



**Consumers
Power**

**POWERING
MICHIGAN'S PROGRESS**

General Offices: 1945 West Parnall Road, Jackson, MI 49201 • (517) 788-1636

Kenneth W Berry
Director
Nuclear Licensing

July 24, 1986

Director,
Nuclear Reactor Regulation
US Nuclear Regulatory Commission
Washington, DC 20555

DOCKET 50-255 - LICENSE DPR-20 - PALISADES PLANT -
EXPANSION OF THE SPENT FUEL POOL STORAGE CAPACITY - RESPONSE TO REQUEST FOR
ADDITIONAL INFORMATION

Consumers Power Company letter dated February 20, 1986 submitted a Request for Change to Palisades Technical Specifications and supporting Safety Analysis Report (SAR) to increase the storage capacity of the Plant spent fuel pool and tilt pit. This increased capacity will be achieved by installing new spent fuel storage racks in approximately one-half of the main pool and in a portion of the spare tilt pit. By letter dated April 24, 1986, Consumers Power Company committed to submit the Summary Reports for all the analyses performed to support the conclusions in the SAR.

NRC letter dated April 25, 1986 transmitted a request for additional information regarding the expansion of the spent fuel pool. Additional requests for information were also received during discussions with the Palisades Plant NRC Project Manager. Attachment 1, including Enclosure A, provides responses to the questions in the April 25, 1986 NRC letter. Attachment 2, including Enclosure B, provides responses to questions received from the Project Manager. Attachment 3 provides information referenced in the responses to certain questions.

To respond to a specific NRC recommendation (NRC letter dated April 25, 1986, question #2), Consumers Power Company has decided to revise the Technical Specifications Change Request and supporting SAR submitted by our letter of February 20, 1986. These revised documents, which will be submitted to the

8608210088 860724
PDR ADOCK 05000255
PDR

OC0786-0116-NL02

Acc 1
/40

Director, Nuclear Reactor Regulation
Palisades Plant
Expansion of Spent Fuel Pool Storage Capacity - Additional Information
July 24, 1986

2

NRC shortly, together with the responses provided by this letter, are being submitted in lieu of the Summary Reports described above and in our letter of April 24, 1986.

Kenneth W Berry (Signed)

Kenneth W Berry
Director, Nuclear Licensing

CC Administrator, Region III, USNRC
NRC Resident Inspector - Palisades

Attachments



**Consumers
Power**

**POWERING
MICHIGAN'S PROGRESS**

General Offices: 1945 West Parnall Road, Jackson, MI 49201 • (517) 788-1636

Kenneth W Berry
Director
Nuclear Licensing

July 24, 1986

Director,
Nuclear Reactor Regulation
US Nuclear Regulatory Commission
Washington, DC 20555

DOCKET 50-255 - LICENSE DPR-20 - PALISADES PLANT -
EXPANSION OF THE SPENT FUEL POOL STORAGE CAPACITY - RESPONSE TO REQUEST FOR
ADDITIONAL INFORMATION

Consumers Power Company letter dated February 20, 1986 submitted a Request for Change to Palisades Technical Specifications and supporting Safety Analysis Report (SAR) to increase the storage capacity of the Plant spent fuel pool and tilt pit. This increased capacity will be achieved by installing new spent fuel storage racks in approximately one-half of the main pool and in a portion of the spare tilt pit. By letter dated April 24, 1986, Consumers Power Company committed to submit the Summary Reports for all the analyses performed to support the conclusions in the SAR.

NRC letter dated April 25, 1986 transmitted a request for additional information regarding the expansion of the spent fuel pool. Additional requests for information were also received during discussions with the Palisades Plant NRC Project Manager. Attachment 1, including Enclosure A, provides responses to the questions in the April 25, 1986 NRC letter. Attachment 2, including Enclosure B, provides responses to questions received from the Project Manager. Attachment 3 provides information referenced in the responses to certain questions.

To respond to a specific NRC recommendation (NRC letter dated April 25, 1986, question #2), Consumers Power Company has decided to revise the Technical Specifications Change Request and supporting SAR submitted by our letter of February 20, 1986. These revised documents, which will be submitted to the

~~8608210088~~ (136pp)

3720
152

Director, Nuclear Reactor Regulation

2

Palisades Plant

Expansion of Spent Fuel Pool Storage Capacity - Additional Information

July 24, 1986

NRC shortly, together with the responses provided by this letter, are being submitted in lieu of the Summary Reports described above and in our letter of April 24, 1986.

Kenneth W Berry (Signed)

Kenneth W Berry

Director, Nuclear Licensing

CC Administrator, Region III, USNRC

NRC Resident Inspector - Palisades

Attachments

53

1

3720

ATTACHMENT 1

Consumers Power Company
Palisades Plant
Docket 50-255

SPENT FUEL POOL STORAGE CAPACITY EXPANSION

RESPONSE TO QUESTIONS TRANSMITTED BY
NRC LETTER DATED APRIL 25, 1986

July 24, 1986

84 Pages

154

3720

RESPONSES TO NRC REQUEST FOR ADDITIONAL INFORMATION

PALISADES SPENT FUEL STORAGE EXPANSION

Question 1: What type of administrative controls are employed to evaluate the burnup of a fuel assembly prior to its placement in Region II?

Response: The following is an outline of the administrative controls that will be invoked.

1. Unless a documented engineering analysis and associated safety evaluation proves the present criticality analysis and burnup versus enrichment curve to be bounding for fuel batch K and future batches, only batches A through J will be considered for storage in Region II.
2. Assembly burnup values will be obtained from the incore analysis system which calculates the individual assembly burnup values based on core power distribution and core average burnup. This system is the same one used to monitor Technical Specification limits for peaking factors.
3. A 10% uncertainty will be applied to the documented burnup value. A lower uncertainty value may be utilized in the future if: 1) The current incore detector analysis system, INCA, is determined to be more accurate, 2) INCA is replaced with an improved code such as CECOR, or 3) assemblies are actually tested to verify burnup. Any change in the uncertainty value will be documented.
4. The active fuel documentation file maintained by the Reactor Engineer will be utilized to identify assemblies that have been modified from their original condition (eg, reconstitution, poison rod removal or fuel rod removal). The modified assemblies will be evaluated to determine if the criticality analysis bounds the "as-is" condition.
5. Actual serial numbers will be read on either: 1) assemblies that are acceptable for Region II storage, or 2) assemblies that are NOT acceptable for Region II storage. Both methods have advantages and disadvantages, and the best option is presently being evaluated. When a serial number is read, the assembly will be physically marked. The marker should be designed to be visible (with adequate lighting) from the 649 foot elevation in the spent fuel pool area. These markings should allow easy, definitive verification of correct assembly storage at any desired time.

6. During refueling operations, items 1 through 4 above will be applied to an assembly prior to placement into Region II. Within 90 days following completion of all refueling operations (ie, after the new core loading is verified), item 5 above will be performed, as necessary.
7. New fuel assemblies will not be allowed in Region II. New fuel can be easily distinguished from spent fuel and special identification marking is unnecessary.
8. Plant procedures will be revised to require all fuel assembly movements into Region II racks be approved first by the Reactor Engineer or designate.

1 5 6

1

3 7 2 0

Question 2: Since the spent fuel burnup requirements for storage in Region II are given in terms of weight percent of U-235, we recommend that the references to 41.24 grams of U-235 per axial centimeter in Tech Spec 5.4.2 be changed to weight percent of U-235 for consistency.

Response: A revised Technical Specifications change request will be submitted which will include the change to section 5.4.2 recommended by the NRC.

3 7 2 0
1 5 7

Question 3: Please identify the organization and provide assurance that the organization that performs the criticality analyses has been previously qualified to perform these type of calculations.

Response: The Westinghouse Nuclear Fuel Division is responsible for the criticality analysis. This division performs all Westinghouse core design calculations and has been responsible for fuel rack and shipping container criticality analysis since the early 1970's.

3 7 2 0
1 5 3

Question 4: The standard deviation of the K_{eff} values for the 27 critical experiments used as benchmarks (Table 3-1) is significantly lower than that previously obtained by other licensees using the same calculational method. Describe your derivation of the 95/95 uncertainty in the method bias in more detail.

Response: It has long been known that the original Westinghouse procedure for handling the bias uncertainties in the criticality analysis was conservative. As a result, a new procedure was implemented in 1984 based on the method presented in "Statistical Methods in Nuclear Material Control" by John L. Jaech. This method has been used by Westinghouse since that time and has been licensed in the Zion fuel rack analysis.

From the 27 critical experiments modelled in KENO, the mean K_{eff} of the benchmarks is 0.9998 which demonstrates that there is no significant bias associated with the method. The original treatment of the uncertainty associated with the bias resulted in a 95% probability with a 95% confidence level of 0.013 delta-K. This was based on a standard deviation of the mean of 0.0057 delta-K for the 27 benchmark K_{eff} values. However, a more correct treatment of the uncertainties can be used to determine the uncertainty of the bias term applied to the KENO results. This treatment is based on the method in the reference mentioned above. Based on this treatment, the square of the standard deviation of the mean, and the average KENO uncertainty for the 27 critical benchmarks were added and divided by 27. As a result, the uncertainty of the bias term is 0.0014 delta-K. The 95/95 one-sided tolerance limit factor for 27 values is 2.26. Thus, the 95/95 in the bias reactivity due to the method is not greater than 0.0032 delta-K.

3720 159

Question 5: What are the values of the worst case K_{eff} and of the biases and uncertainties referenced in Section 3.1.4.1.1 for Region II?

Response: The values of the worst case K_{eff} , biases and uncertainties are:

K_{worst} - 0.899

B_{method} - 0.0

B_{part} - 0.0045

Ks_{worst} - 0.0035

Ks_{method} - 0.0032

Ks_{re} - 0.01

Substituting the calculated values results in a maximum K_{eff} - 0.9155.

3 7 2 0
1 6 0

Question 6: It appears that the only certainty accounted for due to reactivity equivalencing is that due to uncertainty in the plutonium reactivity. Justify why the uncertainty in reactivity as a function of burnup was not included also.

Response: Although the reactivity uncertainties associated with plutonium and fuel burnup are not independent, it should be considered that the reactivity of fuel as a function of irradiation depends implicitly on the production rate of plutonium. These uncertainties are so closely related that accounting for them twice is considered very conservative. As a result, a term was defined to account for the uncertainty associated with the burnup dependent reactivities.

A value of 0.01 delta-K is given to the uncertainty term associated with the burnup dependent reactivities computed with PHOENIX. This uncertainty is considered to be conservative since comparison between PHOENIX results and the Yankee Core experiments and the 81 benchmark experiments indicates much closer agreement.

3720
161

Question 7: What is the maximum clad temperature predicted to occur in the spent fuel pool for normal storage condition and for any abnormal or accident condition?

Response: Maximum clad temperatures were calculated for three conditions - normal storage; 80% flow blockage of the rack coolant inlet at the rack base plate; and total loss of cooling in the spent fuel pool. For the first two cases water inlet temperature was conservatively taken as 150°F. For the third case water inlet temperature was 212°F. Decay heat value correspond to 36 hours after reactor shutdown. The chart below shows maximum clad surface temperature for a peak rod of 1.6 times heat output for an average rod.

Condition	Max. Clad Surface Temp (°F)
Normal Operation	258.2
80% Flow Blockage at Base Plate	291.8
Loss of Cooling	< 300

Note that the calculations were performed for fuel stored in the main pool and the spare tilt pit. Therefore the results given above apply to fuel stored in either location.

3 7 2 0
1 6 2

Question 8: The request for Technical Specification change from Consumers Power Company dated February 20, 1986, does not provide sufficient information to perform an adequate review of certain aspects of material considerations mentioned in (or omitted from) Section 4 of PALSFP-4-NL02. The following information is needed for the staff to complete this review:

- a. Identification of subsections, articles, subarticles and paragraphs of Sections III and IX of the ASME Boiler and Pressure Vessel Code that pertain to spot welding referenced in PALSFP-4-NL02,
- b. The fabrication, control, and inspection methods utilized in spot welding, and
- c. The long term environmental compatibility of the spot welds with fuel pool storage conditions.

Response: Spot welding is used on the spent fuel rack to attach the poison wrapper to the cell. The function of the poison wrapper is to cover the Boraflex poison material. Thus, the spot welds are not part of the primary load path of the rack structure and are, therefore, outside the jurisdiction of the ASME Boiler and Pressure Vessel Code.

The spot welds on the racks are made using the plasma arc fusion welding process or the gas tungsten arc welding process, Westinghouse has developed process specifications for this weld using the intent of American Welding Society specification C1.1. The procedures were qualified by testing using the same material alloy and thickness as the wrapper and cell. Testing included visual examination, peel tests, shear load tests and material sensitization tests. In each case, on the sheer load test weld strength greatly exceeded design requirements. For the material sensitization test the weld and heat affected zone were tested and passed per Practice A of ASTM A262.

Spot welds are made using calibrated equipment on which all welding variables are preset. Prior to each working shift a weld sample is made with each welding head using the same material alloy and thicknesses as the wrapper and cell. Each sample is visually inspected and peel tested to determine fusion nugget diameter. In addition, each weld made during a shift is visually inspected.

Sample spot welds were tested and passed per ASTM A262 Practice A during procedure qualification. This test showed that the material is not sensitized by the spot welds. Thus the long term environmental compatibility of the spot welds in the fuel storage pool conditions will be the same as 304 stainless steel and should not be a problem.

3 7 2 0
1 6 3

Question 9: SPENT FUEL RACK STRUCTURAL ANALYSIS

With respect to the analysis of spent fuel rack modules, please provide the following information:

- a. For the Region I racks already in place, provide descriptions and sketches of the fuel racks, their method of lateral restraint (attachment to the pool walls), and a full description of the displacement analysis indicating that the Region I racks will not be displaced to impact the new Region II racks.

Response:

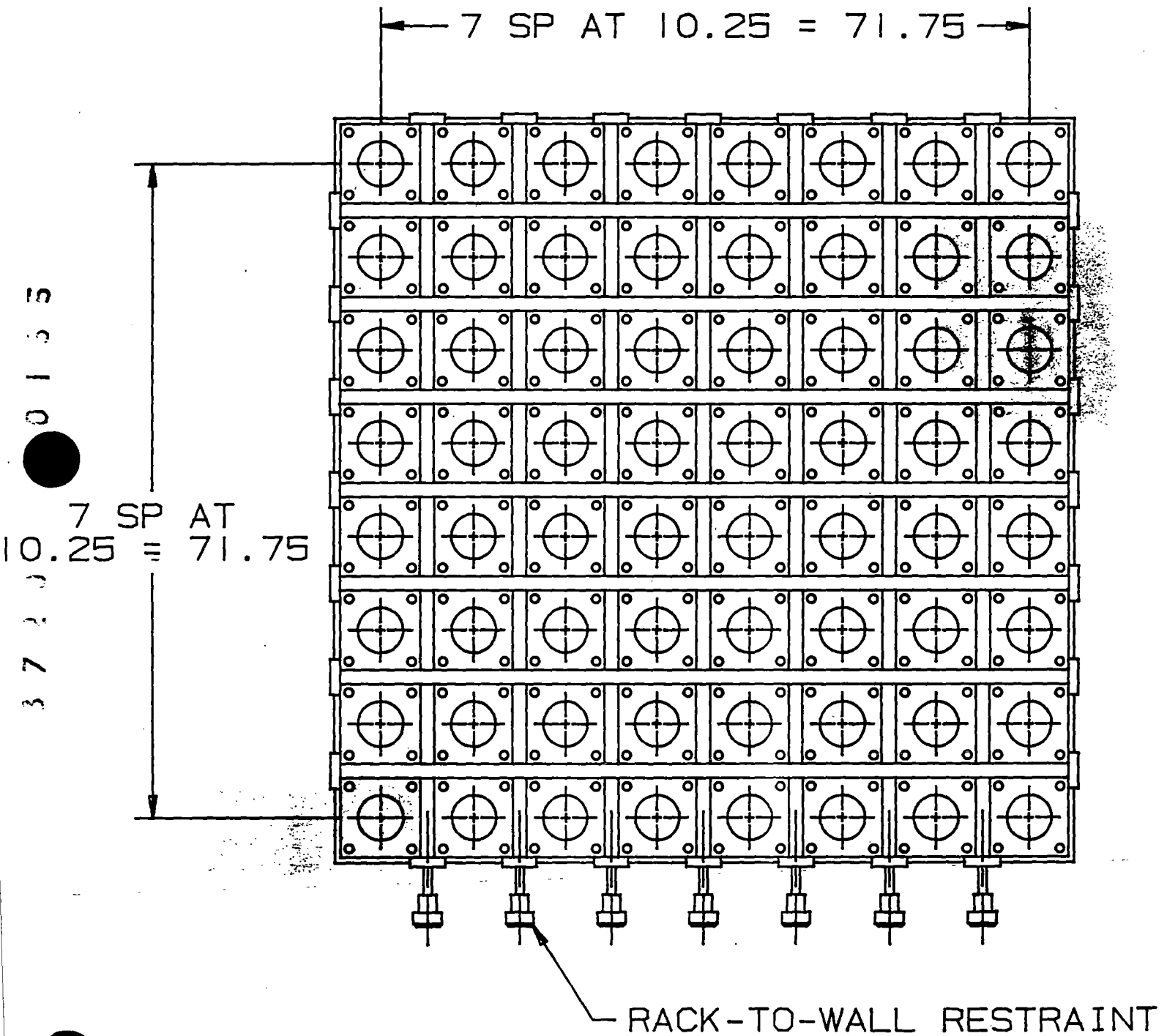
The existing Region I racks are 8x8 with 10.25 inch center-to-center cell spacing and are supported on the pool floor at four locations. The rack-to-wall lateral restraint assembly (see Sketch 9a) is a bolt with integral bearing pad which threads into the ends of both the top and bottom grid members. (Note that the north end of the Region I racks will have no lateral restraint.)

The non-linear time history analyses of the Region I and Region II racks show that the maximum relative displacement between the Region I and Region II racks due to sliding, rocking, structural deflection, and thermal effects is 0.54 inches. This is much less than the 1.75 inch minimum clearance and therefore precludes impact between the Region I and Region II racks.

3 7 2 0
1 5 4

SKETCH 9a

TYPICAL REGION I RACK - PLAN VIEW



Question 9b: Document the source of the earthquake data and describe the methods by which the earthquake acceleration time histories were generated for use in the rack displacement analysis.

Response: The acceleration time histories applied to the fuel rack models were obtained by synthesizing the 1940 El Centro earthquake such that the resulting response spectra envelop the Palisades Floor Response Spectra. The Palisades Floor Response Spectra employed here is that of the original design of the Plant. That response spectra was generated from the modified Taft 1952 earthquake.

3 7 2 0
1 6 6

Question 9c: Describe the number of independent horizontal earthquake acceleration components used, as well as the directional orientation of the horizontal components relative to the long and short sides of the racks analyzed.

Response: The analysis accounts for two horizontal shocks and one vertical shock simultaneously. Since the North-South and East-West horizontal shocks are identical, the rack response is independent of the directional orientation.

3 7 2 0
1 6 7

Question 9d: Identify the rack modules chosen for analysis and provide the technical justification that the choice of racks for analysis brackets, or bounds, the response of all the rack modules in the spent fuel pool and tilt pit.

Response: The main spent fuel pool has two (2) 11x11 rack modules and two (2) 7x11 rack modules, while the tilt pool has a 6x6 rack module and 6x7 rack module. In order to determine which rack response would be limiting, loads were calculated for both the 11x11 and 7x11 in the main pool. For racks in the tilt pool, loads were calculated for the 6x7 rack, which enveloped the response of the 6x6 rack.

3 7 2 0
1 6 8

Question 9e: Provide the clearance space between each adjacent rack module and between the rack modules and the pool walls.

Response: The minimum clearance space between each adjacent rack module is 1.50 inches. The minimum clearance between the rack modules and the pool walls is 1.80 inches.

3 7 2 0
1 6 9

Question 9f: For adjacent rack modules, describe how the clearance space between the rack modules was apportioned to each module for the purposes of comparing the rack displacement to the available apportioned clearance space.

Response: The maximum rack relative displacement between rack modules was found to be 0.439. This value is much less than the available 1.50 inch clearance space.

3 7 2 0
1 7 0

Question 9g: Document the computer codes used for the three-dimensional elastic analysis and for the nonlinear dynamic displacement analysis. Include justification of the choice of the computer codes.

Response: An analysis of the racks is performed on the Westinghouse Electric Computer Analysis (WECAN) Code, which has been developed over many years by Westinghouse. It is a general purpose finite element code with a great variety of static and dynamic capabilities. These elements have been fully verified by benchmark problems and are on a configuration control code which is maintained in compliance with strict quality control requirements.

The general WECAN code has been reviewed by the NRC through the submittal of Westinghouse document WCAP-8929, "Benchmark Problem Solutions Employed for Verification of the WECAN Computer Program." For review of additional capabilities which pertain to the fuel rack non-linear dynamic analysis, the following documents are provided in the "References" section of this letter.

- a. Shah, V N, Gilmore, C B, "Dynamic Analysis of a Structure with Coulomb Friction," ASME Paper No. 82-PVP-18, presented at the 1982 ASME Pressure Vessel Piping Conference, Orlando, FL, June 1982.
- b. Gilmore, C B, "Seismic Analysis of Freestanding Fuel Racks," ASME Paper Number 82-PVP-17, presented at the 1982 ASME Pressure Vessel Piping Conference, Orlando, FL, June 1982.

3720
2171

Question 9h: Describe the features and limitations (if any) of the frictional model used to compute static and sliding friction in the dynamic displacement analysis.

Response: The three-dimensional friction element used in the non-linear model is composed of a gap in series with a parallel combination of impact spring and impact damper with a frictional spring orthogonal to the gap. This element, which is used to model the support pad interface with the pool floor, is designed to represent two surfaces which may slide relative to each other, and may separate or contact each other. The dynamic displacement analysis is performed for friction coefficients of $\mu = .2$ and $.8$. The maximum sliding distance (rack base horizontal displacement) of the rack module is obtained for the $\mu = .2$ case. The maximum rack loads and structural deflections are obtained for the $\mu = .8$ case.

3720 172

Question 91: A statement on Page 4-9 indicates that "the hydrodynamic mass of a submerged fuel rack assembly is modeled by general mass matrix elements connected between the cell and the pool wall." Please provide the theoretical premise by which this was modeled, and justify the use of the model for hydrodynamic mass and hydrodynamic coupling between adjacent rack modules, between a rack module and the pool walls and walls, and between a fuel assembly and the storage cell walls. Does this underestimate or overestimate the hydrodynamic coupling?

Response: The hydrodynamic mass between the rack cells and the pool wall was calculated by evaluating the effects of the gap between the rack modules and the pool wall using the method outlined in the paper by R. J. Fritz ("The Effect of Liquids on the Dynamic Motions of Immersed Solids," Journal of Engineering for Industry, February 1972). The close proximity of adjacent racks, as well as the size of the racks relative to the gap between racks, is such that extremely large hydrodynamic masses are produced if the racks attempt to respond out of phase. It is this large hydrodynamic mass which causes the racks to respond in phase. The seismic analysis treats the racks as if they are hydrodynamically coupled (move in phase), which gives the highest loads and displacements. The hydrodynamic mass between the fuel assembly and the cell walls is based upon the fuel rod array size and cell inside dimensions using the technique of potential flow and kinetic energy. The hydrodynamic mass is calculated by equating the kinetic energy of the hydrodynamic mass with the kinetic energy of the fluid flowing around the fuel rods. The concept of kinetic energy of the hydrodynamic mass is discussed in a paper by D F DeSanto ("Added Mass and Hydrodynamic Damping of Perforated Plates Vibrating in Water." ASME Journal of Pressure Vessel Technology, May 1981).

Both papers cited above are provided in the "References" section of this letter.

3 7 2 0
1 7 3

Question 9j: Document the source of the impact spring stiffness and impact damping between a fuel assembly and the storage cell walls, and justify the value of impact damping used.

Response: To determine the spacer grid impact stiffness and impact damping, the following test was performed in air. (Note that water will increase the damping effects from those of air.) A weight was dropped onto a spacer grid mounted vertically to a load cell. The top end of the spacer grid is free. Sections of fuel rod cladding are inserted into the spacer grid to simulate the fuel's effects on stiffness and damping. A displacement transducer follows the vertical motion of the dropweight and displacement of the top surface of the spacer. The results of this test are summarized below.

Drop Height of Weight; in	0.25		0.50	
	X	Y	X	Y
Direction Relative to Spacer Orientation				
Natural Frequency; Hz	31.6	21.0	26.2	21.2
Spacer Impact Stiffness; lbs/in	14,544.	6,402.	9,970.	6,510.
Spacer Impact Damping; % of Critical Damping	15.8	12.3	18.0	17.7

3 7 2 0
0 1 7 4

Question 9k: For the non-linear dynamic displacement analysis, describe the numerical integration method used, as well as the procedures that were employed to assure that the numerical integration remained stable and that the resulting displacements represent a fully converged solution.

Response: For the non-linear dynamic analysis, the modal superposition method was employed to obtain displacements as a function of time. In order to determine if the solution was fully converged, a time increment study was performed. Different time increments were used, and it was shown that the results were the same for the time increments of 0.0013 seconds and 0.0025 seconds. Thus, for the seismic analysis, the time step chosen was 0.0025 seconds.

3 7 2 0
1 7 5

Question 91: Provide a summary of rack displacements that includes elastic distortion (if significant), sliding and tipping displacement as well as their sum.

Response: The maximum single rack displacement including elastic distortion and tipping is 0.2579 inches, and the maximum single rack sliding displacement is 0.0053 inches. The maximum relative displacement between adjacent racks is 0.439 inches.

3 7 2 J 0 1 7 6

Question 9m: Provide tables of computed stresses in the rack structure and support legs, and their comparison to allowable values in accordance with the acceptance criteria cited in the licensing report.

Response: The following table provides a summary of the computed stresses in the rack structure and support structure along with the allowable values and their margins of safety.

3720
177

REGION II RACKS
SUMMARY OF DESIGNS STRESSES AND MINIMUM MARGINS OF SAFETY
NORMAL & UPSET CONDITIONS

	Design Stress (psi)	Allowable Stress (psi)	Margin of Safety
<u>1.0 Support Pad Assembly</u>			
1.1 Support Pad Shear	2801	11000	2.93
Axial and Bending	11538	16500	.43
Bearing	9805	24750	1.52
1.2 Support Pad Screw Shear	8030	11000	.37
1.3 Support Plate Shear	2802	11000	2.93
Weld Shear	16100	24000	.49
<u>2.0 Cell Assembly</u>			
2.1 Cell Axial and Bending	.86	1.0**	.16
2.2 Cell to Base Plate Weld Weld Shear	17695	24000	.36
2.3 Cell to Cell Weld Weld Shear	22652	27500*	.21
2.4 Cell to Wrapper Weld Weld Shear	9053	11000	.21
2.5 Cell Seam Weld Weld Shear	19173	24000	.25
2.6 Cell to Cover Plate Welds Weld Shear	20431	24000	.18

*Thermal Plus OBE Stress is limiting

**Allowable per Appendix XVII-2215 Eq (24)

3720 0173

Question 9n: Provide the amount and characteristics of mounting foot lift-off from the pool floor associated with dynamic rack displacement, and show that the resulting impacts with the floor were considered in the stress analysis.

Response: The maximum pad (mounting foot) lift-off from the pool floor is 0.342 inches. This pad is modeled using an impact/gap element which allows impact to be accounted for in the dynamic analysis. The loads developed from this dynamic analysis are in turn used in the stress analysis.

3 7 2 0
1 7 9

Question 9o: Provide an analysis of rack module stability in the tipping mode, considering the worst case of off-center fuel load possible.

Response: For the evaluation of rack stability, the rack is evaluated for both partially and fully loaded conditions. It was determined that the partial loading of two rows of fuel, coupled with the limiting condition of the six-cell direction of the rack (ie, the side of the rack comprised of six storage cells), yielded a minimum factor of safety against overturn of 32. This value is much greater than the 1.5 minimum required by the NRC Position Paper.

3720
0180

Question 9p: Provide a detailed description of the recessed cask area (cask pit), showing its location in the spent fuel pool and geometric relationship of the cask pit to any adjacent spent fuel rack modules. Include full descriptions of any structures, or other provisions, present to preclude damage to any adjacent fuel rack modules during cask operations, or to prevent any adjacent fuel rack modules from entering the pit.

Response: A 9-foot by 9-foot area in the northeast corner of the spent fuel pool is recessed to accommodate a shipping cask. Technical Specifications section 5.4.2, item "f", prohibits fuel shipping casks from being moved to the fuel storage building until the NRC approves the cask drop evaluation. With regard to preventing any adjacent fuel rack from entering the recessed cask pit, a review of the Region II rack configuration shows that the centerline of the fuel rack support closest to the cask pit is 3.5 inches from the edge of the pit. Comparing this distance to the sliding distance given in the response to Question 91 (0.0053 inches), shows that the racks will not enter the pit.

3720181

Question 10a: SPENT FUEL POOL STRUCTURAL ANALYSIS

With respect to analysis of the spent fuel pool under the increased loads of higher density fuel storage, the Licensee is requested to provide the following information to supplement the analysis outline provided in the licensing report:

- a. Describe how the dynamic interaction between the pool structure and the rack modules was considered, including the value of any associated dynamic amplification factors.

Include all assumptions made regarding the summation and phase of all rack loads.

Response:

The response of the spent fuel racks was determined by a nonlinear time history analysis. The seismic time histories applied to the racks were synthesized from pool floor response spectra which account for the pool floor amplification. Applying the time histories to the nonlinear dynamic fuel rack model, the loads on the pool were determined. Since the dynamic model accounts for possible rack lift and then pad impact on pool floor, the results of the nonlinear dynamic analysis provide the proper rack to pool interaction and the use of additional dynamic amplification factors is not necessary. The structural model of the pool was loaded assuming that all the individual racks were responding in phase. See also the response to Question 9c.

3720 0182

Question 10b: Provide analysis proving the adequacy of the pool floor and liner under the local maximum rack module dynamic mounting foot loads.

Response: The analysis of the pool floor is discussed in the response to Question 10c. This analysis considers the local maximum rack module dynamic mounting foot loads. From the stress summary Tables provided in the response to Question 10c, it is apparent that the pool floor is adequate for these local loads. The structural adequacy of the liner for these local loads is demonstrated below.

Two types of fuel racks (W and NUS) are used in the pool. Both racks are free standing with circular pads used to transfer the rack loads to the pool floor. The basic design characteristics are shown in Figure 1-10b. The W pad and the NUS pad are 5 inches in diameter. The liner on which the pads rest is 3/16 inches in thickness and is SA-167, Type 304L stainless steel anchor plate. The liner rests on the concrete pool floor. This is also shown in Figure 1-10b.

The loads transferred through the pads are both vertical and horizontal. The maximum loads that a particular pad will transfer is a function of the type and configuration of the rack. This is seen in Table 1-10b.

By the nature of free standing rack design, the only way that a horizontal load can be transmitted to the pool floor is by friction. The friction load, as well as the vertical load, is transferred directly to the pool floor at the location of a pad. This is shown in Figure 2-10b. As seen in this figure, two types of local stresses are induced into the liner, shear stress and bearing stress. Since the NUS fuel racks have the highest loads (See Table-10b), the highest local liner stresses will occur at the location of the NUS pads. The maximum local stresses that will be produced in the liner for the defined design seismic events are given in the following.

Local Liner Bearing Stress (P):

30

$$\text{Pad Bearing Area} = 3.14 \times (5/2) \times (5/2)$$

$$\text{Pad Bearing Area} = 19.63 \text{ sq in}$$

$$\text{SSE Event: } P = 94.2/19.63$$

$$P = 4.8 \text{ ksi}$$

$$\text{OBE Event: } P = 60.94/19.63$$

$$P = 3.1 \text{ ksi}$$

The local liner bearing stresses calculated above are well within the liner plate allowable stresses defined below.

$$\text{SSE Bearing Allowable Stress} = 1.6 \times 0.9 F_y$$

Where F_y = Liner Yield Stress

F_y = 25 ksi at 100 degrees Fahrenheit

$$\begin{aligned} \text{SSE Bearing Allowable Stress} &= 1.6 \times 0.9 \times 25 \\ &= 36.0 \text{ ksi} \end{aligned}$$

$$\text{OBE Bearing Allowable Stress} = 0.9 F_y$$

$$= 0.9 \times 25 = 22.5 \text{ ksi}$$

3720 0134

Local Liner Shear Stress (V):

$$\text{SSE Event: } V = 60.5/19.63$$

$$V = 3.1 \text{ ksi}$$

$$\text{OBE Event: } V = 30.24/19.63$$

$$V = 1.5 \text{ ksi}$$

The local liner shear stresses are also well within the liner allowable shear stresses as seen below.

$$\text{SSE Shear Stress Allowable} = 1.6 \times 0.4 \times F_y$$

$$= 1.6 \times 0.4 \times 25 = 16 \text{ ksi}$$

$$\text{OBE Shear Stress Allowable} = 0.4 \times F_y$$

$$= 0.4 \times 25 = 10 \text{ ksi}$$

As seen from the analysis given above, and the analysis reported in response to question 10c, the pool floor and liner is adequate for the local maximum rack module dynamic mounting foot loads.

The wall rack loads are bearing forces only. The bearing loads are smaller than the floor bearing forces and are therefore enveloped by the analysis performed above.

3 7 2 0
1 8 5

MAXIMUM PAD LOADS (kips)					
RACK ARRAY	WESTINGHOUSE RACKS				NUS RACKS
	11 x 11	11 x 7	7 x 6	6 x 6	8 x 8
<u>SSE</u> Load Condition					
Vertical	75	75	68	68	94.2
Hor: N-S	25	25	16	16	60.5
E-W	47	47	16	16	13.83
<u>OBE</u> Load Condition					
Vertical	46	46	46	46	60.94
Hor: N-S	12.5	12.5	8.0	8.0	30.24
E-W	23.5	23.5	8.0	8.0	6.92

TABLE 10-1b: MAXIMUM PAD LOADS

0186

3720

3720 2187

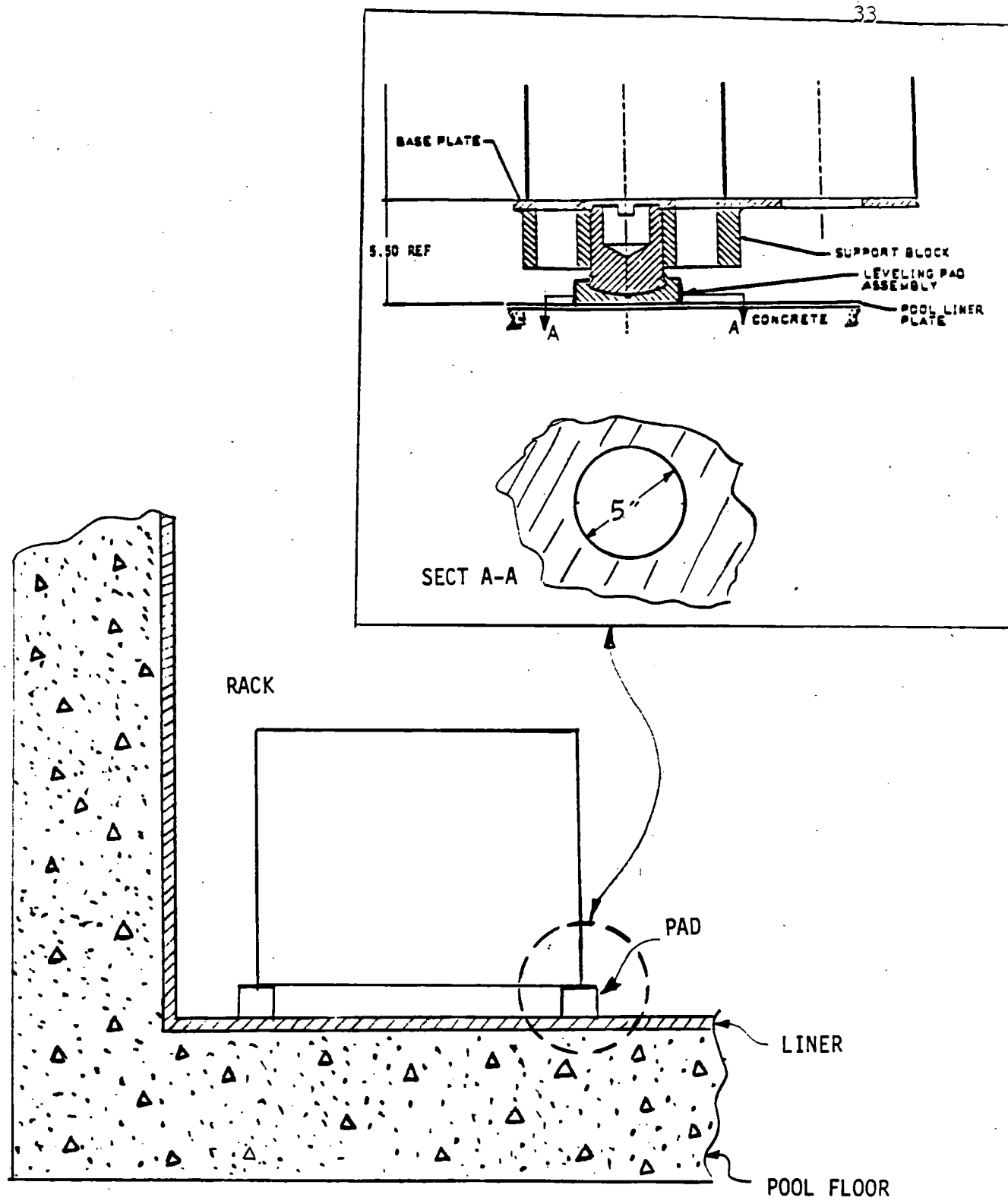


FIGURE 1-10b: RACK MODULE AND MOUNTING PAD DESIGN CHARACTERISTICS

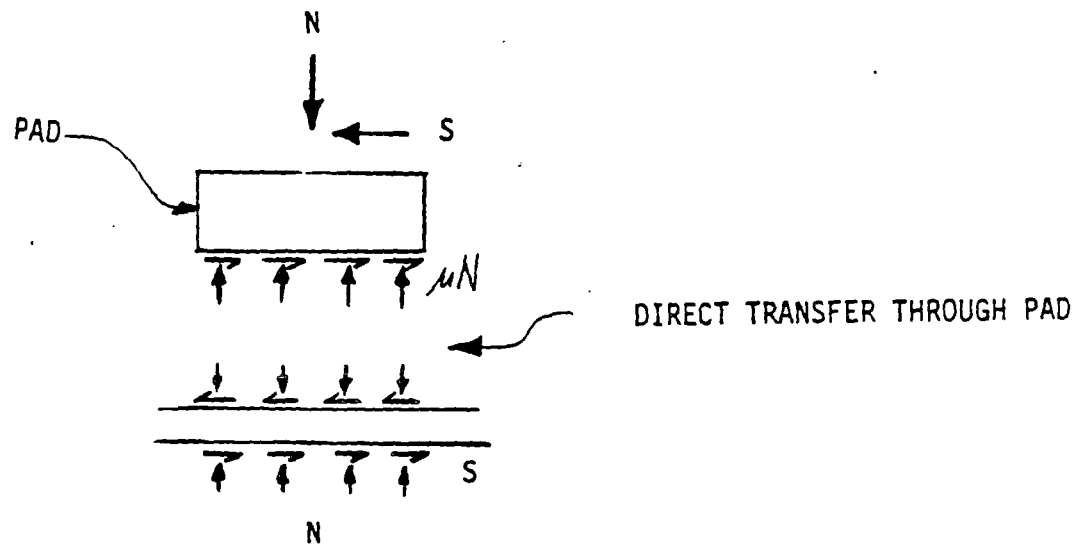
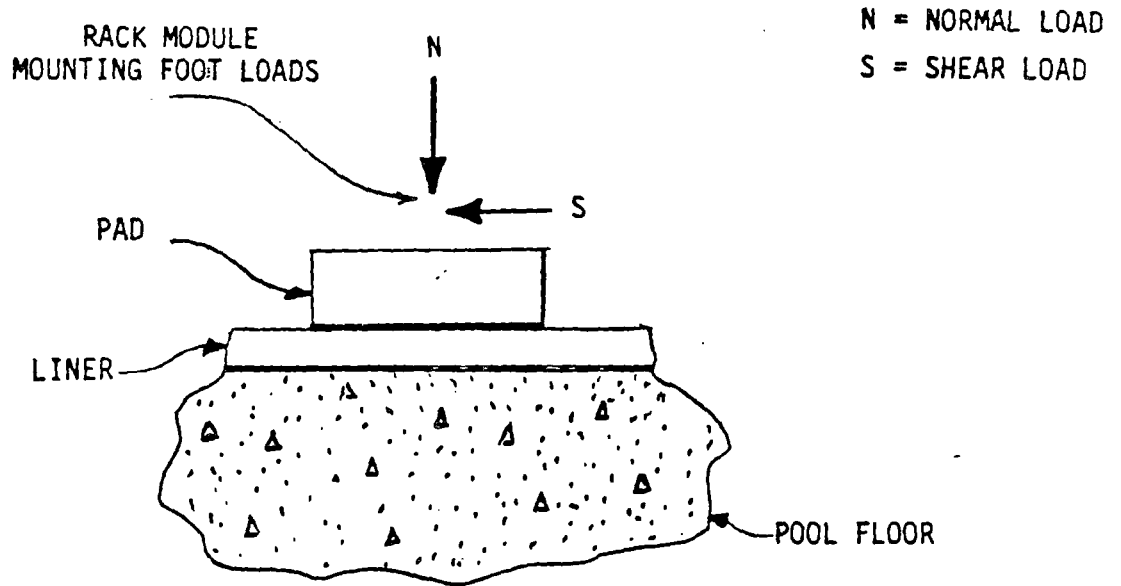


FIGURE 2-10b

MAXIMUM RACK MODULE DYNAMIC MOUNTING FOOT LOADS

3720 0133

Question 10c: Provide identification of the most critical regions of the pool structure. List the stresses (thermal, deadweight, seismic and rack dynamic loads) and their comparison to allowable values, including the source and justification of the use of the allowable values.

Response: The requested information is provided in Enclosure A that follows. The criteria and loading conditions employed to evaluate the Palisades Spent Fuel Pool Structure are given, as well as the stresses associated with the most critical regions of the pool. Specifically provided in this attachment are the following:

1. Loading Combinations
2. Material Properties
3. Design Allowable Stress Limits with Basis of Allowable Values
4. Table of Critical Stresses and Location (A1 to A2)
5. Figures Defining Element No. Used to Define Critical Stress Locations per Tables A1 to A2 (Figures B1 through B7 and D1 through D31)

3 7 2 0
1 3 9

Question 11: FUEL ASSEMBLY ACCIDENT ANALYSIS

The following information is requested with respect to the analysis of a dropped fuel assembly covered in Paragraph 4.6.4 of the Licensee's report:

- a. For the first accident condition, provide the extent of deformation predicted by the analysis to occur on the top of the spent fuel rack as well as to occur on the dropped fuel assembly. Indicate whether there is a possibility for the damage to release radioactive material.
- b. Documentation of the second accident condition should be provided in a manner similar to that requested for question 11a above.
- c. Provide a description of the analysis methods for the third accident condition, including justification of assumptions. Provide the maximum velocity reached by the fuel assembly and verify that the kinetic energy of the fuel assembly can be absorbed as strain energy in the structure without damage to the pool liner or release of radioactive material from the fuel assemblies.

Response:

For fuel drop accident conditions, the double contingency principle of ANSI N16.1-1975 is applied. This states that one is not required to assume two unlikely, independent, concurrent events to ensure protection against a criticality accident. Thus, for accident conditions, the presence of soluble boron in the storage pool water can be assumed as a realistic initial condition since not assuming its presence would be a second unlikely event.

The presence of approximately 1720 ppm boron in the pool water will decrease reactivity by about 30 percent ΔK . In perspective, this is more negative reactivity than is present in the poison plates (18 percent ΔK), so K_{eff} for the rack would be less than 0.95 even if the poison plates were removed by a drop accident. In fact, with 1720 ppm boron in the pool water, there is no deformation that could reasonably be achieved by the drop of a fuel assembly that would cause the criticality acceptance criteria to be exceeded for fuel meeting the burnup criteria for Region II storage. This applies to all of the three drop accident conditions.

The radiological consequences of a fuel drop accident are described in Section 5.3.1 of February 20, 1986, submittal. This Section shows that the potential offsite doses are less than the guidelines of 10CFR100. Furthermore, an analysis has been performed which shows that a large number of fuel elements could be failed without exceeding the guidelines of 10CFR100.

ENCLOSURE A

Consumers Power Company
Palisades Plant
Docket 50-255

SPENT FUEL POOL STORAGE CAPACITY EXPANSION

July 24, 1986

3720 191

ENCLOSURE A

A. CRITERIA AND LOADING CONDITIONS

This section presents the loading conditions, material properties, seismic requirements, criteria employed and design specifications and codes used to evaluate the structures.

A.1 LOADS

The following loads were considered in the evaluation of the pool integrity.

- Dead Load, includes pool structure self-weight, racks and fuel assemblies, and hydrostatic loads. In addition, all floor live loads, dead loads of adjacent structures and superstructure crane loads are included.
- Operating basis earthquake
- Safe shutdown earthquake
- Thermal loads
- Hydrostatic loads are considered for a water level at elevation 648 feet in the spent fuel pool and tilt pits
- Sloshing effects of water - hydrodynamic loads

To determine the adequacy of the structure, the criterion outlined in Appendix A "Design Bases" to the FSAR Update was adopted.

Based on the Palisades FSAR Update (Reference Document 1) the following critical load combinations were considered in the analysis of the pool structure.

$$1.25D + 1.25T_o + 1.25E \text{ (Normal Operating Condition)}$$

$$1.0D + 1.0T_o + 1.0E' \text{ (Abnormal Operating Condition)}$$

where

- D = Dead load defined above including hydrostatic loads
- E = Seismic (OBE) load including hydrodynamic (sloshing) loads
- E' = Seismic (SSE) load including hydrodynamic (sloshing) loads
- T_o = Thermal gradient load for normal operating condition

3720
192

Two additional load combinations were considered to evaluate the isolated effects of the mechanical loads and to evaluate the abnormal event of a full core off load case. The additional load combinations are:

$$\begin{aligned} &1.25 D + 1.25 E \\ &1.0 D + 1.0 T_{ab} \end{aligned}$$

where

T_{ab} = Thermal gradient for abnormal operating condition

3 7 2 0
1 9 3

A.2 MATERIAL PROPERTIES

CONCRETE:

f'_c = Compressive Strength at 28 days = 3000 psi

W = Specific Weight of Concrete = 150 pcf

E_c = Modulus of Elasticity of Concrete

$E_c = W^{1.5} (33) \sqrt{f'_c} = 3.32056 \times 10^6 \text{ psi} = 3.321 \times 10^3 \text{ ksi}$

ν = Poisson's Ratio = 0.14

ρ = Mass Density = 4.6583 P-sec²/ft⁴

G = Modulus of Rigidity = 1.4563 x 10³ ksi

α = Coef. of thermal Expansion = 5.5 x 10⁻⁶ per °F

REINFORCEMENT BARS:

ASTM-A-615, Grade 40

Yield Strength = 40 ksi

E_s = 29000 ksi

ν_s = Poisson's Ratio = 0.33

G = 10694 ksi

α = Coeff. of thermal Expansion = 6.5 x 10⁻⁶ per °F

3720
195

A.2 DESIGN ALLOWABLE STRESS LIMITS

The design allowable stress limits outlined in "Building Code Requirements for Reinforced Concrete (ACI 318-71)" were considered the basis of evaluation for the spent fuel structure.

To determine the adequacy of structure, the stress criterion outlined in FSAR Update Appendix A (Reference 1) was adopted. The load combinations considered for evaluation are:

- | | | |
|---|---|--------------------------------|
| 1. $Y = \frac{1}{\phi} (1.25D + 1.25T + 1.25E)$ | } | (Normal Operating Condition) |
| 2. $Y = \frac{1}{\phi} (1.25D + 1.25E)$ | | |
| 3. $Y = \frac{1}{\phi} (1.0D + 1.0T + 1.0E')$ | } | (Abnormal Operating Condition) |
| 4. $Y = \frac{1}{\phi} (1.0D + 1.0 T_{ab})$ | | |

where:

D, T, T_{ab} , E and E' are defined in Section A.1, and

Y = Required yield strength of the material

ϕ = Yield capacity reduction factor per ACI 318-71 for both reinforcement and concrete

A.3 STRESS SUMMARY

The reinforcement and concrete stresses of the critical sections in the pool walls and slabs, in the substructure walls and in the foundation mat have been identified in Tables A-2 and A-3. Sketches to help identify the critical sections have been included in Attachment A in Figures B-1 to D-31.

A.4 REFERENCES

Palisades FSAR Update Appendix A, Design Bases for Structures, Systems, and Equipment for Palisades Plant.

TABLE A1

MAXIMUM REINFORCEMENT STRESSES

LOCATION	DIRECTION 1			DIRECTION 2		
	REINF STRESS (ksi)	ELEMENT ³⁾ NO.	LOAD ⁴⁾ COMB.	REINF STRESS (ksi)	ELEMENT ³⁾ NO.	LOAD ⁴⁾ COMB.
<u>MAT & SLABS</u>						
590' (MAT)	30.00	13	2	10.44	13	2
607' - 6"	17.30	54	1	15.8	53	1
610' - 0"	35.1	72	1	12.6	70	1
611' - 0"	34.9	128	1	15.5	128	2
<u>EAST-WEST WALLS</u>						
EW 1	19.3	618	2	28.9	618	2
EW 2	14.5	664	1	18.8	664	2
EW 3	4.0	683	3	31.9	683	4
<u>NORTH SOUTH WALLS</u>						
NS 1	24.8	311	1	20.3	311	4
NS-2	17.0	357	3	22.2	357	2
NS 3	37.4	429	1	16.6	428	1
NS 4	1.1	480	1	17.0	480	2

All reinforcement stresses are below the allowable stress of 40 ksi (yield strength of ASTM-A-615, Grade 40).

1. For Mat and Slabs: Direction 1 = NS, Direction 2 = EW
2. For Walls: Direction 1 = Horizontal, Direction 2 = Vertical
3. Attachment A for Element Locations.
4. Load combinations are defined in Section A.6.

3720 0196

TABLE A2 (Continued)

MAXIMUM REINFORCEMENT STRESSES

LOCATION	DIRECTION 1			DIRECTION 2		
	REINF. STRESS (ksi)	ELEMENT ³⁾ NO.	LOAD ⁴⁾ COMB.	REINF. STRESS (ksi)	ELEMENT ³⁾ NO.	LOAD ⁴⁾ COMB.
<u>SUPPORT WALLS BELOW</u>						
NS 4	20.30	466	2	28.19	466	2
NS 5	32.53	501	1	7.51	494	2
NS 6	29.0	513	2	2.0	513	2
NS 7	18.9	526	1	2.0	526	2
NS 8	6.1	536	1	6.1	536	2
NS 9	20.7	546	1	3.9	546	1
NS 10	35.7	561	2	18.1	561	2
EW4	10.5	690	3	2.0	690	3
EW 5	16.6	696	2	28.0	696	2
EW 6	23.9	705	4	2.0	705	1
EW 7	35.2	715	1	2.0	715	2
EW 8	29.8	718	2	3.9	718	3
EW 9	21.1	720	2	23.7	720	2
EW 3	26.0	677	3	2.0	677	1

All reinforcement stresses are below the allowable stress of 40 ksi (yield strength of ASTM-A-615, Grade 40).

1. For Mat and Slabs: Direction 1 = NS, Direction 2 = EW
2. For Walls: Direction 1 = Horizontal, Direction 2 = Vertical
3. See Attachment A for Element Locations.
4. Load Combinations are defined in Section A.6.

TABLE A2
MAXIMUM CONCRETE STRESSES

LOCATION	DIRECTION 1			DIRECTION 2		
	CONC. STRESS (ksi)	ELEMENT ³⁾ NO.	LOAD ⁴⁾ COMB.	CONC. STRESS (ksi)	ELEMENT ³⁾ NO.	LOAD ⁴⁾ COMB.
<u>MAT & SLABS</u>						
590' (MAT)	0.5	13	2	0.2	13	2
607' - 6"	0.3	53	1	0.3	54	4
610' - 0"	1.3	71	2	0.5	71	1
611' - 0"	0.5	128	1	0.3	128	2
<u>EAST-WEST WALLS</u>						
EW 1	0.3	618	2	0.1	618	1
EW 2	0.7	664	1	0.6	664	1
EW 3	1.4	685	1	0.1	685	3
<u>NORTH SOUTH WALLS</u>						
NS 1	0.4	311	1	0.2	311	4
NS 2	0.6	360	1	0.6	353	4
NS 3	0.6	428	1	0.4	428	1
NS 4	0.1	480	1	0.1	480	2

All concrete stresses are below the allowable stress of 3 ksi (concrete compressive stress at 28 days).

1. For Mat and Slabs: Direction 1 = NS, Direction 2 = EW
2. For Walls: Direction 1 = Horizontal, Direction 2 = Vertical
3. See Attachment A for Element Locations.
4. Load Combinations are defined in Section A.6.

3720 0193

TABLE A2 (Continued)

MAXIMUM CONCRETE STRESSES

LOCATION	DIRECTION 1			DIRECTION 2		
	CONC. STRESS (ksi)	ELEMENT ³⁾ NO.	LOAD ⁴⁾ COMB.	CONC. STRESS (ksi)	ELEMENT ³⁾ NO.	LOAD ⁴⁾ COMB.
<u>SUPPORT WALLS BELOW</u>						
NS 4	0.1	466	2	0.3	465	3
NS 5	0.1	503	2	0.8	503	3
NS 6	0.3	512	2	0.8	512	1
NS 7	0.3	518	2	1.5	526	1
NS 8	0.1	536	1	1.4	536	2
NS 9	0.2	545	3	1.4	545	3
NS 10	0.1	561	3	0.1	561	2
EW 4	0.1	686	2	1.2	686	2
EW 5	0.1	692	2	1.0	692	2
EW 6	0.1	705	3	1.2	705	1
EW 7	0.1	715	3	0.7	715	3
EW 8	0.1	718	3	0.9	718	3
EW 9	0.1	720	2	0.5	720	2
EW 3	0.1	677	3	1.0	677	3

All concrete stresses are below the allowable stress of 3 ksi (concrete compressive stress at 28 days).

1. For Mat and Slabs: Direction 1 = NS, Direction 2 = EW
2. For Walls: Direction 1 = Horizontal, Direction 2 = Vertical
3. See Attachment A for Element Locations.
4. Load Combinations are defined in Section A.6.

LIST OF FIGURES

<u>FIGURE</u>	<u>TITLE</u>
B-1	Plan at El. 590 ft
B-2	Plan at El. 611 ft
B-3	Section A-A - El. 590 ft to 696 ft
B-4	Section B-B - El. 590 ft to 649 ft
B-5	Section C-C - El. 590 ft to 649 ft
B-6	Section F-F - El. 590 ft to 649 ft
B-7	Section H-H - El. 590 ft to 649 ft
D-1	Perspective View - El. 590 ft thru 602 ft
D-2	Perspective View - El. 602 ft thru 611 ft
D-3	Perspective View - El. 611 ft thru 649 ft
D-4	Foundation Mat at El. 590 ft
D-5	Slab at El. 602 ft
D-6	Slab at El. 607.6 ft
D-7	Slab at El. 610 ft
D-8	Slab at El. 611 ft
D-9	Slab at El. 622 ft
D-10	Slab at El. 634 ft
D-11	North/South Wall 1
D-12	North/South Wall 2
D-13	North/South Wall 3
D-14	North/South Wall 4
D-15	North/South Wall 5
D-16	North/South Wall 6
D-17	North/South Wall 7
D-18	North/South Wall 8
D-19	North/South Wall 9
D-20	North/South Wall 10
D-21	East/West Wall 1
D-22	East/West Wall 1A
D-23	East/West Wall 2
D-24	East/West Wall 2A
D-25	East/West Wall 3
D-26	East/West Wall 4
D-27	East/West Wall 5
D-28	East/West Wall 6
D-29	East/West Wall 7
D-30	East/West Wall 8
D-31	East/West Wall 9

3 7 2 0

3720 201

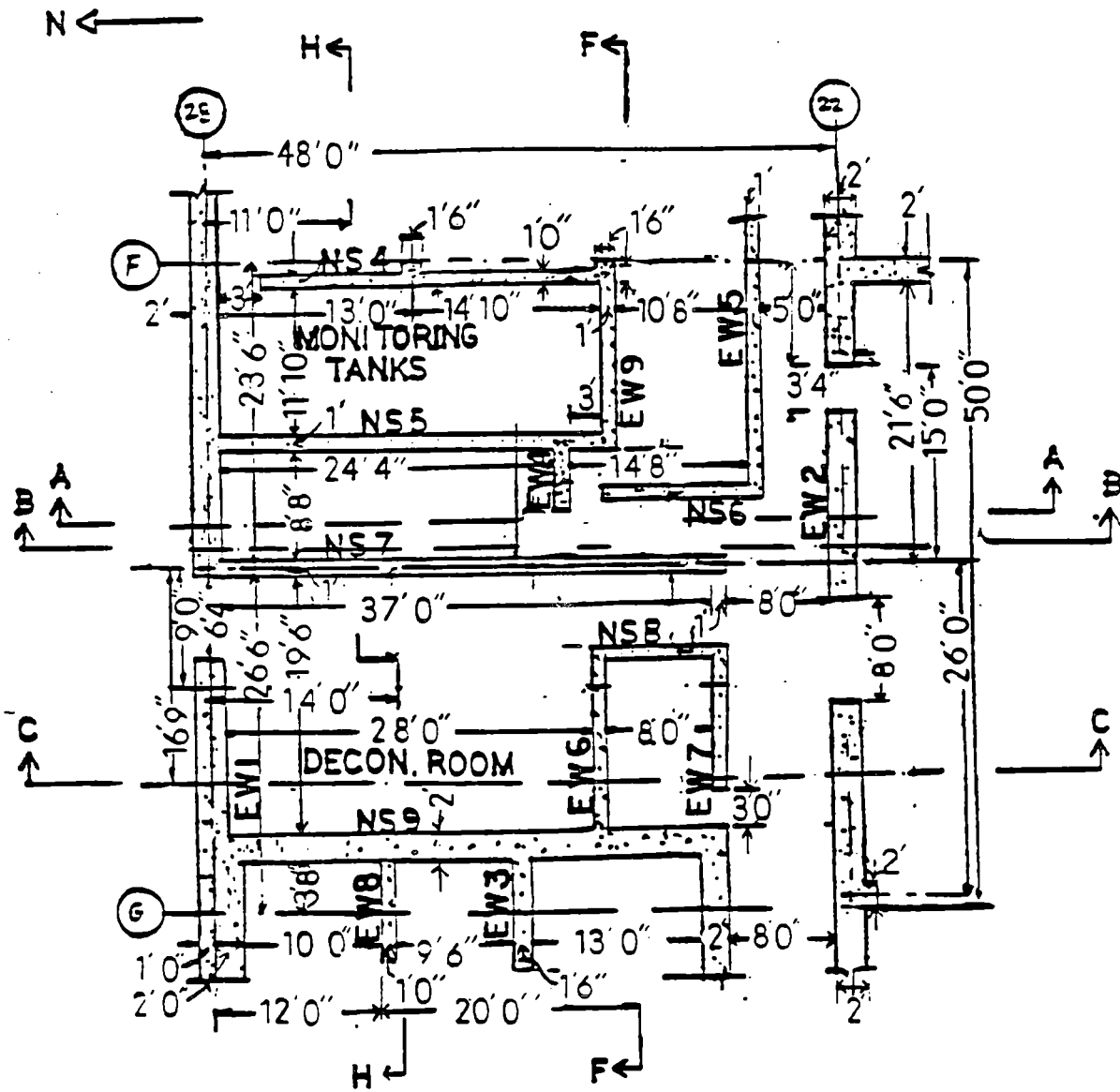


FIGURE B-1: PLAN AT EL. 590 FT

202

3720

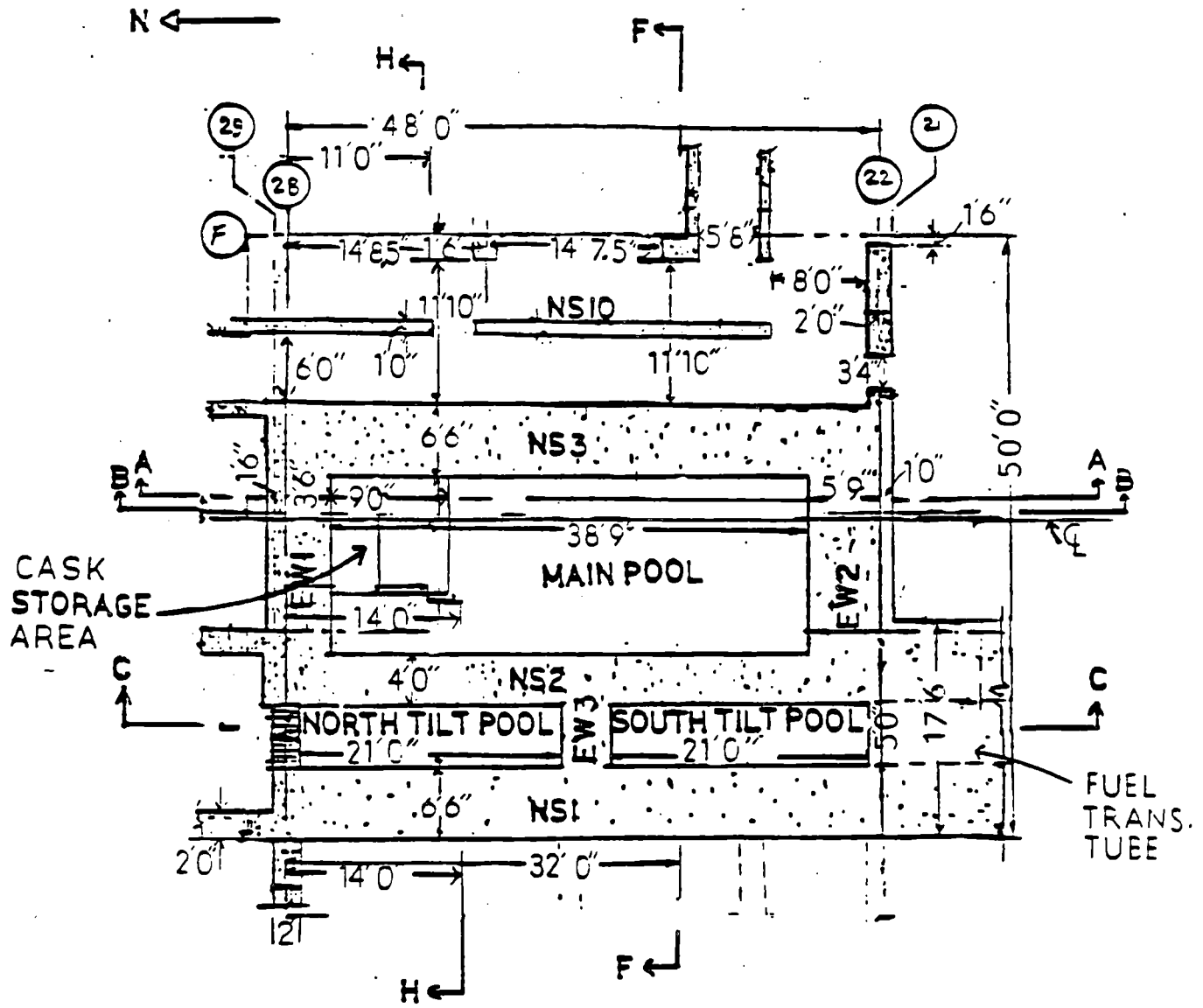


FIGURE B-2: PLAN AT EL. 611 FT

3 7 2 0 2 0 3

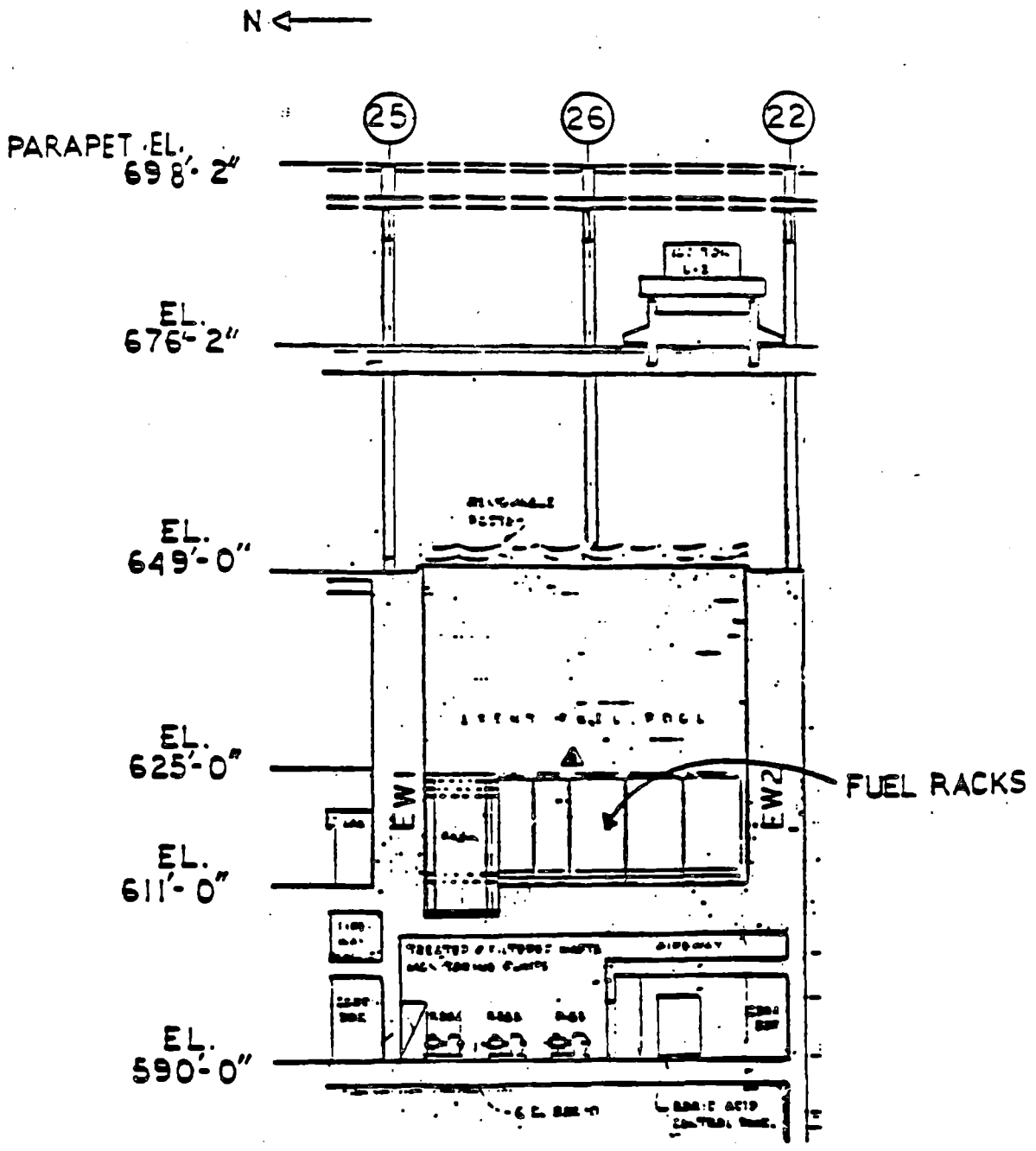


FIGURE B-3: SECTION A-A - EL 590 FT TO 696 FT

3 7 2 0
2 0 5

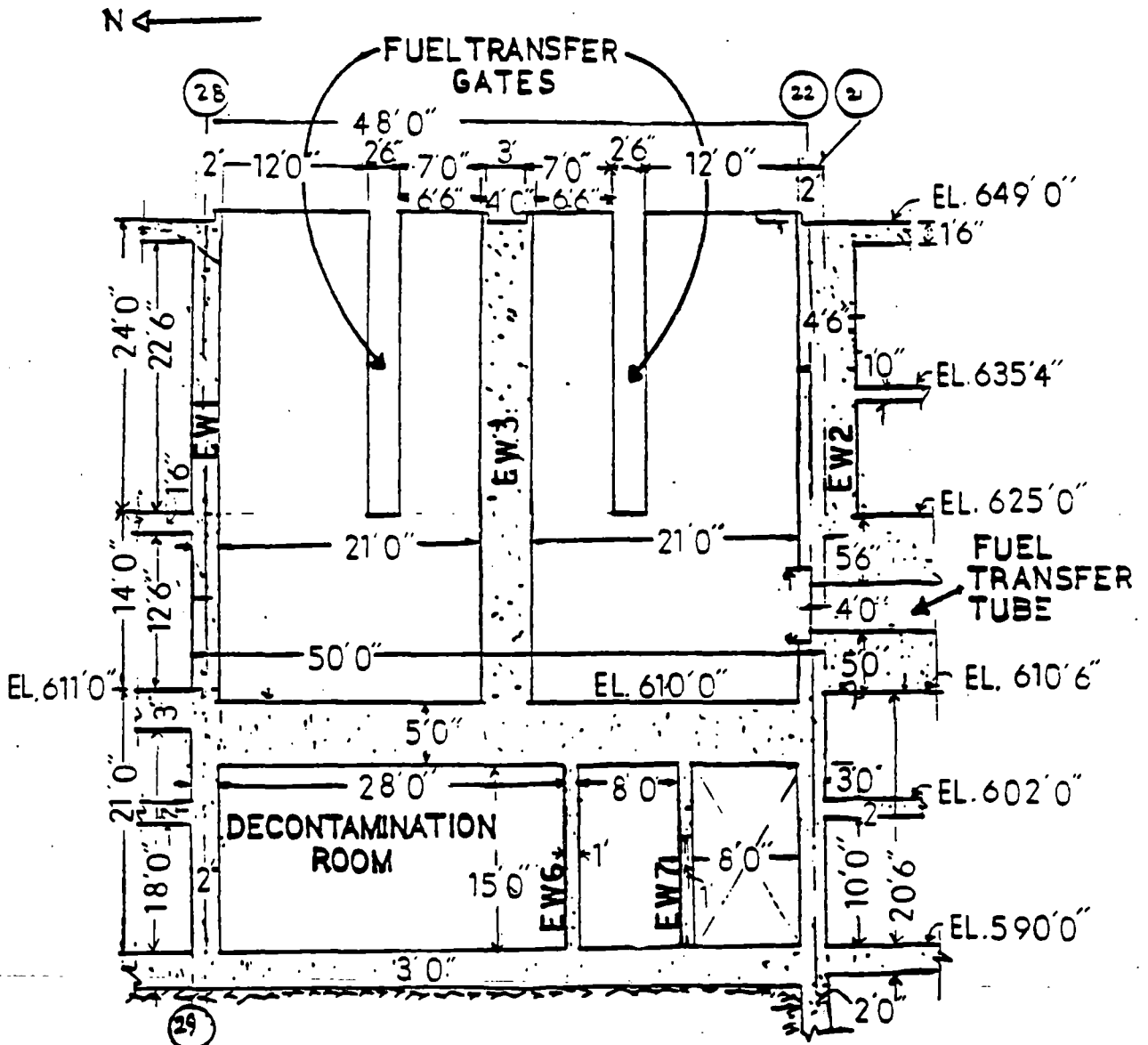


FIGURE B-5: SECTION C-C - EL. 590 FT TO 649 FT

3720 206

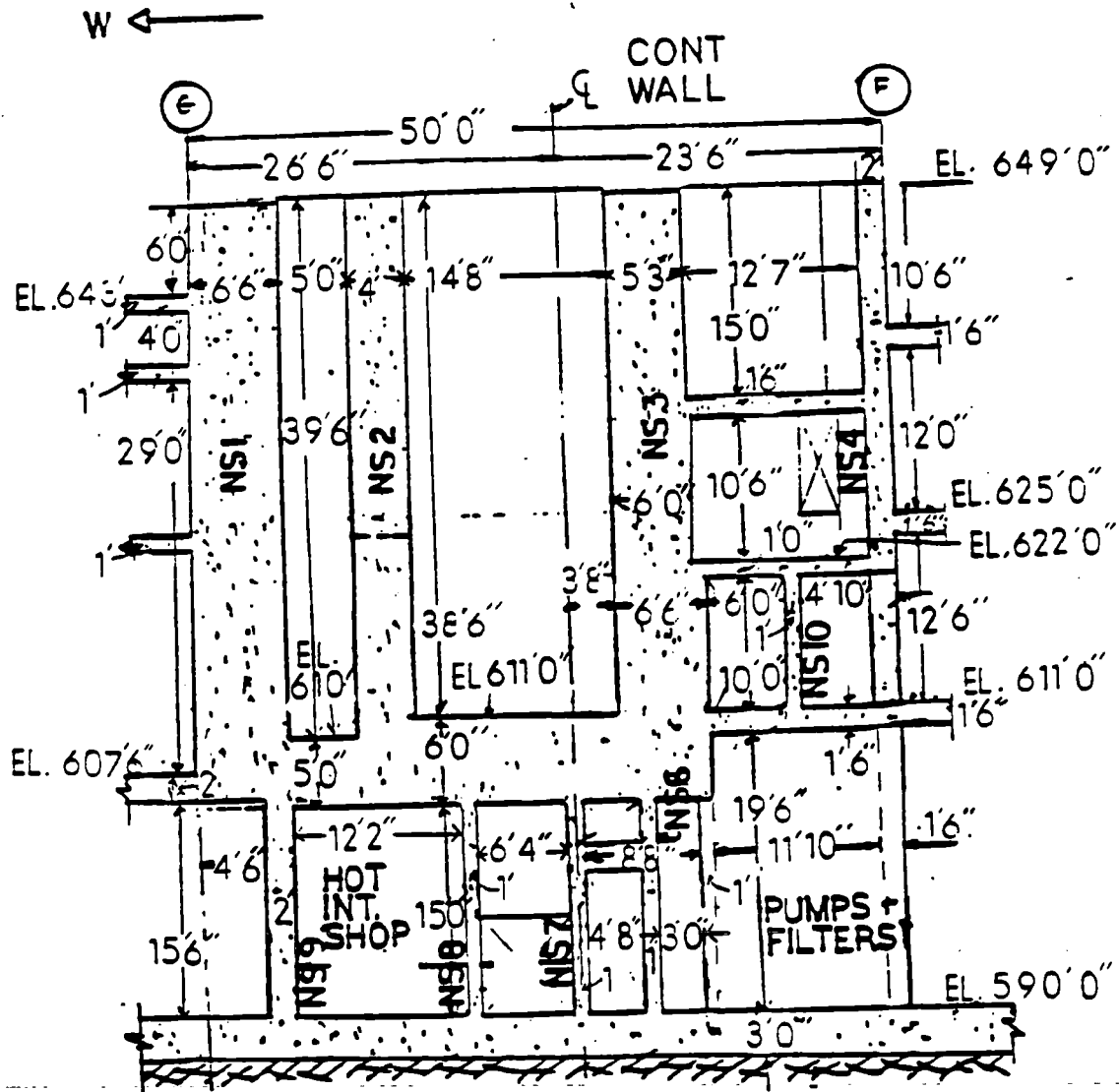


FIGURE B-6: SECTION F-F - EL. 590 FT TO 649 FT

3720 207

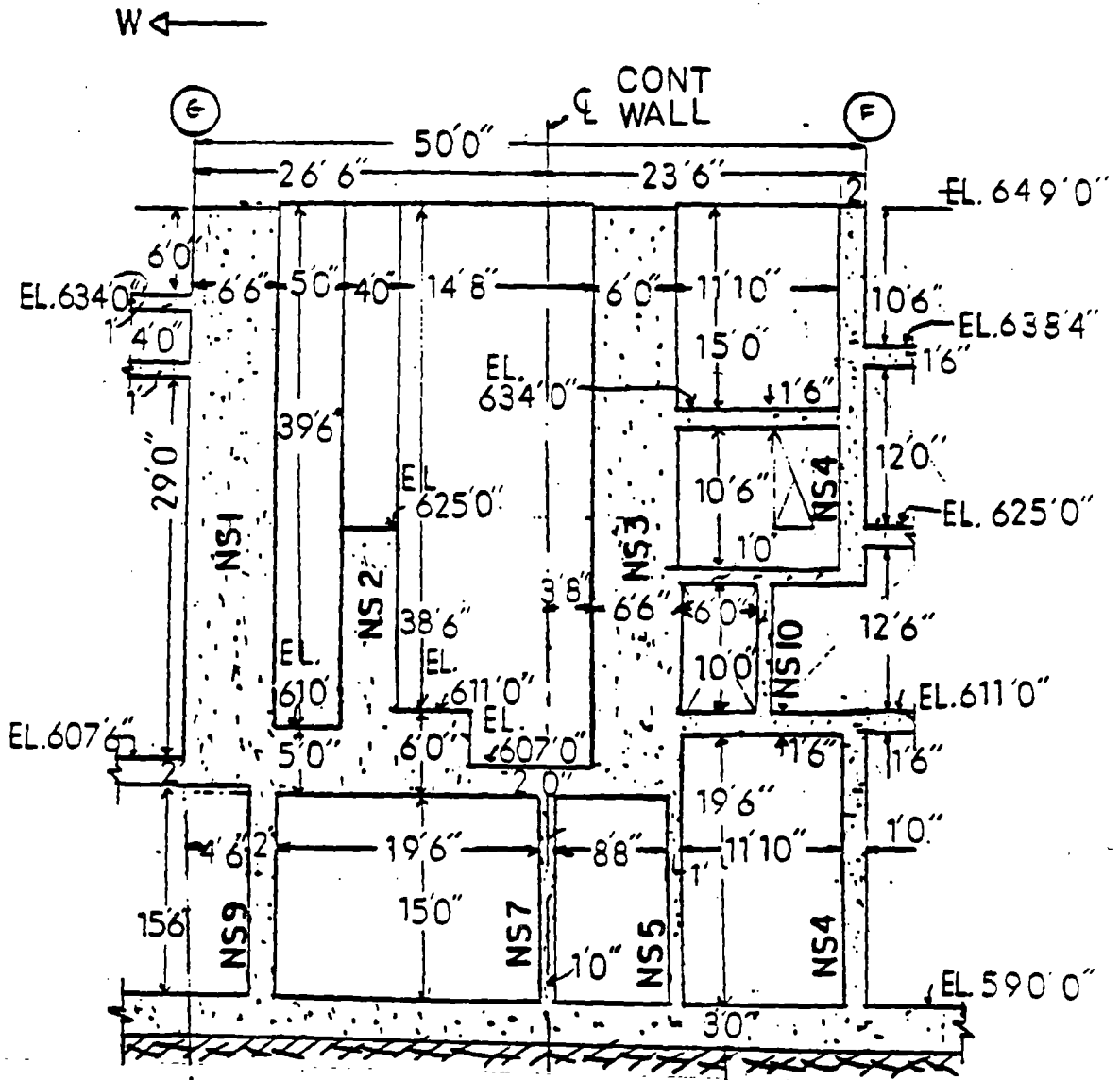


FIGURE B-7: SECTION H-H - EL. 590 FT TO 649 FT

3720 203

PERSPECTIVE VIEW 1 OF 590 THRU 602

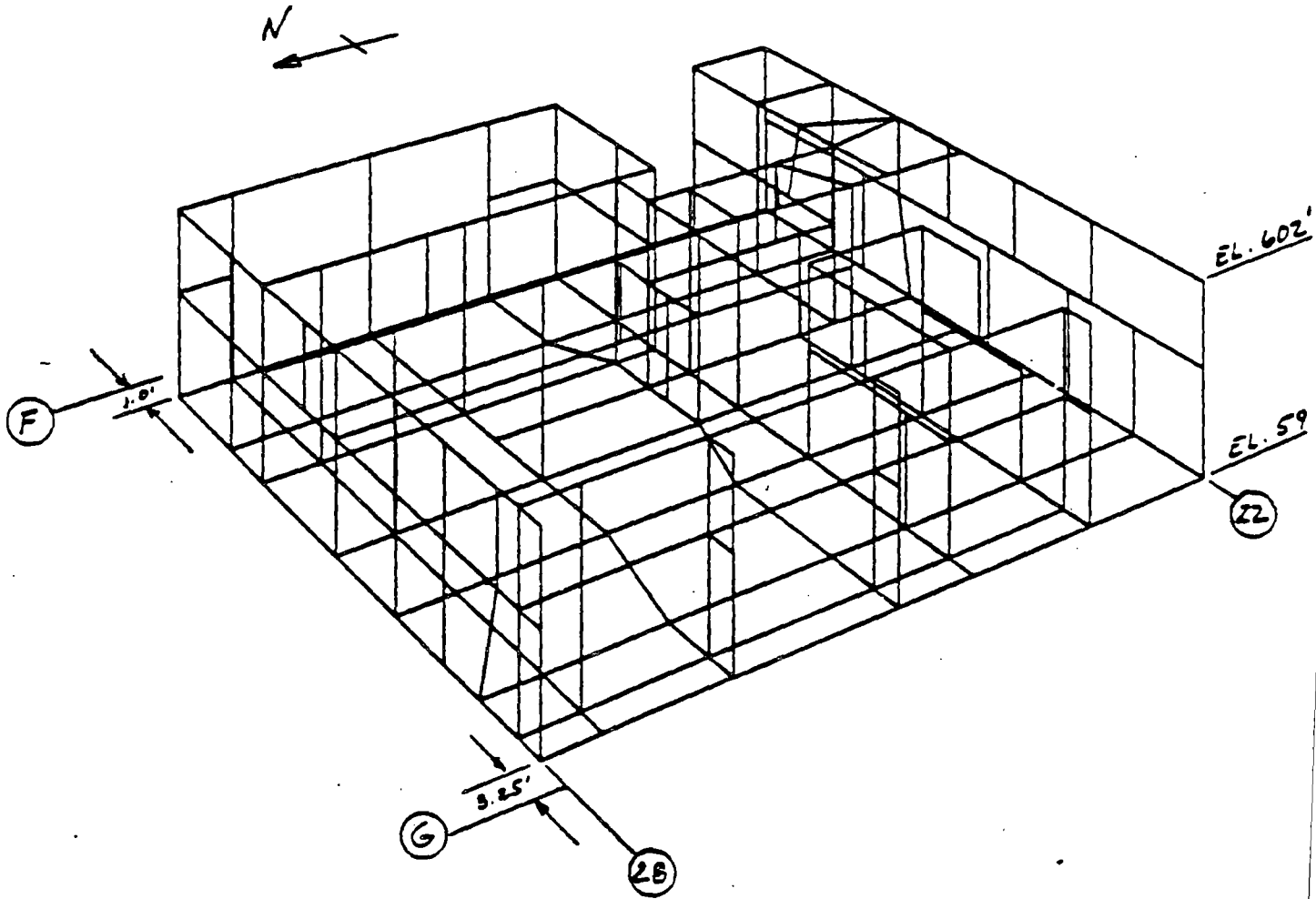
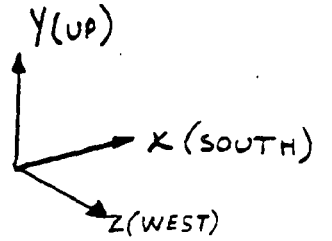
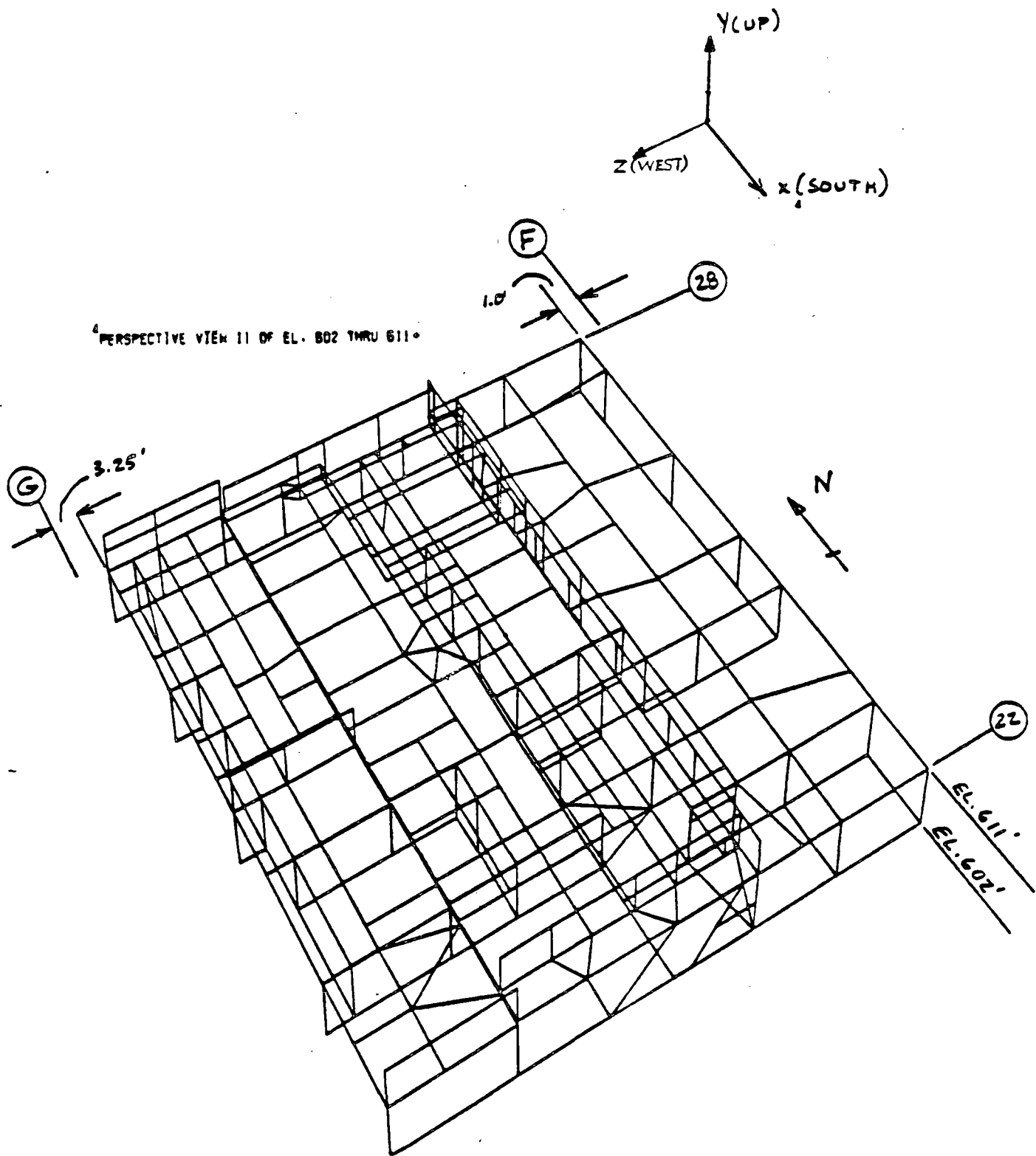


FIGURE D-1: PERSPECTIVE VIEW - EL. 590 FT. THRU 602 FT.

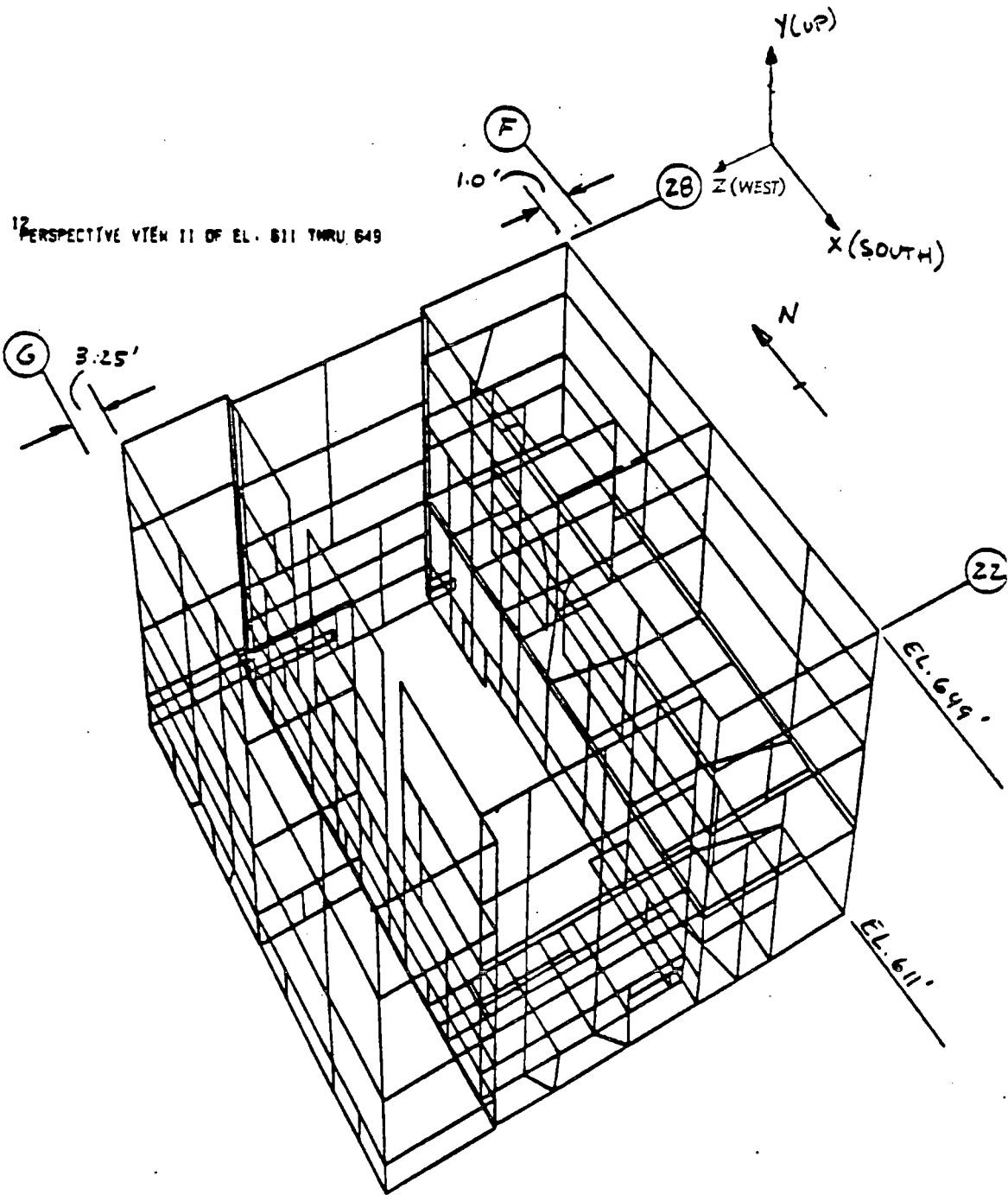
3720 209



PERSPECTIVE VIEW II OF EL. 602 THRU 611

FIGURE D-2: PERSPECTIVE VIEW - EL. 602 FT. THRU 611 FT.

3720 210



NOT TO SCALE EXCEPT SIZE: SEE VETC

FIGURE-D-3: PERSPECTIVE VIEW - EL. 611 FT THRU 649 FT.

3 7 2 0 2 1 1

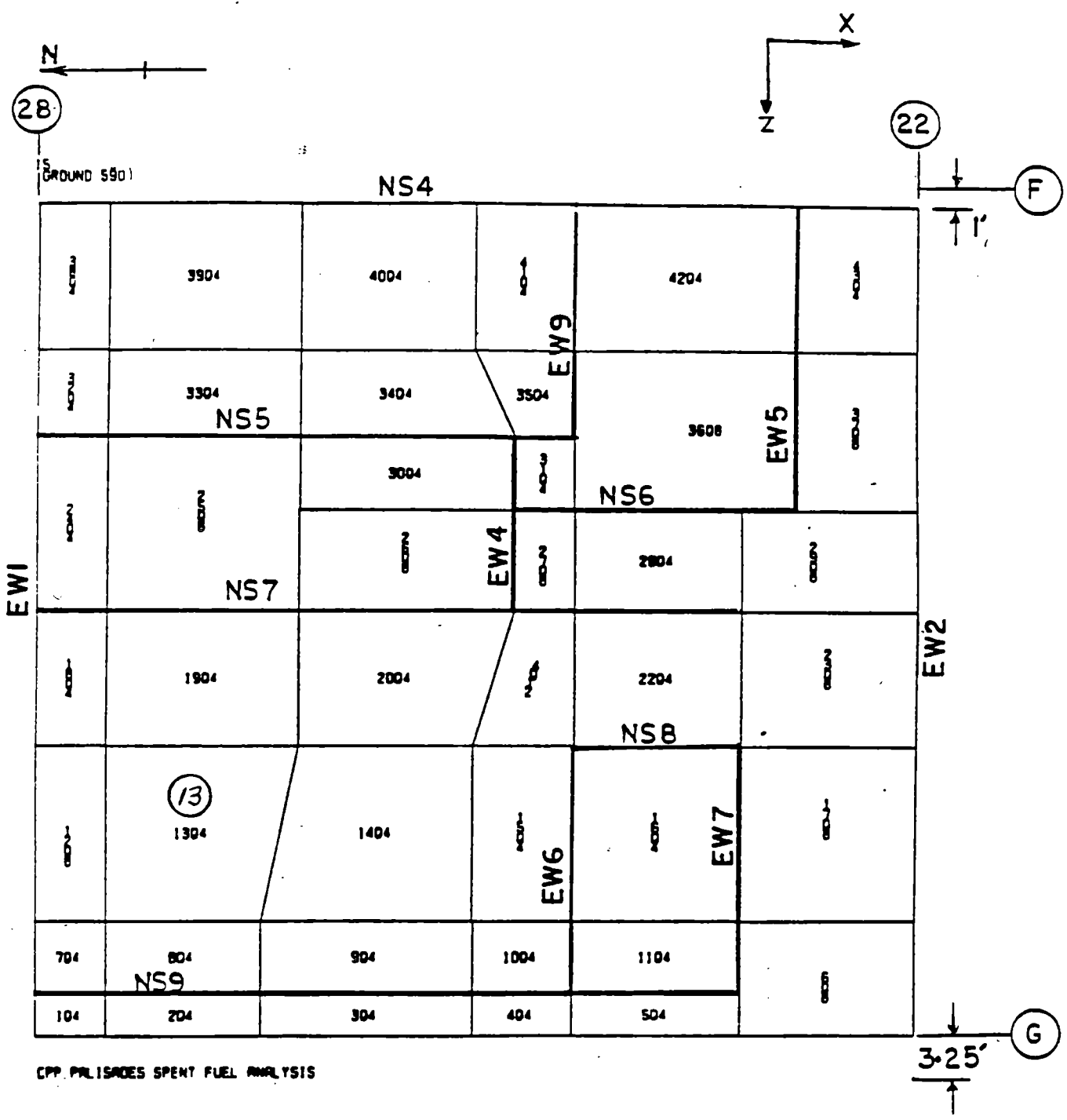
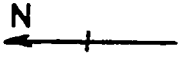
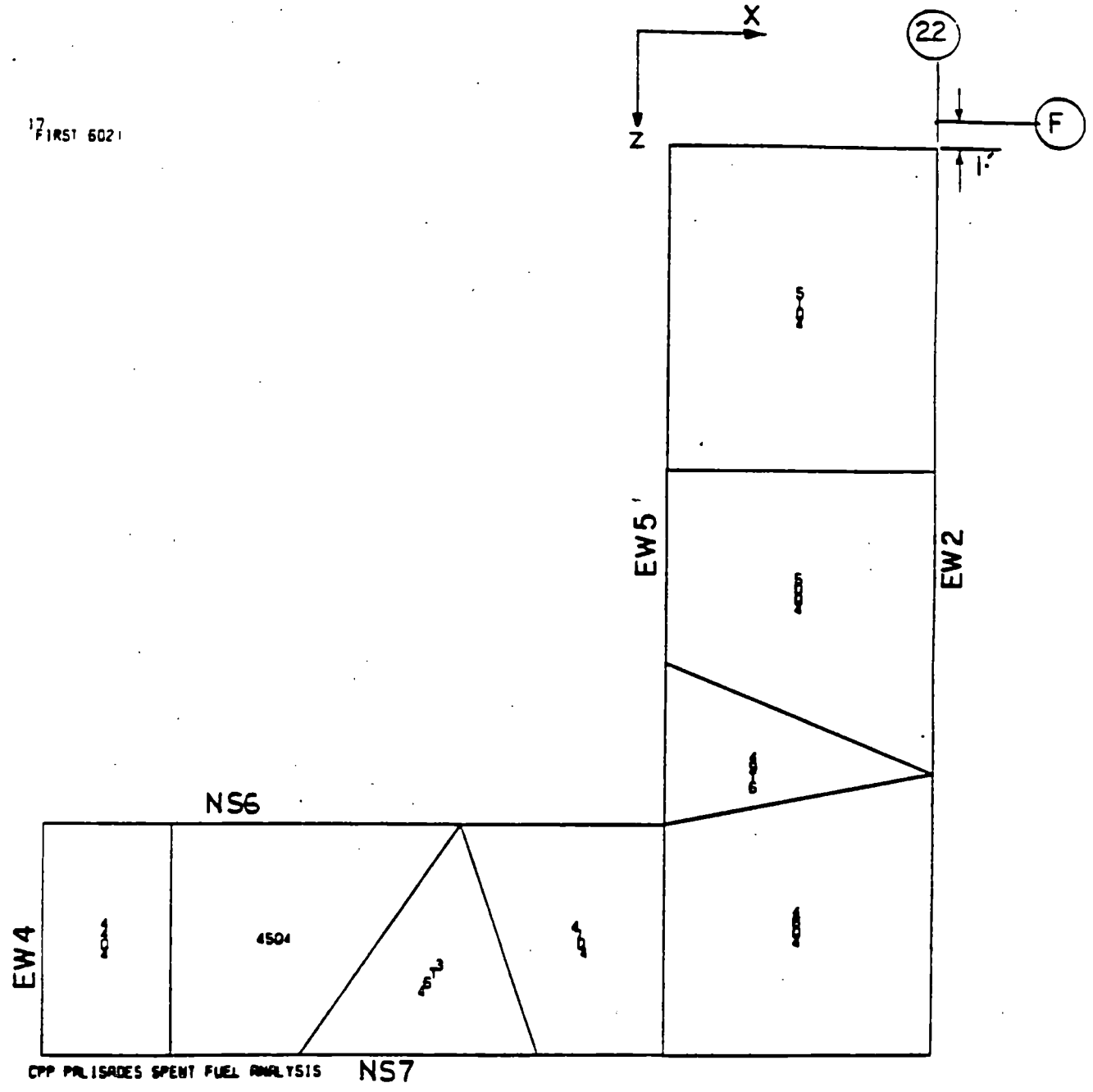


FIGURE D-4: FOUNDATION MAT AT EL. 590 FT.



17
FIRST 6021

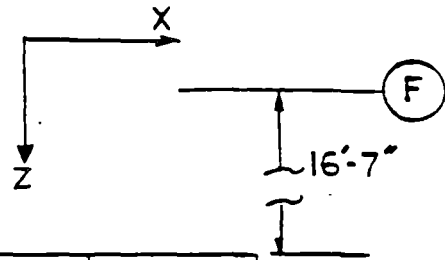
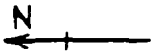


Note:

Structural slab not adjacent to spent fuel pool region. The reinforcement and concrete stresses in this slab are less than the allowables.

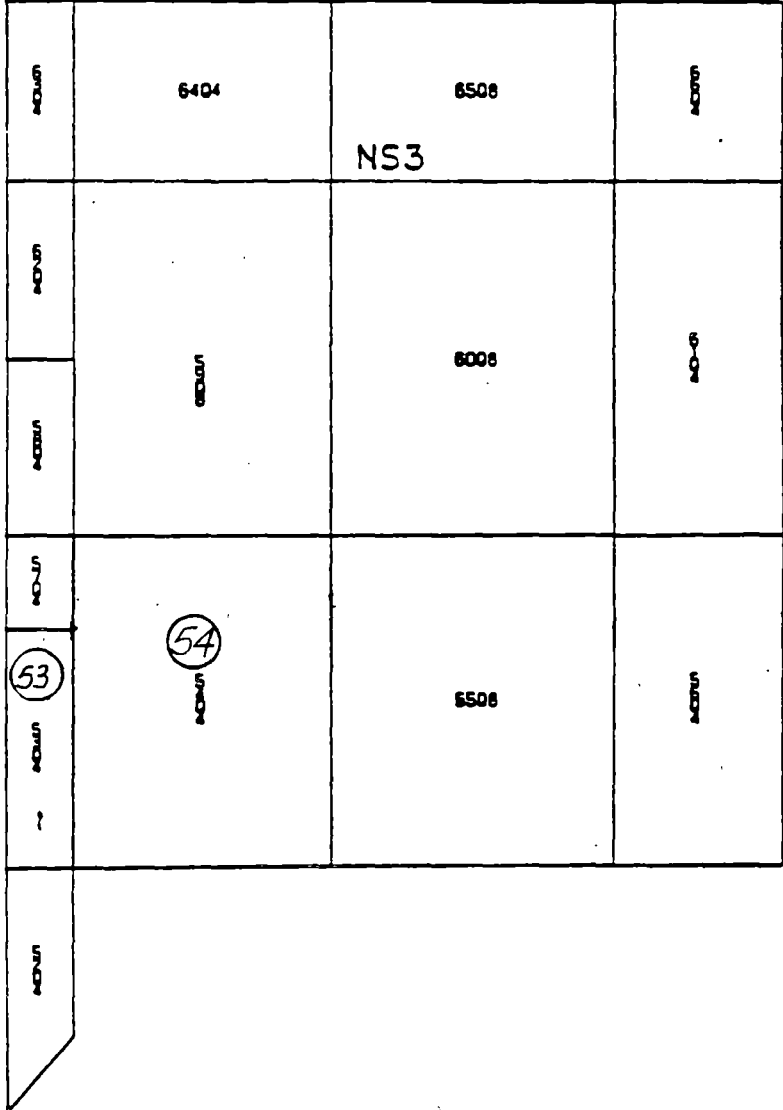
FIGURE D-5: SLAB AT EL. 602 FT.

3 7 2 0
0 2 1 2



(28)

1st SECOND 607.51



PPP PW ISADES SPENT FUEL ANALYSIS

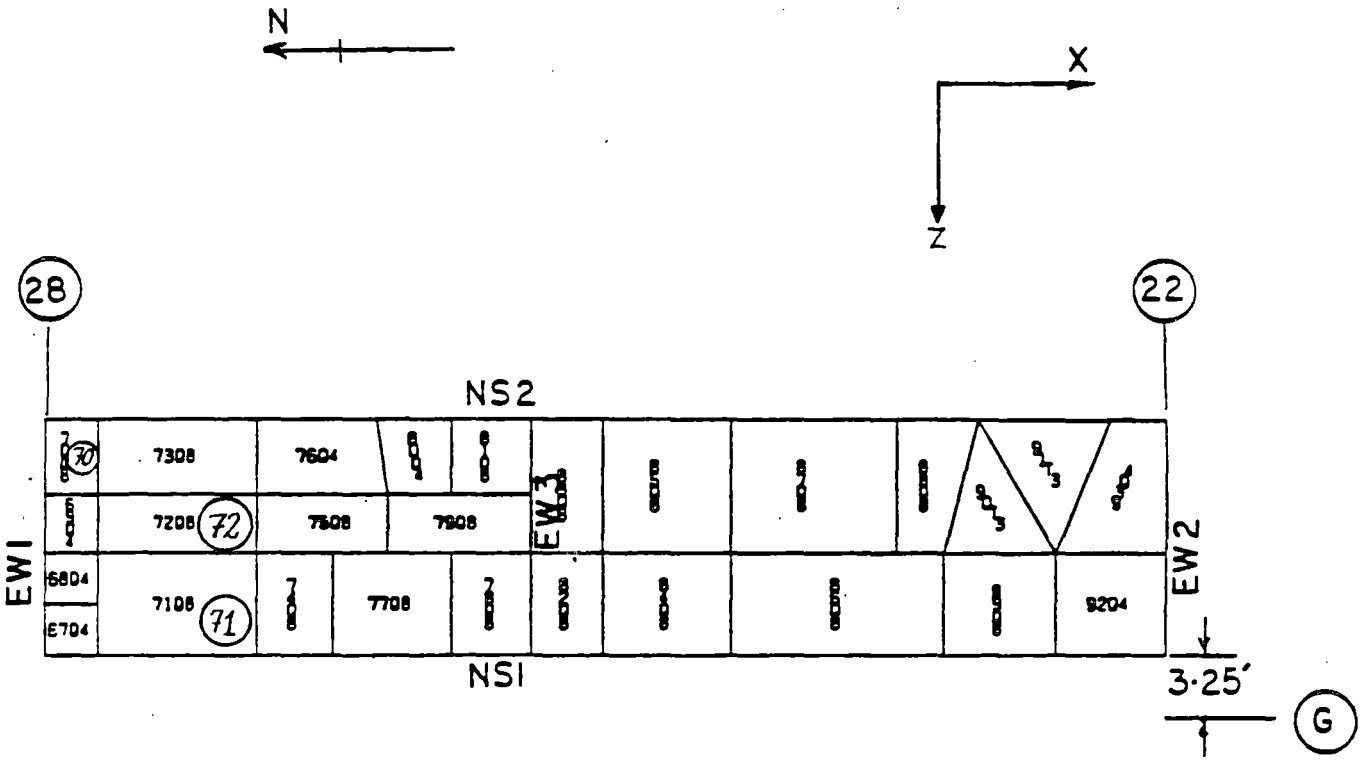
3 7 2 0
2 1 3

FIGURE D-6: SLAB AT EL. 607.5 FT.

214

3720

21 MIRD 6101



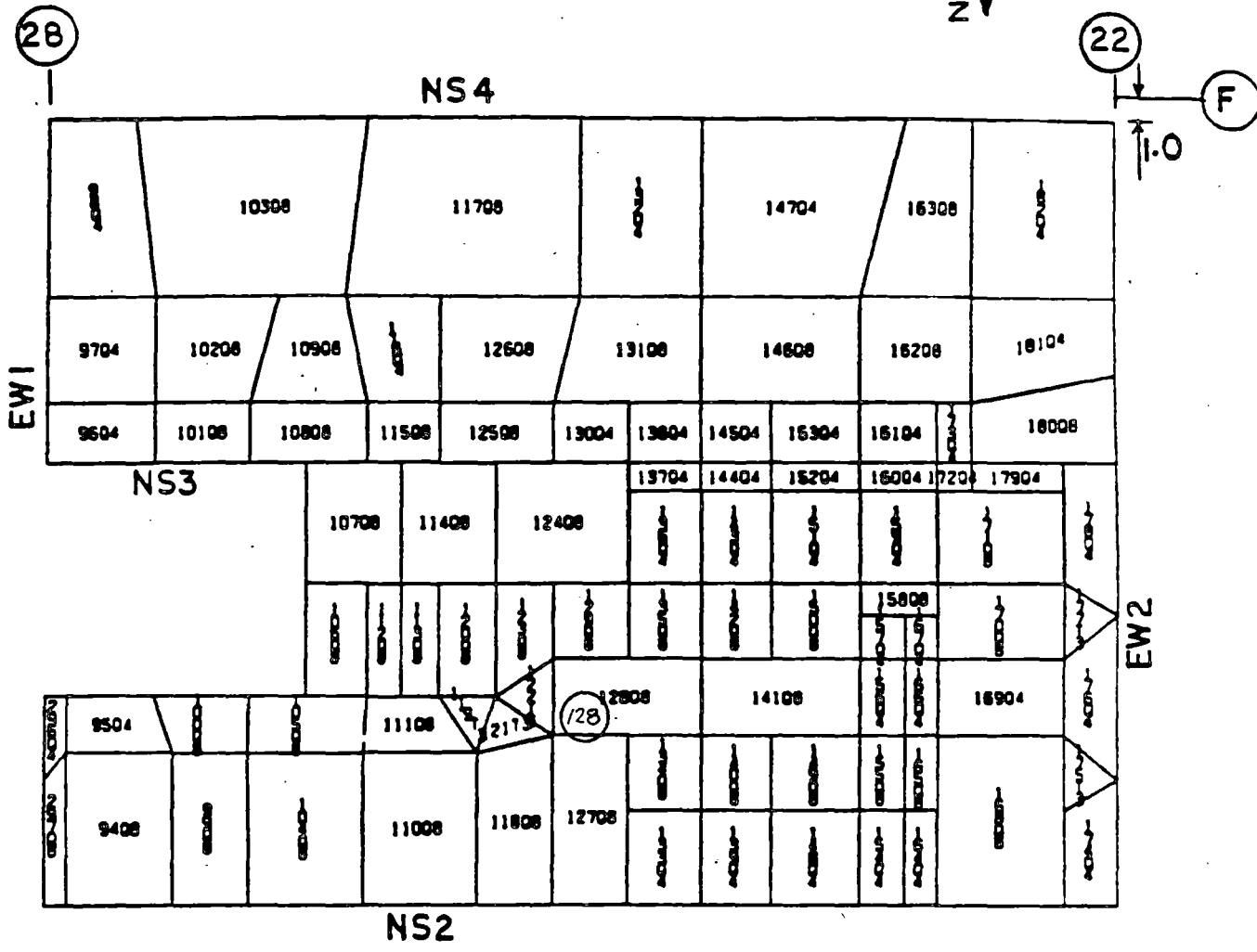
CPP_PALISADES_SPEMI_FUEL ANALYSIS

FIGURE D-7: SLAB AT EL. 610 FT.



FOURTH 6111

23



CPP PALISADES SPENT FUEL ANALYSIS

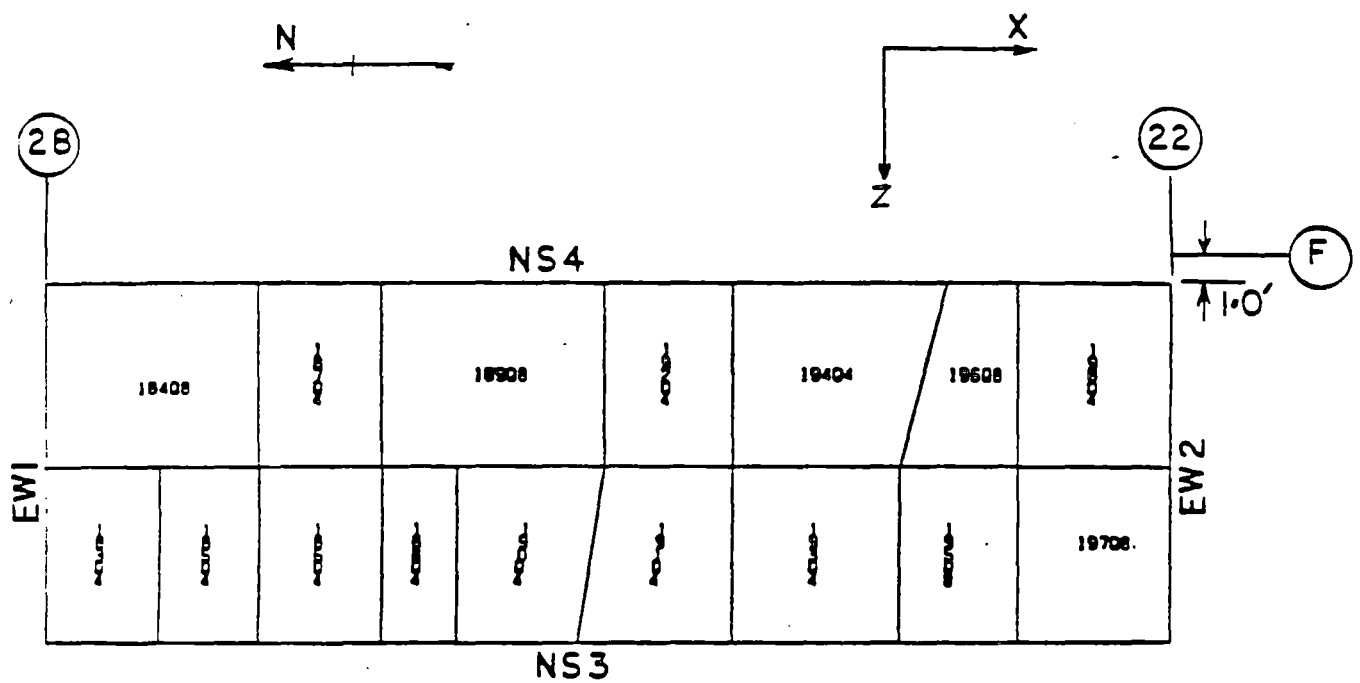
FOURTH 6111 9/19/83

24

FIGURE D-8: SLAB AT EL. 611 FT.

3720 0.215

25
FJETH 6221



Note:

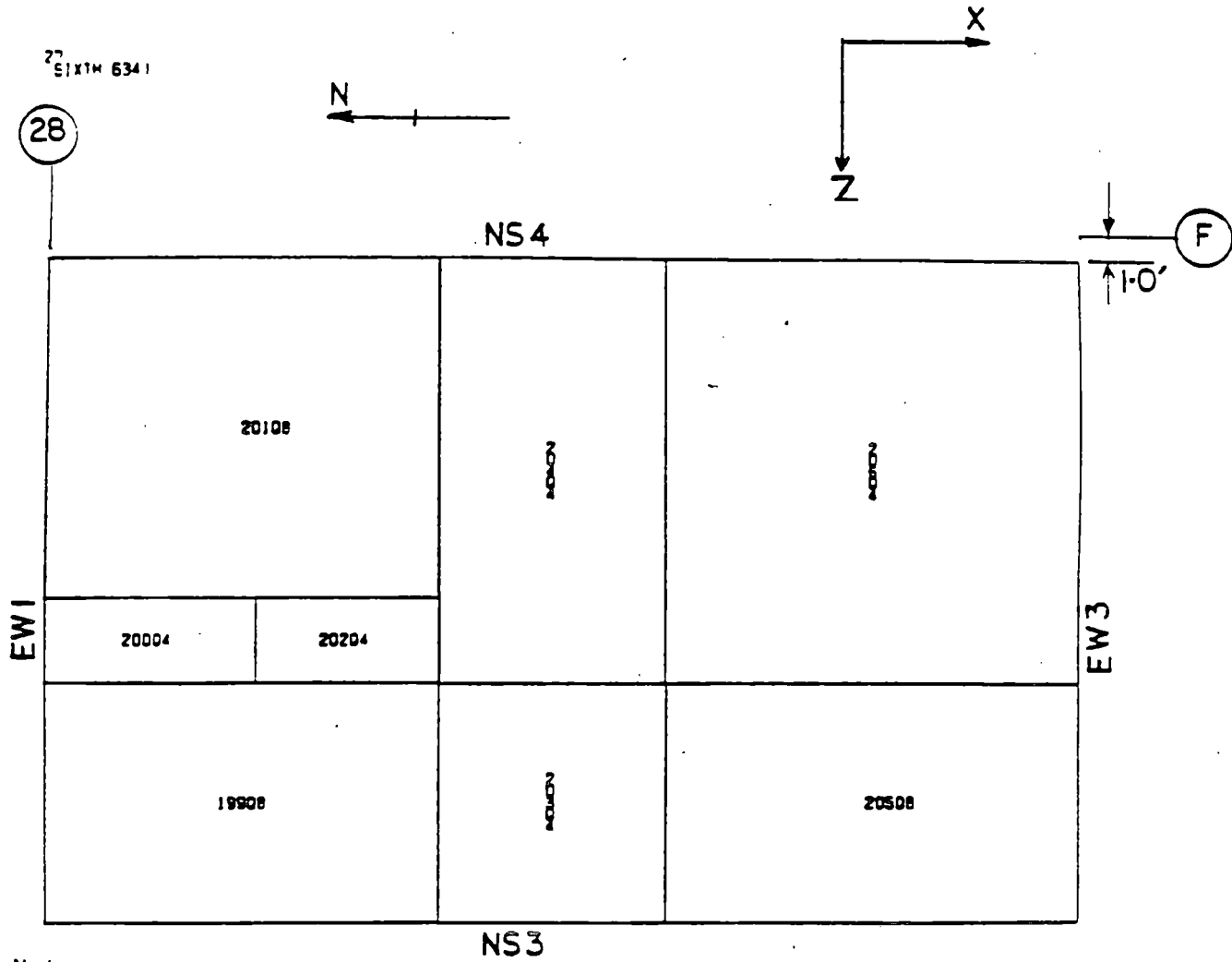
Structural slab not adjacent to spent fuel pool region. The reinforcement and concrete stresses in this slab are less than the allowables.

CPP, PRL, SADES, SPEVI, FUEL ANALYSIS

FIGURE D-9: SLAB AT EL. 622 FT.

3720 216

3720 217



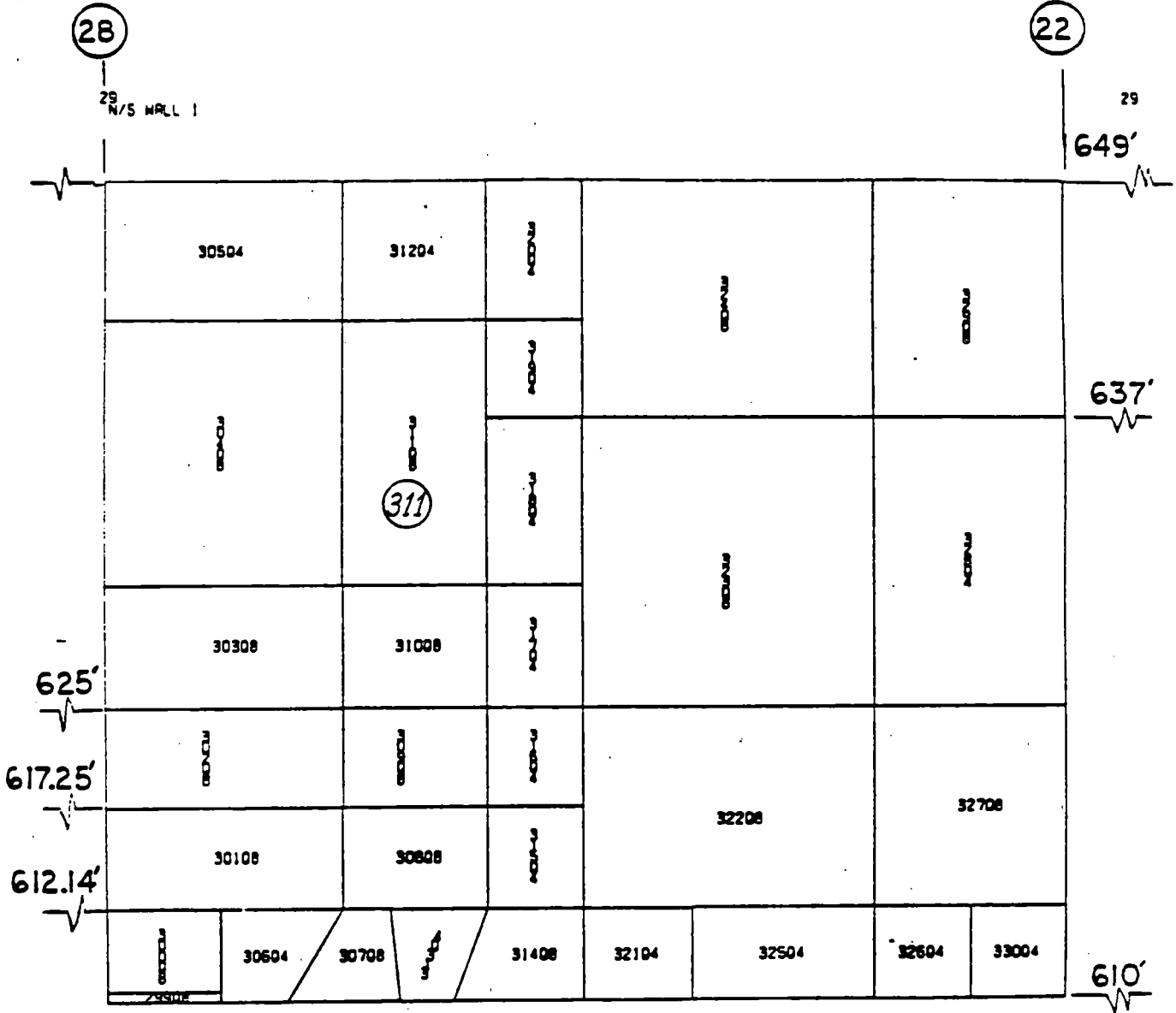
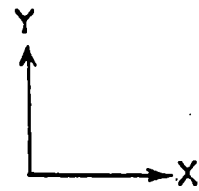
Note:

Structural slab not adjacent to spent fuel pool region. The reinforcement and concrete stresses in this slab are less than the allowables.

CPP_PALISADES_SPENT_FUEL_ANALYSIS

FIGURE D-10: SLAB AT EL. 634 FT.

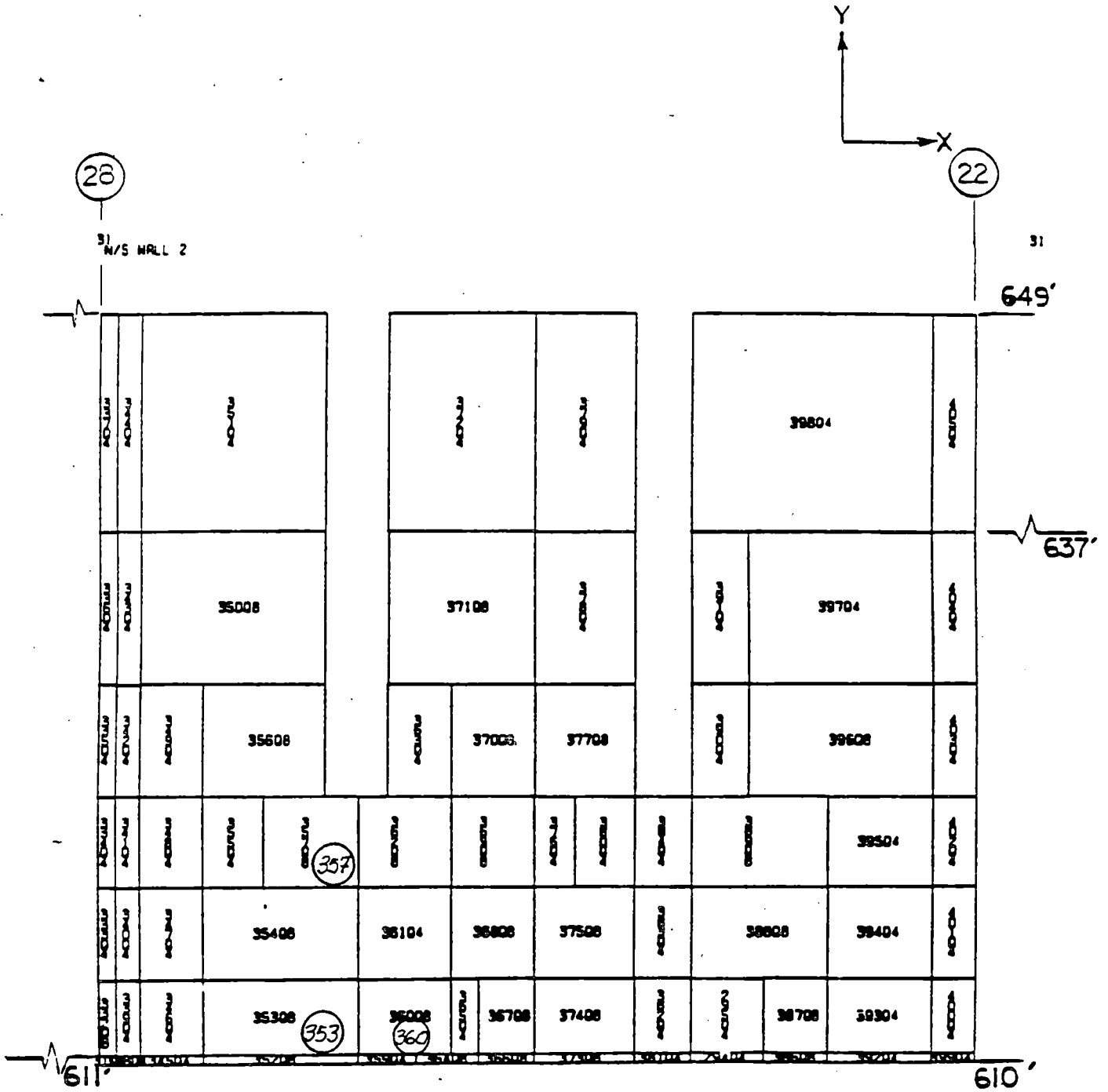
3720 218



CPP PALISADES SPENT FUEL ANALYSIS

FIGURE D-11: NORTH/SOUTH WALL 1

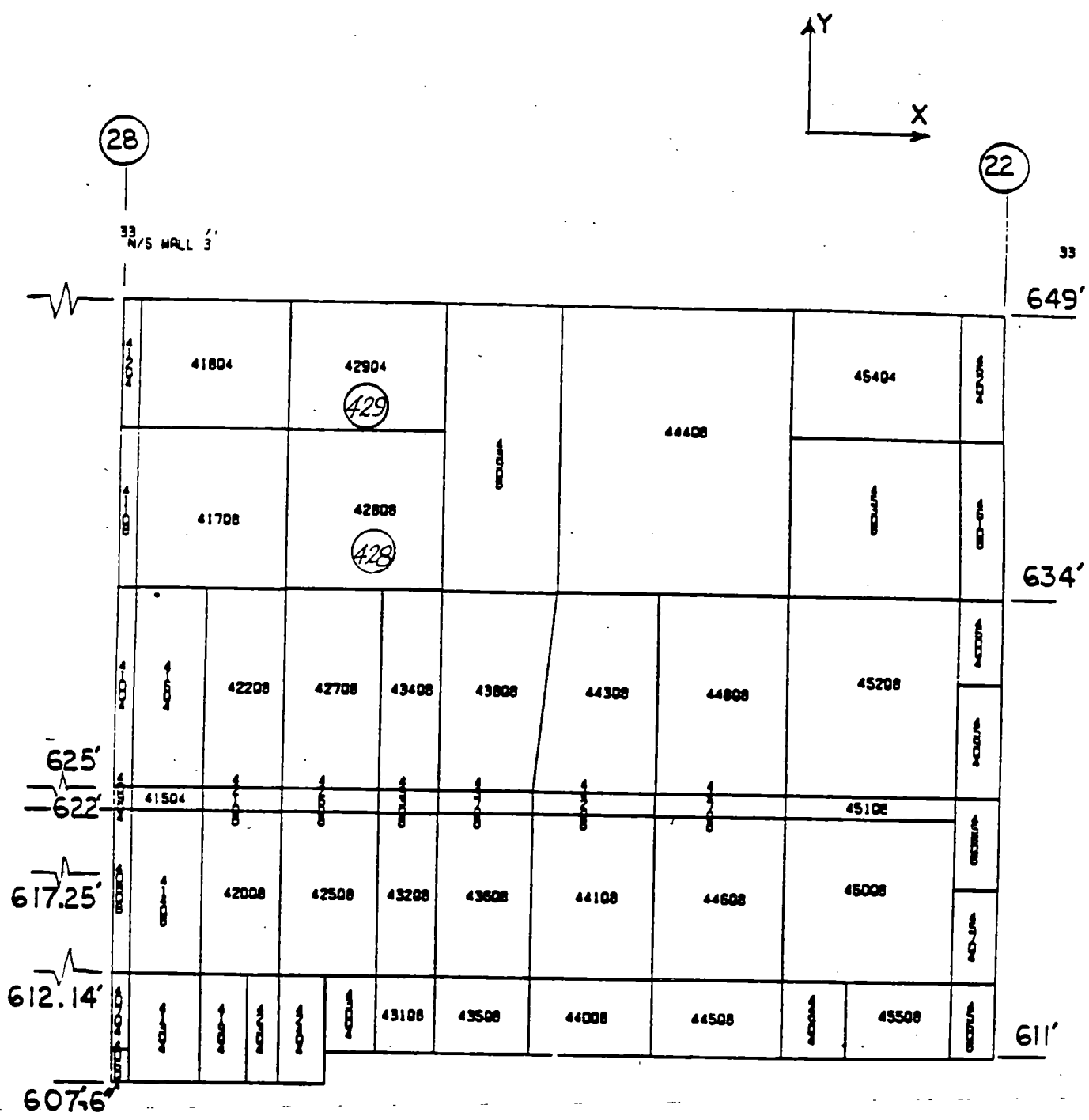
3720 219



CPP PRLISADES SPENT FUEL ANALYSIS

FIGURE D-12: NORTH/SOUTH WALL 2

3 7 2 0
2 2 0



CPP PALISADES SPENT FUEL ANALYSIS

FIGURE D-13: NORTH/SOUTH WALL 3

3720
0221

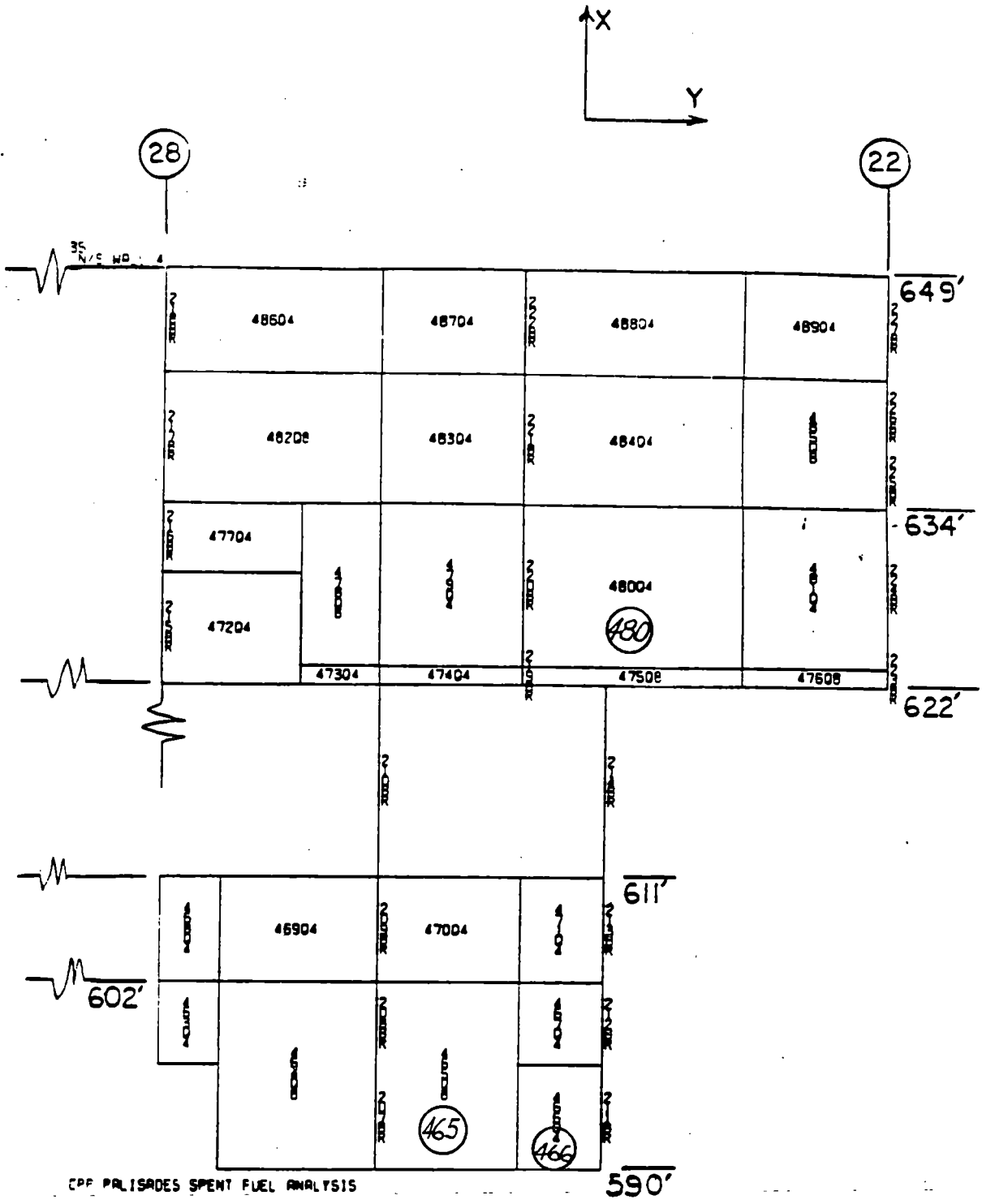
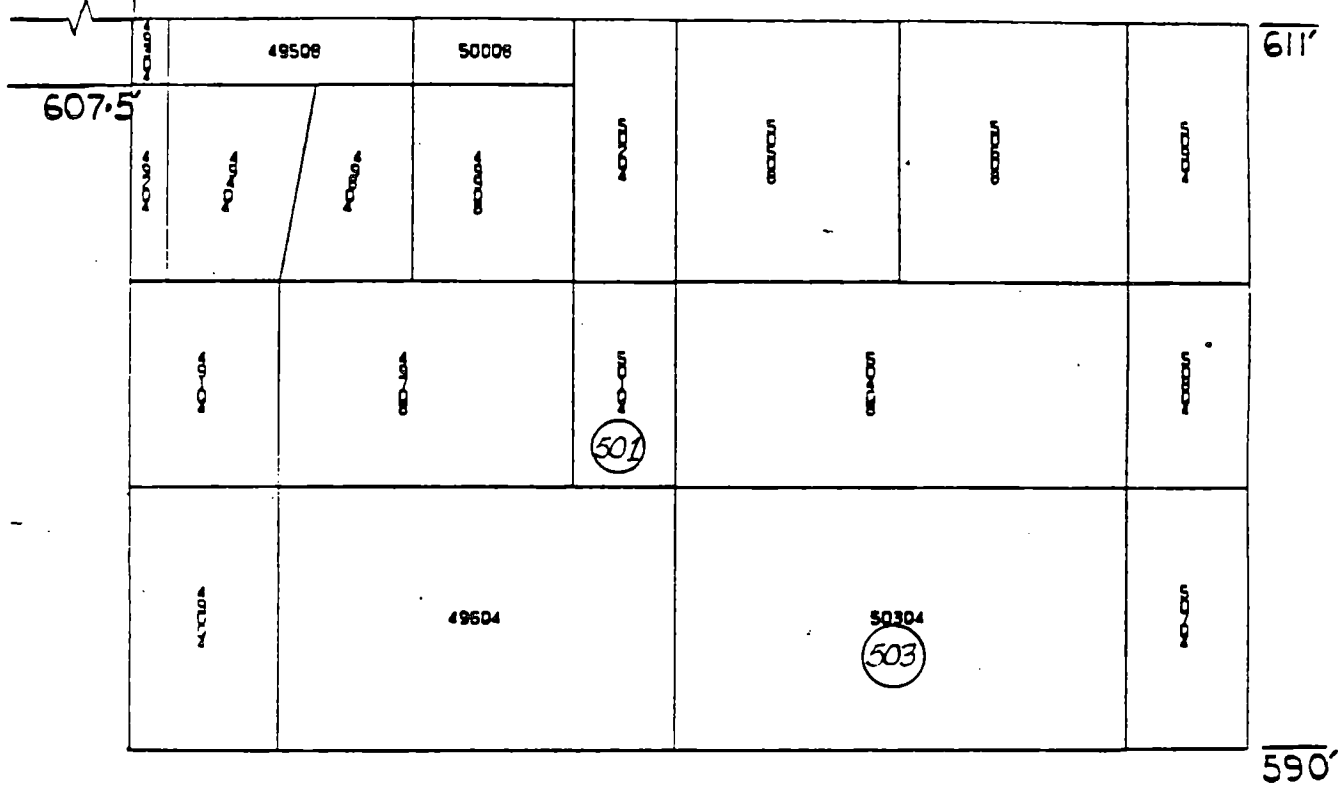
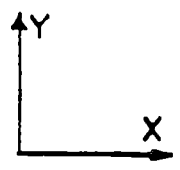


FIGURE D-14: NORTH/SOUTH WALL 4

37
N/S WALL 5

(28)



CPP PALISADES SPENT FUEL ANALYSIS

FIGURE D-15: NORTH/SOUTH WALL 5

3 7 2 0
2 2 2 2

3 7 2 0
0 2 2 3

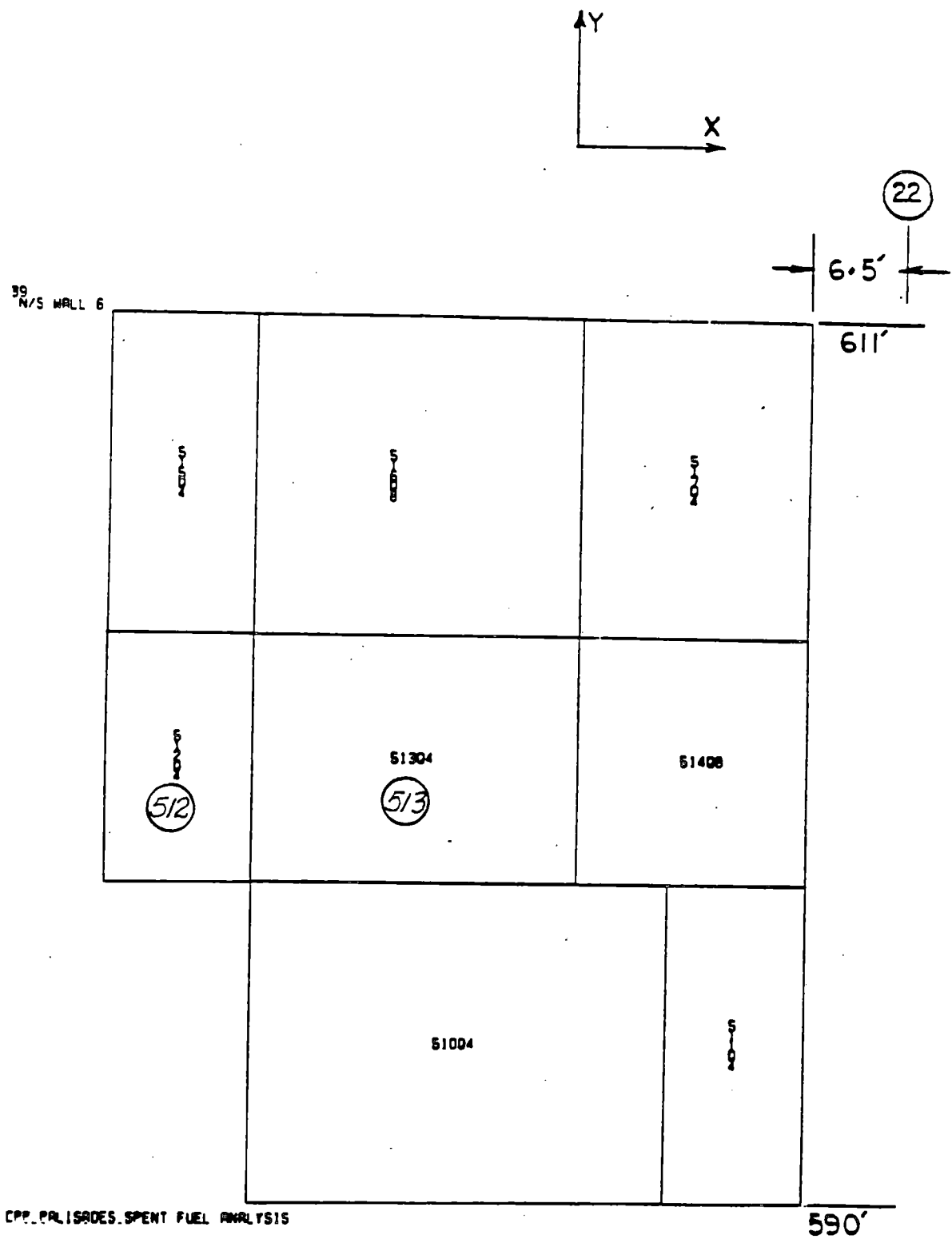
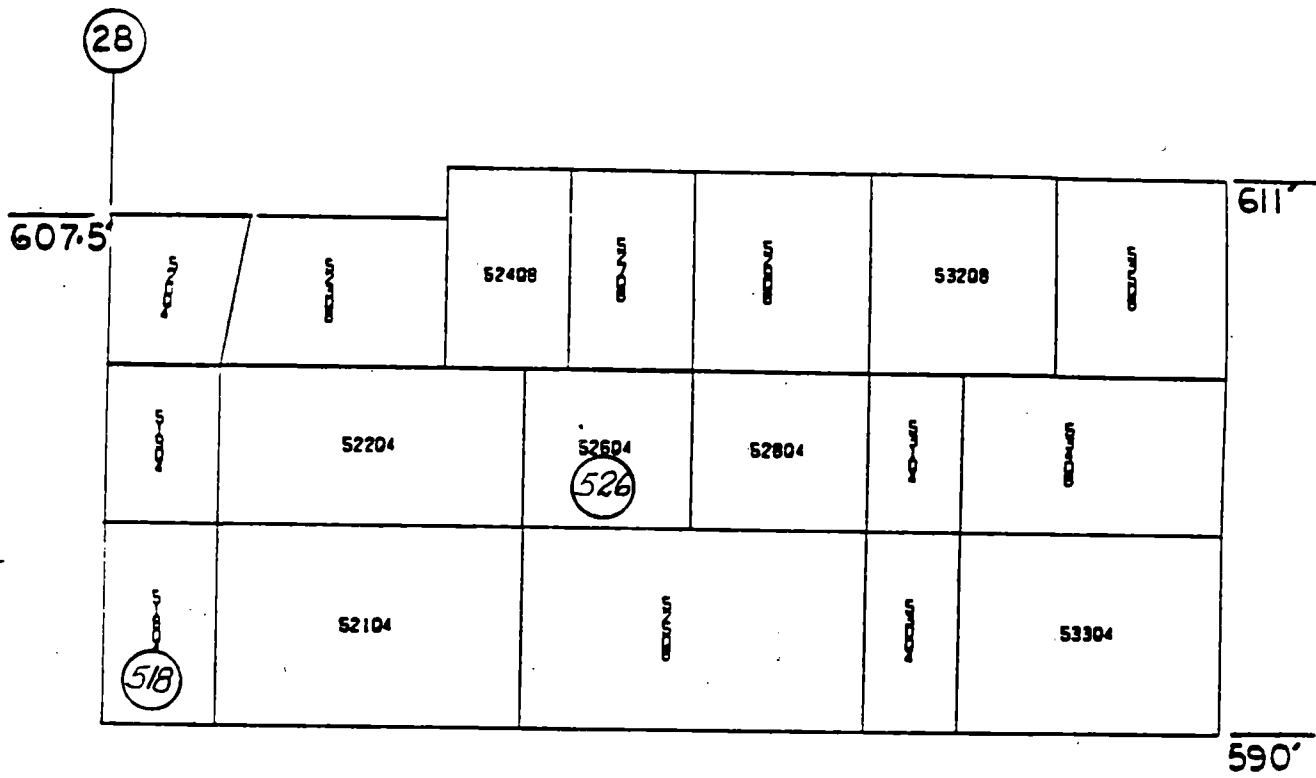


FIGURE D-16: NORTH/SOUTH WALL 6

3 7 2 0
0 2 2 4

N/S WALL 7

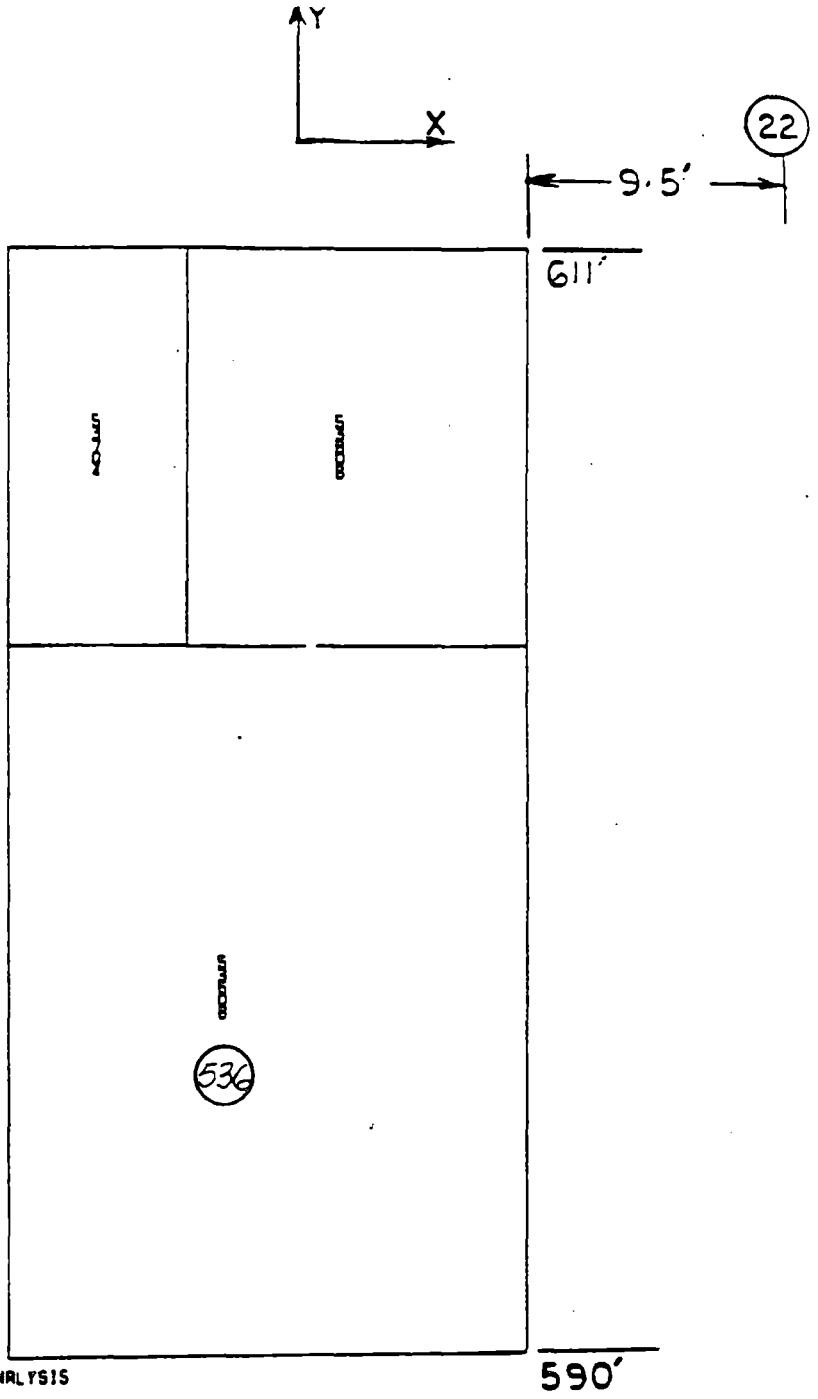


EPP PALISADES SPENT FUEL ANALYSIS

FIGURE D-17: NORTH/SOUTH WALL 7

3720
225

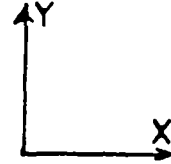
⁴³
N/S WALL 8



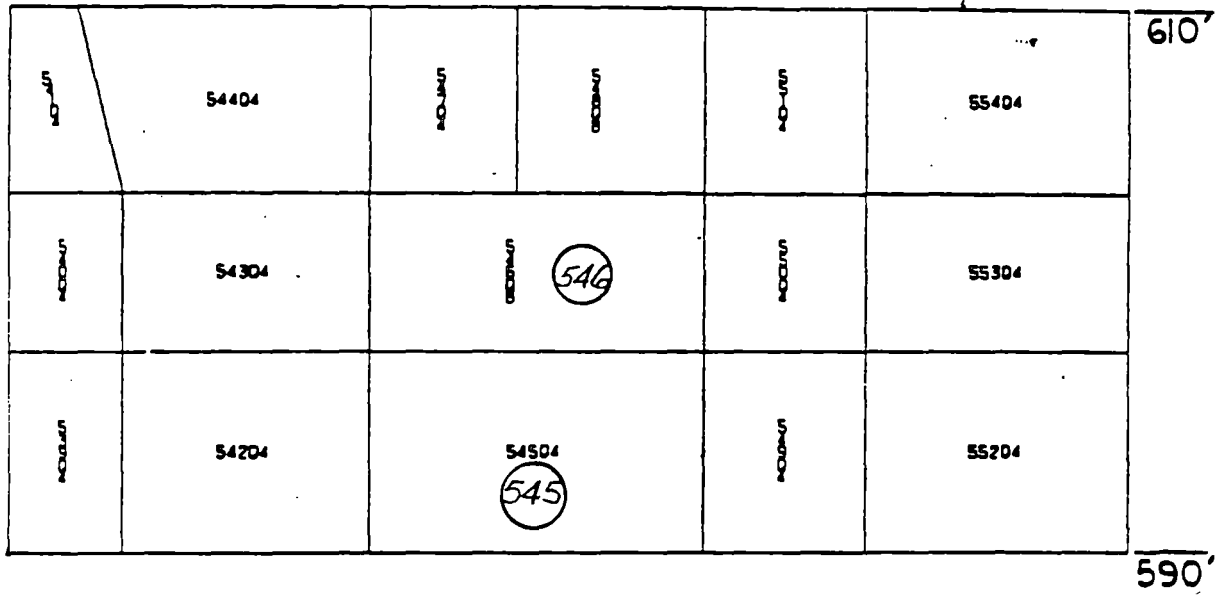
CPP PALISADES SPENT FUEL ANALYSIS

FIGURE D-18: NORTH/SOUTH WALL 8

45
N/S WALL 9



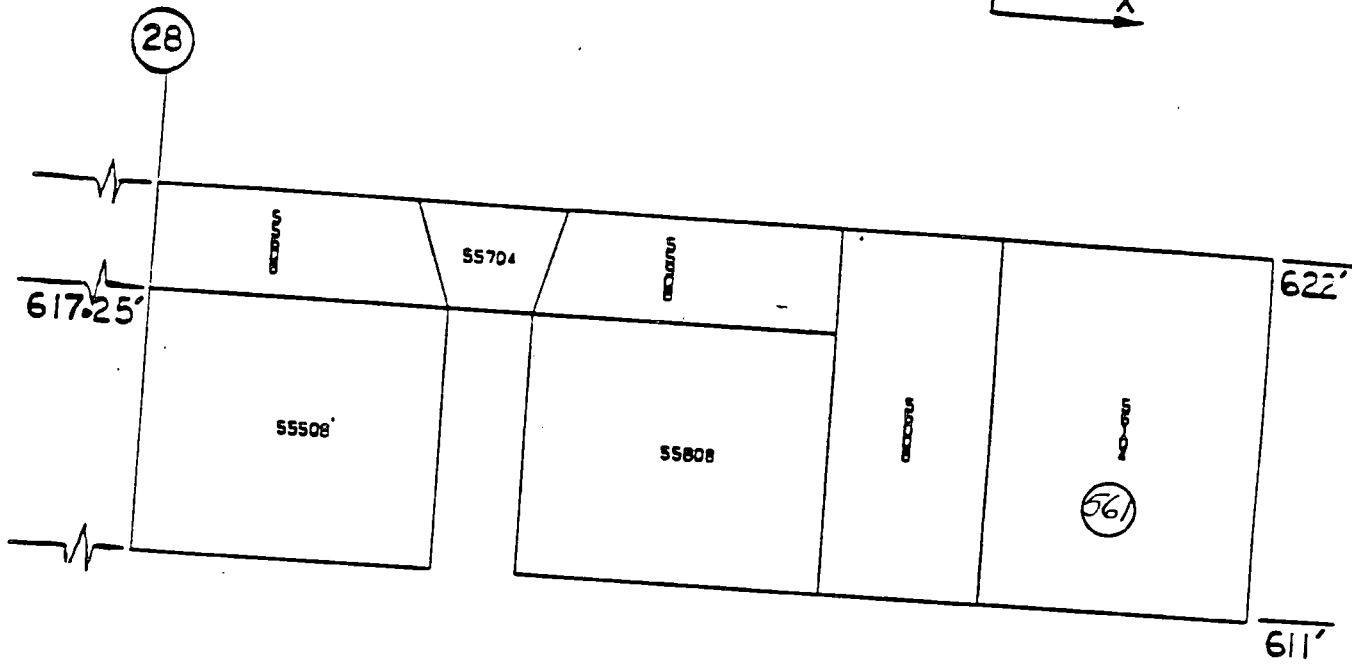
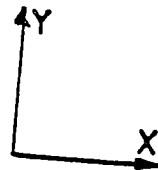
28



CPP PALISADES SPENT FUEL ANALYSIS

FIGURE D-19: NORTH/SOUTH WALL 9

47
N/S WALL 10



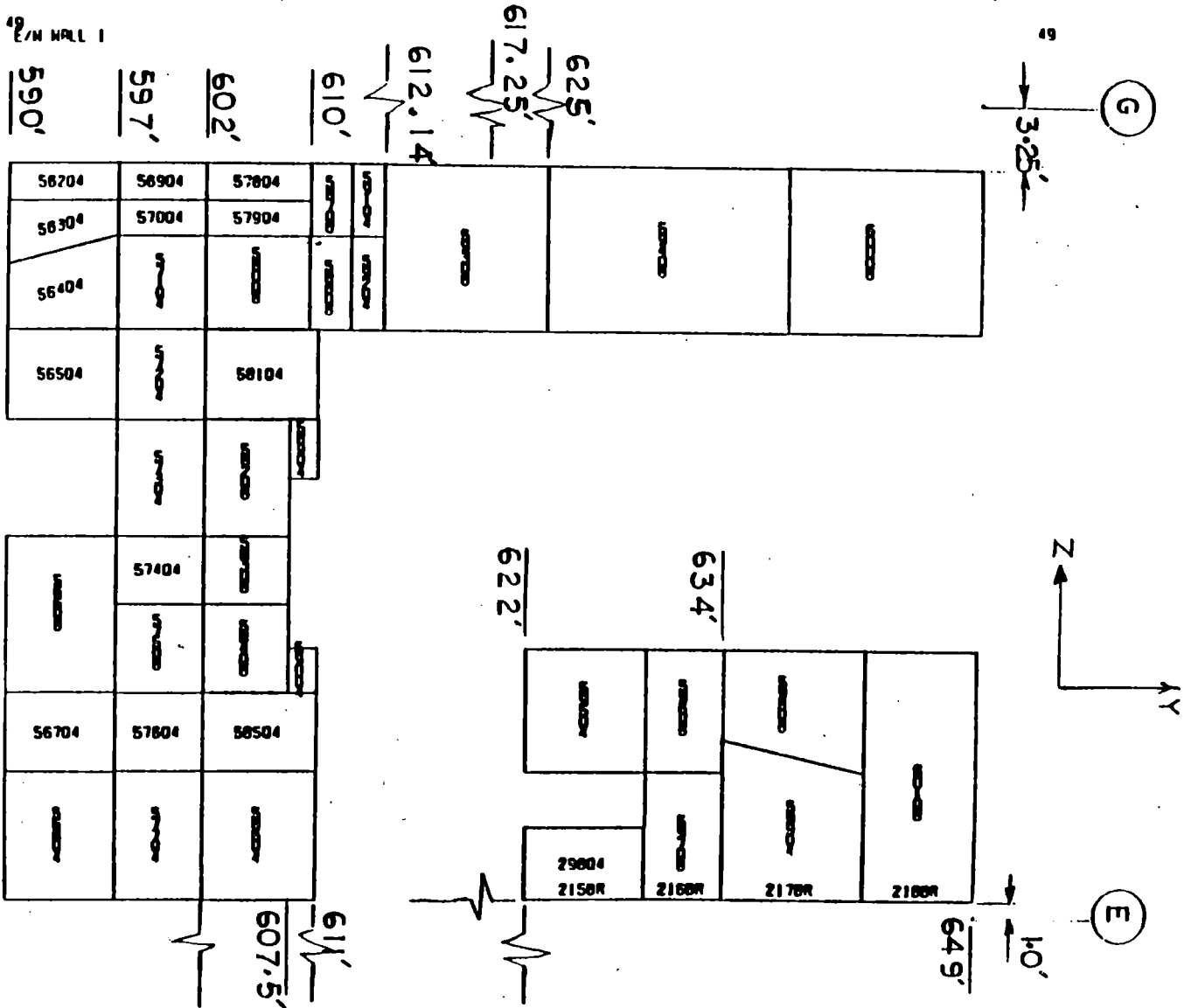
CPP PALISADES SPENT FUEL ANALYSIS

FIGURE D-20: NORTH/SOUTH WALL 10

3 7 2 0
0 2 2 7

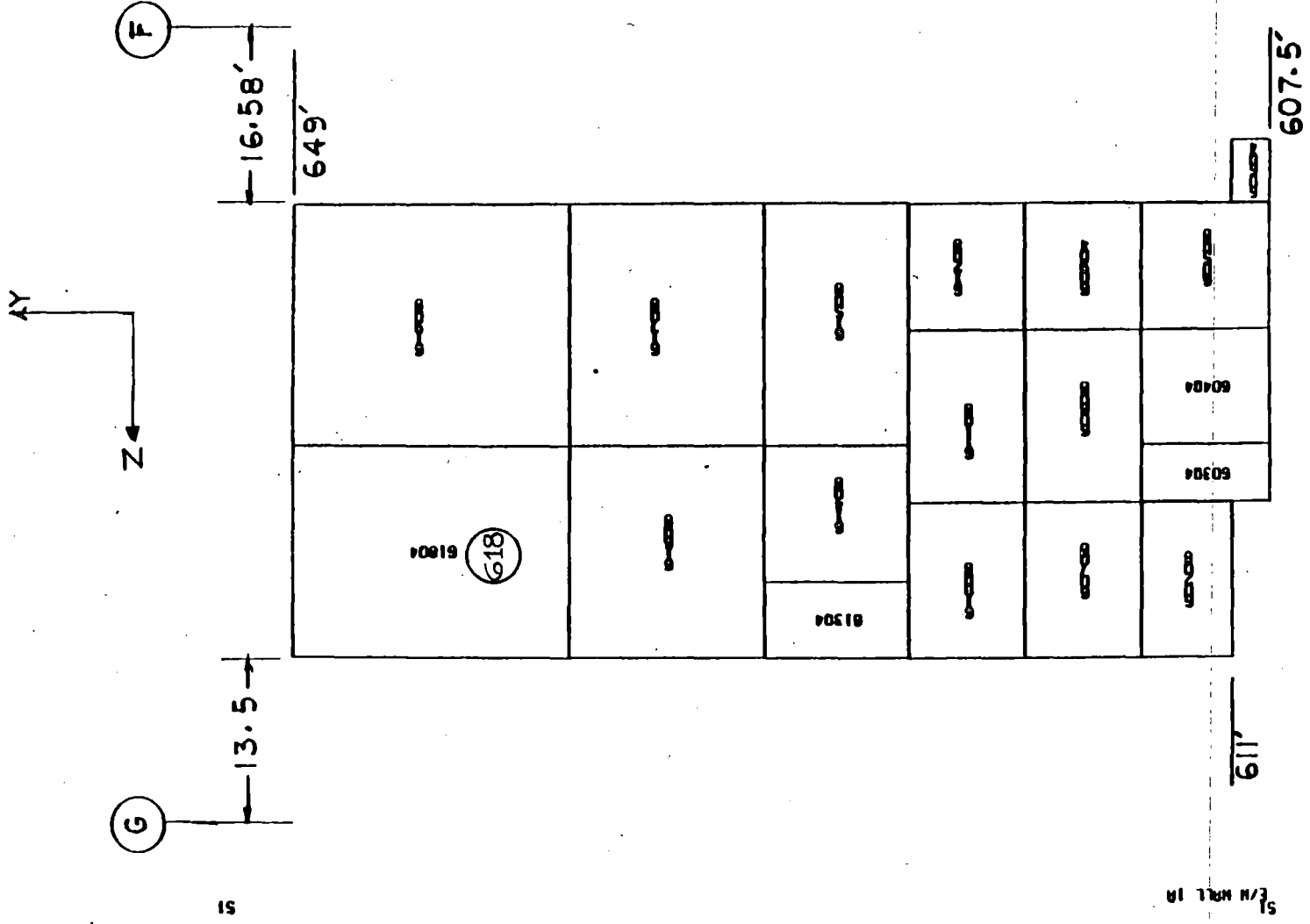
3 7 2 0

2 2 3



CPP PALISADES SPENT FUEL ANALYSIS

FIGURE D-21: EAST/WEST WALL 1



CFR PANELS SPENT FUEL ANALYSIS

FIGURE D-22: EAST/WEST WALL 1A

3 7 2 0
2 2 9

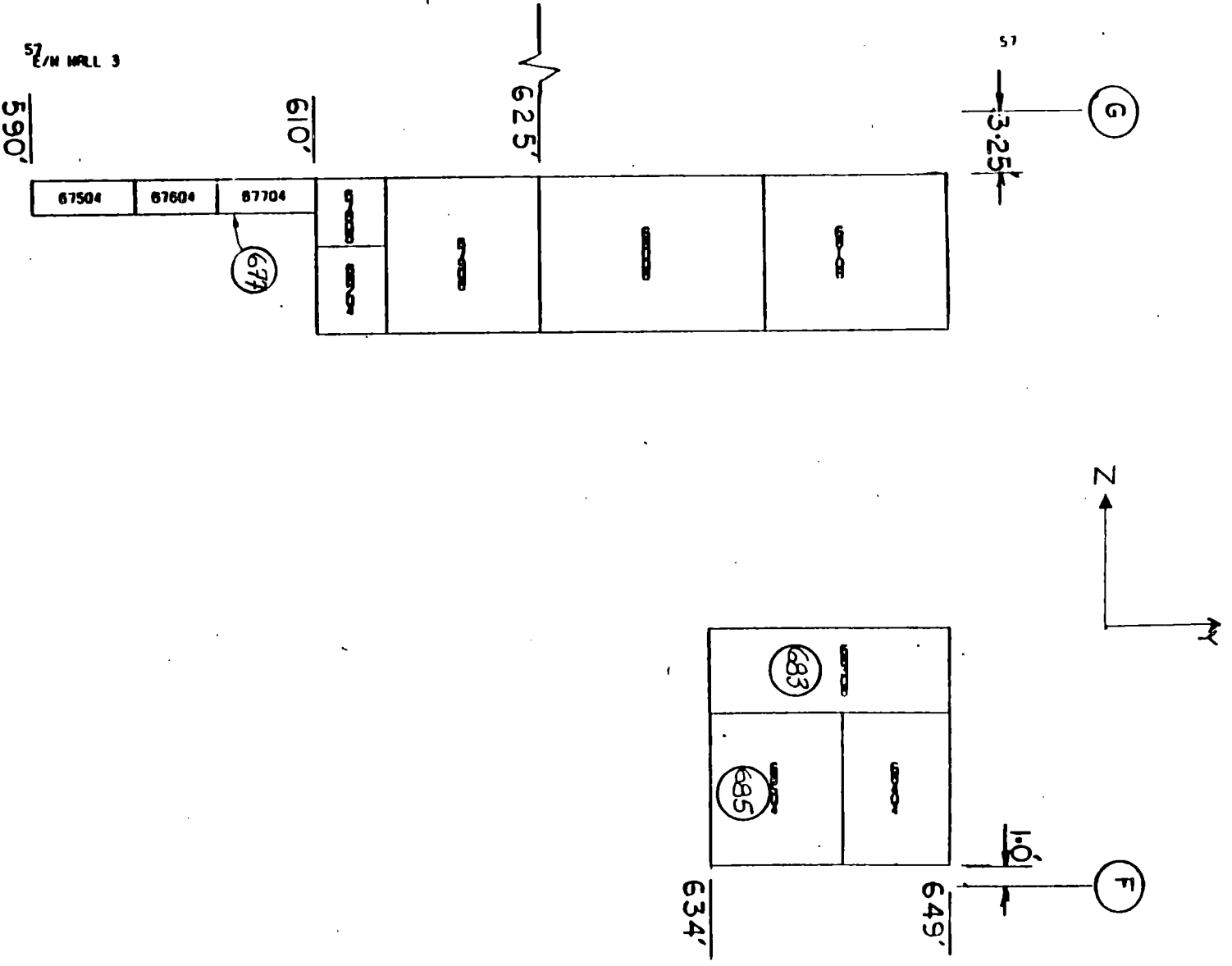


FIGURE D-25: EAST/WEST WALL 3

59
E/W WALL 4

59

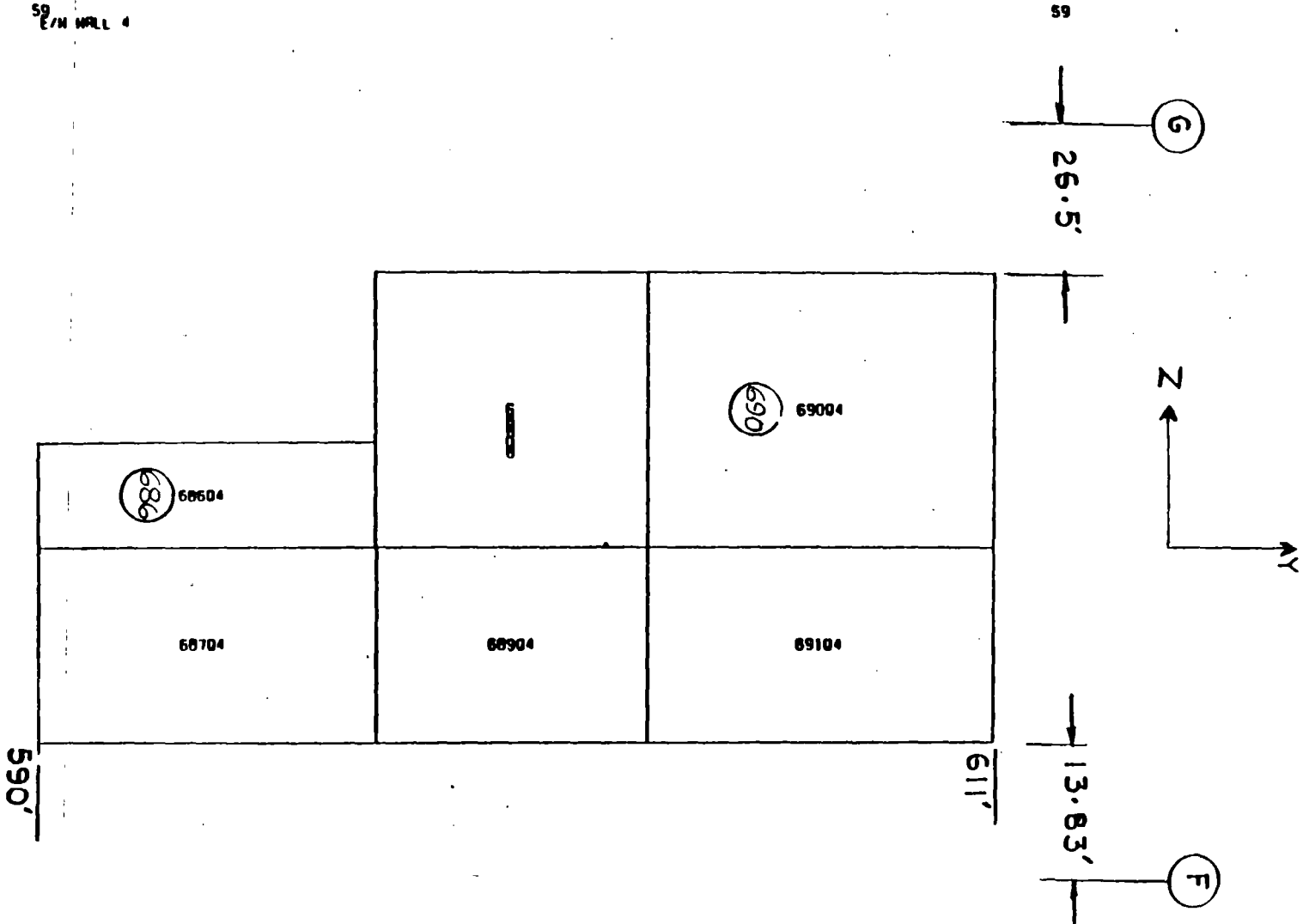


FIGURE D-26: EAST/WEST WALL 4

3 7 2 0 2 3 4

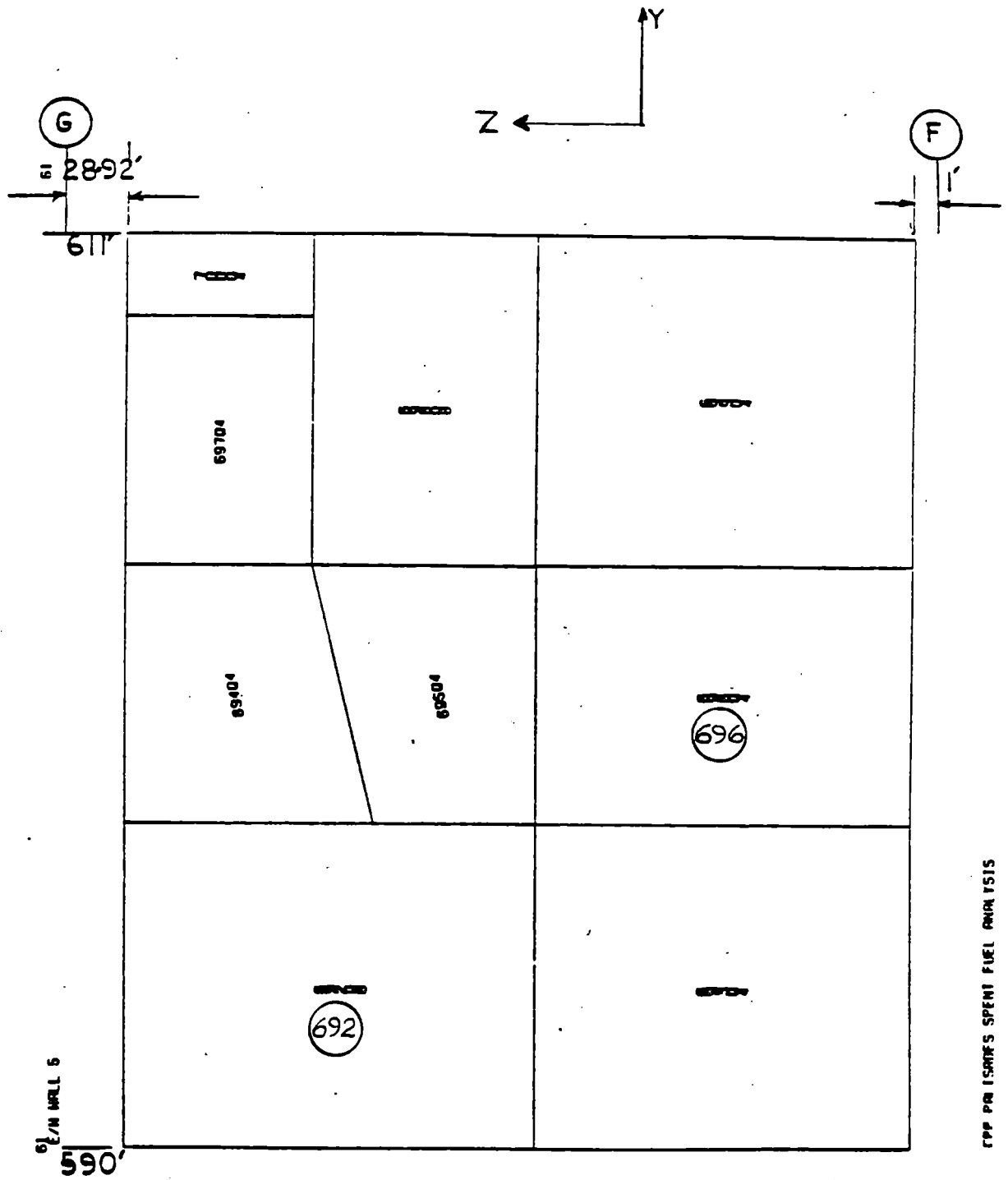


FIGURE D-27: EAST/WEST WALL 5

E/W WALL 6

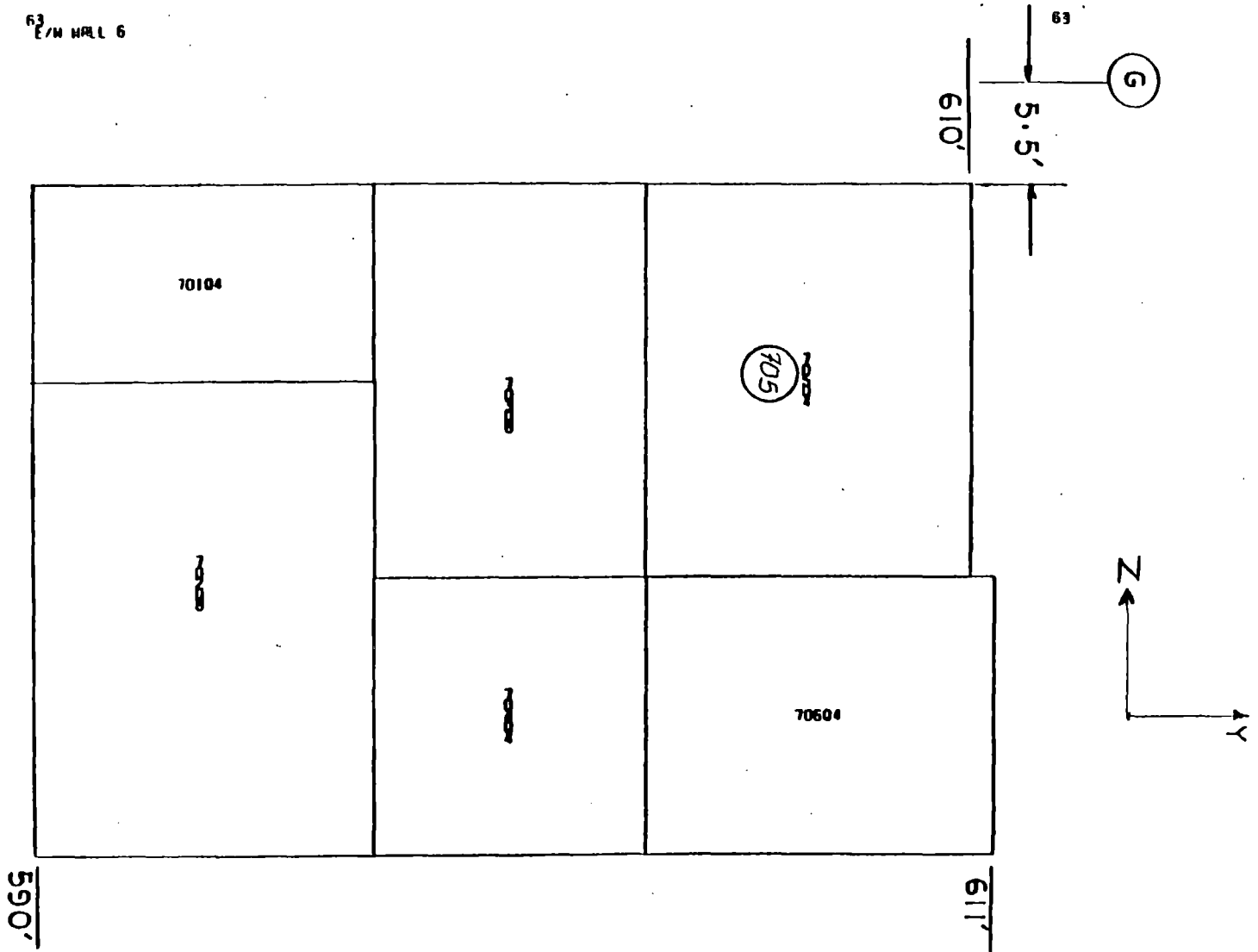


FIGURE D-28: EAST/WEST WALL 6

EFP PALISADES SPENT FUEL ANALYSIS

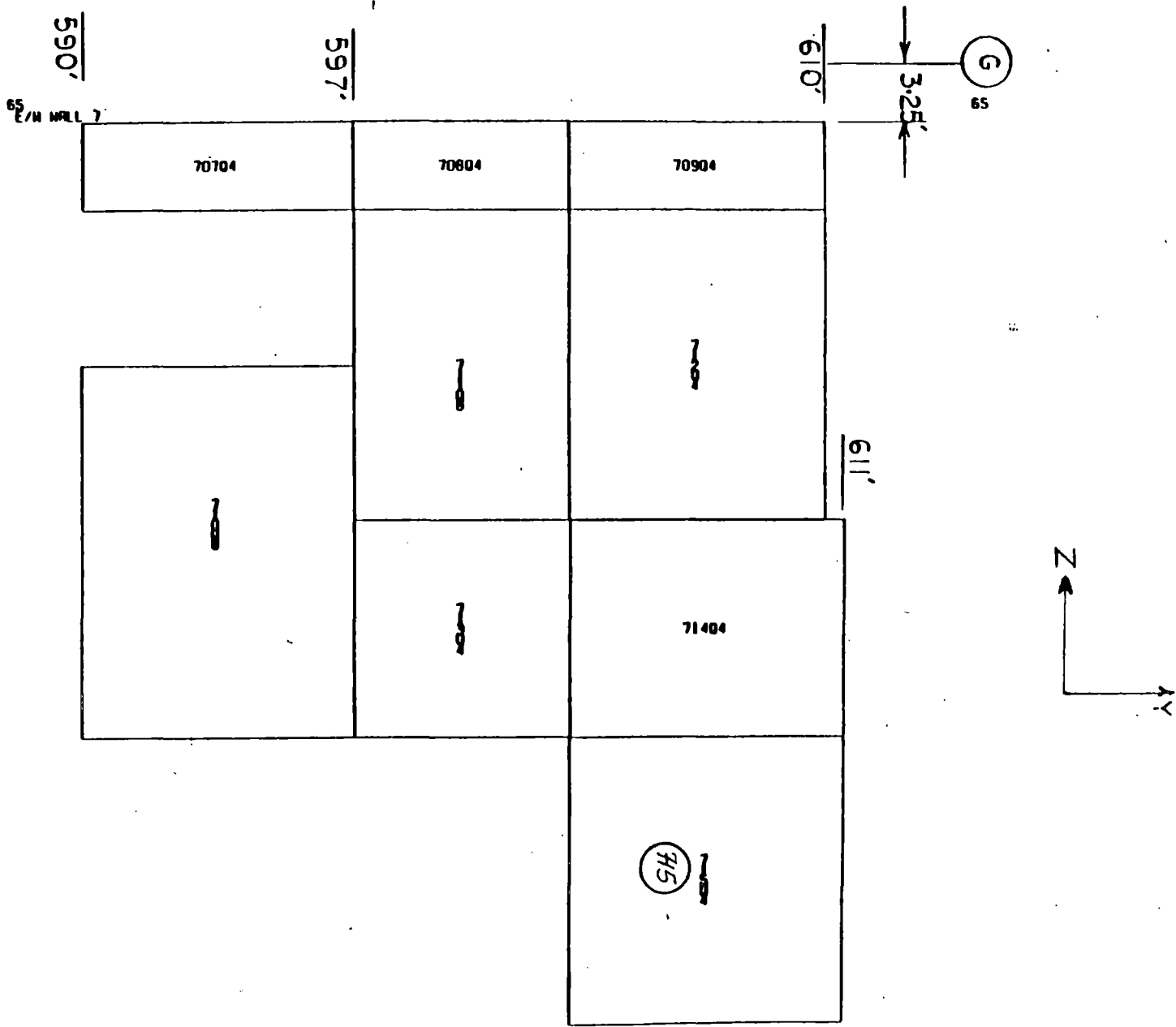


FIGURE D-29: EAST/WEST WALL 7

67
E/W WALL 8

67

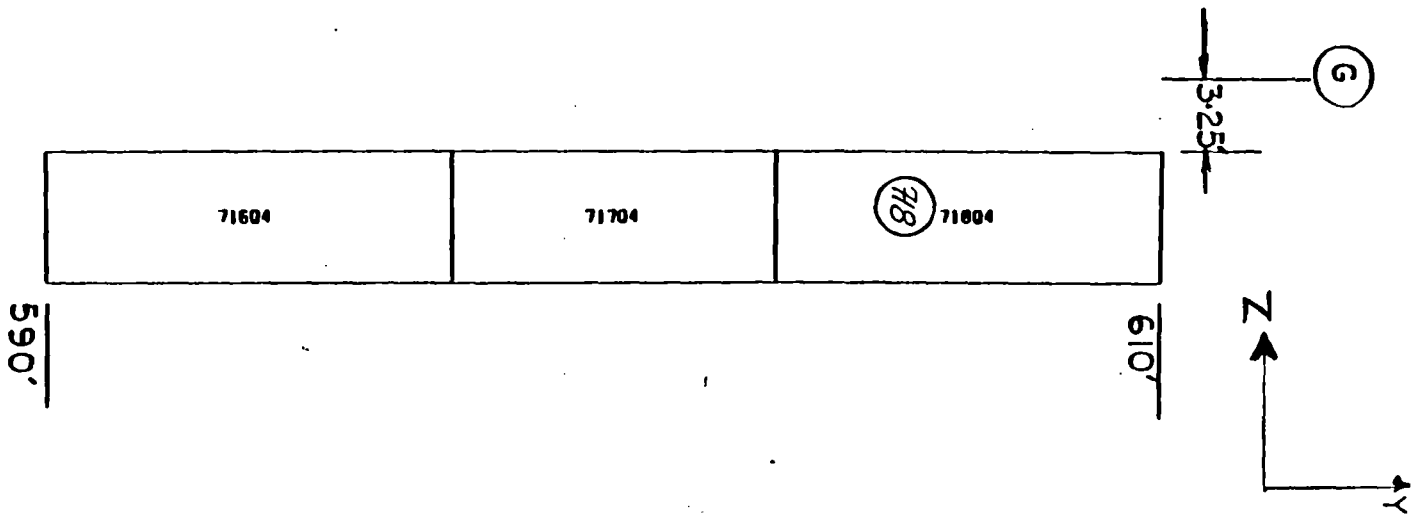


FIGURE D-30: EAST/WEST WALL 8

69
E/W WALL 9

69

590'

611'

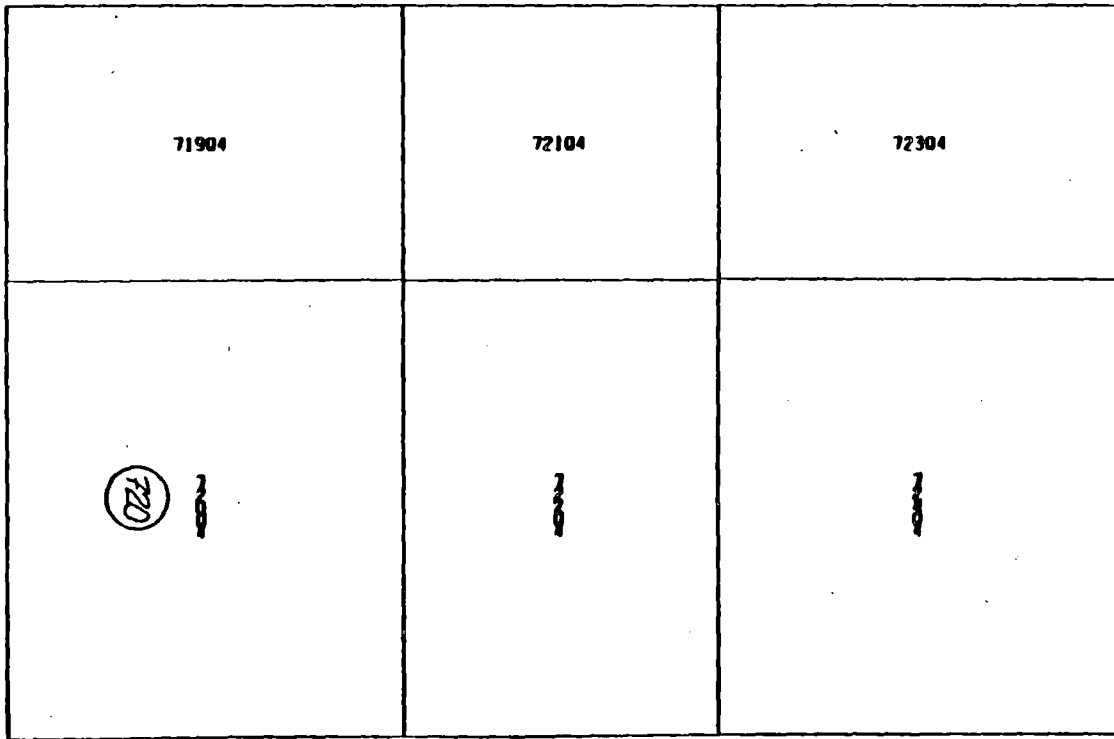


FIGURE D-31: EAST/WEST WALL 9

ATTACHMENT 2

Consumers Power Company
Palisades Plant
Docket 50-255

SPENT FUEL POOL STORAGE CAPACITY EXPANSION
RESPONSE TO QUESTIONS RECEIVED FROM THE NRC PROJECT MANAGER

July 24, 1986

3720
239

RESPONSES TO NRC REQUEST FOR ADDITIONAL INFORMATION

PALISADES SPENT FUEL STORAGE EXPANSION

Question A: Dose rate changes at the sides of the pool concrete shield walls, where occupied areas are adjacent to these walls, should be reviewed as a result of the modification. Increasing the capacity of the pool may cause spent fuel assemblies to be relocated closer to the concrete walls of the pool, resulting in an increase of radiation levels in occupied areas. Discuss this potential problem.

Response: Increasing the capacity of the spent fuel pool and tilt pit will result in spent fuel assemblies stored in portions of the pool and tilt pit being located closer to the concrete pool (shield) walls than their current positions. Radiation levels in occupied areas adjacent to the spent fuel pool and tilt pit walls, however, will increase by more than 1/10 of a percent (0.001). This is due to the fact that occupied areas adjacent to the spent fuel pool and tilt pit walls will be separated from spent fuel assemblies by no less than five feet of concrete and the stainless steel pool and tilt pit liners (ref. NCRP46, App D, Figure 12). Supporting calculations using the Rockwell Nuclear Shielding Design Manual will be available on site.

3 7 2 0
2 4 0

Question B: Provide or explain why the following descriptive information was not included in your modification for the spent fuel storage facility:

- i. the manner in which occupational exposure will be kept ALARA during the modification including the need for and manner in which cleaning of the crud on SFSF walls will be performed to reduce exposure rates in the SFSF area;
- ii. vacuum cleaning of SFSF floors if divers are used;
- iii. clean-up of the SFSF water;
- iv. the distribution of existing spent fuel stored in racks to allow maximum water shielding to reduce dose rates to divers;
- v. pre-planning of diver work as required; and
- vi. the provision for surveillance and monitoring of the work area by health physics personnel.

Response:

- i. Westinghouse, the organization performing the modification, does not intend to deviate from existing SFSF operations. Water levels will be maintained at their normal height during SFSF modifications, thus ALARA concerns would be virtually unchanged. Nevertheless, ALARA concerns will be addressed during the ALARA reviews of procedures governing the modification process.
- ii. SFSF Floors will be vacuumed only at spent fuel rack locations. Vacuum operations will be performed by using a swarp clean-up system. Rack removal and installation efforts will be done remotely. At this time, the use of divers is not anticipated.
- iii. SFSF Water will be kept clean by utilizing Palisades SFSF Cavity Filtration System.
- iv. Removal and installation efforts will be performed using remote tooling. Existing spent fuel stored in racks to be removed will be shuffled to empty racks. Westinghouse does not intend to use divers.
- v. At this time, the use of divers is not anticipated, and divers will only be used as a last option. A contingency plan will be developed, however, if diving operations are found to be necessary.

- vi. All radiological protection monitoring and surveillance of work performed in conjunction with the expansion of the SFSF will be conducted by qualified Radiation Protection Department personnel. The monitoring and surveillance activities will be performed in accordance with approved Plant Health Physics and Administrative Procedures, and controlled by specific requirements on a standard Radiation Work Permit.

3 7 2 0
2 4 2

Question C: In Section 4.7.2, 3rd paragraph, pg. 4-12, provide the analytical basis including specific assumptions that support your conclusion that the maximum gas generation would be less than 0.01 percent of the total room volume during irradiation.

Response: The calculation for gas generation being less than .01 percent of room volume uses the average gas generation over one year's time assuming the number of locations equivalent to one third core is filled with freshly discharged fuel and all other locations are filled with fuel one or more years old. The calculation also assumes the atmosphere in the spent fuel area is renewed at an average rate of the total room volume per week.

3 7 2 0
2 4 3

Question D: For the disposition of existing racks, describe the following:

- i. The method that will be used to remove, decontaminate and dispose of the old racks. Disposal alternative should include crating intact racks for disposal at a low-level waste burial site or cutting and drumming them for burial. If the racks are to be decontaminated and stored on-site, then this alternative should be described.
- ii. The number of workers that will be required for each operation including divers, if necessary.
- iii. The dose rate associated with each phase of rack removal and disposal, occupancy times and the total man-remS that will be received by all workers.

Response:

- i. As part of the old rack removal process, each individual storage cell and all other surfaces of the rack shall be hydrolased. Decontamination shall proceed until average contact radiation readings are less than 50 mrem/hr.

The racks will then be removed from the spent fuel pool and dried in the cask washdown area. They shall be moved to a loading area and placed in a fiber reinforced plastic bag. This bag serves as a protective layer against the release of radioactive contaminants from the racks. The racks shall then be placed in strongtight shipping containers for transport to the Westinghouse Decontamination, Disposal and Recycling (DDR) facility located near Madison, Pennsylvania.

The number of workers necessary for the above efforts and their exposures have been addressed as part of the on site effort (see Enclosure B).

Upon arrival at the DDR facility the racks will be placed into a contaminated materials storage area while appropriate process areas are being cleared of other work. Once the processing area is free, the racks will be handled as follows:

- 1) The racks will be surveyed and appropriate samples obtained and analyzed to meet the waste classification requirements of 10CFR61.
- 2) Any rack with excessive average contact radiation readings (greater than 50 mrem/hr) will be abrasively decontaminated to reduce the radiation levels and consequent man-rem dose. The decision regarding abrasive cleaning of the racks with hot spots will be determined on a per rack basis.

3 7 2 0 2 4 4

- 3) Racks will be mechanically volume reduced and packed in strongtight shipping containers to both reduce total burial volume and meet licensed burial site waste stability requirements.
- 4) Volume reduced fuel racks will be shipped to a licensed commercial low level waste burial facility for burial.

Experience indicates that a crew of four men can volume reduce spent fuel racks of this type and number to approximately 35% of their original volume in about 8 weeks.

Given the radiation levels above, exposures average approximately 15 to 20 mrem per man per week. Total man-rem exposure at the DDR facility for the volume reduction of the Palisades spent fuel racks will therefore range between .480 and .640 man-rem.

- ii. Rack deconning, removal and packaging for shipment will be performed by a seven (7) man crew: six (6) technicians and one (1) engineer. At this time, the use of divers is not anticipated.
- iii. See Enclosure B.

Question E: Has the spent fuel pool cooling system been modified to provide a direct cooling water supply for the tilt pit that is used for fuel storage?

Response: As stated in Consumers Power Company letter dated January 11, 1977, cooling water will be supplied to the tilt pit from the existing fill line which penetrates the pool wall near the top of this pit. A 90-degree elbow has been welded to the end of this pipe at the liner penetration to direct the cooling water downward. The nozzle welds are capable of withstanding seismic, thermal, and hydraulic loads. This line can be used to direct water from the spent fuel pool cooling pump discharge to the tilt pit for cooling purposes.

3 7 2 0
2 4 6

Question F: Provide a summary of the evaluation of the spent fuel pool (bulk) cooling system. State the assumptions used and the results concerning (1) normal refueling heat loads, (2) full core offload heat loads, (3) temperatures with single failure, and (4) time to reach 212°F with no forced cooling.

Response: Fuel decay heat values for the spent fuel pool (bulk) cooling system were calculated using the method provided in NRC Branch Technical Position ASB 9-2. All storage cells were assumed to be filled (892 assemblies). Decay heat from fuel assemblies in the tilt pit was included with the decay heat from fuel assemblies in the main pool. Loading of the spent fuel pool was begun 36 hours after reactor shutdown and proceeded at the rate of 3 fuel assemblies per hour. For the full core offload case, the offload was assumed to occur just before a normal refueling which gives the highest decay heat values. The chart below shows the results of this analysis and lists the comparable results for the existing configuration.

Condition	798 Assemblies (existing)	892 Assemblies (expanded)
Normal Refueling		
Heat Load, BTU/hr	16.9E6	16.2E6
Outlet Temperature (2 pumps), °F	116	114.3
Outlet Temperature (1 pump), °F	118*	137.6
Time to Reach 212°F (0 pumps), hrs	8.5+	8
Full Core Offload		
Heat Load, BTU/hr	26.4E6	34.1E6
Outlet Temperature (2 pumps), °F	134	141.5
Outlet Temperature (1 pump), °F	103*	191.9
Time to Reach 212°F (0 pumps), hrs	6.3+	3

*This value was determined by accounting for the spent fuel pool cooling that is provided by the Shutdown Cooling System, assuming that fuel transfer tube is open and allows communication between the spent fuel pool water and the containment refueling cavity.

+These times were calculated assuming an initial outlet temperature of 118°F for normal refueling conditions, and 103°F for full core offload conditions.

Note that the normal refueling heat load for the existing configuration (16.9E6 BTU/hr) is greater than the expanded configuration (16.2E6 BTU/hr), even though the expanded configuration accounts for 94 more fuel assemblies. The major reason for this apparent anomaly is the difference in the times at which the decay heat load was calculated. For the 798 assemblies case representing the current pool capacity, all 68 fuel

assemblies discharged from the reactor were assumed to be in the spent fuel pool at 36 hours after reactor shutdown. In the 892 assemblies case representing the expanded pool capacity, refueling (ie, discharge of fuel assemblies from the reactor) was assumed to begin 36 hours after shutdown and was completed at 60 hours after shutdown, the time at which the maximum heat load occurred. Note that both of these cases are conservative since the Palisades Technical Specifications prohibits initiation of refueling operations until 48 hours after reactor shutdown.

To put the two cases on a common basis, the heat load for the 798 assemblies case was corrected to 60 hours after shutdown using the NRC Branch Technical Position ASB 9-2. The resultant heat load is $14.6E6$ BTU/hr, which is 10% lower than the heat load for the 892 assemblies case.

Also, for full core offload conditions, the heat load for the 798 assemblies case was calculated at seven days after shutdown, and the heat load for the 892 assemblies case was calculated at 108 hours after shutdown.

Note also that all calculations for the expanded 892 assemblies case were performed for fuel stored in the main pool and the spare tilt pit. Therefore, the results given above apply to fuel stored in either location.

3 7 2 0
0 2 4 3

ENCLOSURE B

Consumers Power Company
Palisades Plant
Docket 50-255

SPENT FUEL POOL STORAGE CAPACITY EXPANSION

July 24, 1986

249

3720

SPENT FUEL RACK REPLACEMENT
PERSONNEL EXPOSURE SUMMARY

The Personnel Exposure Estimate Worksheets contain the exposure estimate for various tasks involved in Spent Fuel Rack Replacement. These estimates include only the Westinghouse crew.

Summary of Exposure Estimates to W Personnel:

I. Prerequisite and Clean-up Task	0.122 man-rem
II. Removal of Existing NUS Racks	0.688 man-rem
III. Installation of <u>W</u> Racks	<u>1.620</u> man-rem
Total	2.430 man-rem

Assumptions for Estimates:

The overall average exposure in the spent fuel building was found to be 0.69 millirem per hour. While the average dose rate directly above the SFP was 1.5 millirem per hour.

3 7 2 0
2 5 0

PALISADES PLANT SPENT FUEL RACK REPLACEMENT
PERSONNEL EXPOSURE ESTIMATES

I. Prerequisite and Clean-up Task

<u>Description of Task</u>	<u>Responsibility</u>	<u>Radiation Levels mr/hr</u>	<u>Number of Men</u>	<u>Task Hrs</u>	<u>Total Exp Per Task (Man-rem)</u>	<u># of Times Task Performed</u>	<u>Total Man-rem</u>
A. Fuel Shuffle	CPCo	1.5	1	52.2	78.3	1	0.078
B. Interference Removal & Installation	CPCo	4	4	40	640	1	0.640
C. Temporary Shed Facility Erection	CPCo	No Exposure					
D. W Personnel Platform	<u>W</u>	No Exposure					
E. Personnel Platform/ Positioning in Spent Fuel Building	<u>W/</u> CPCo	1.5 1.5	5 2	8 8	60.0 24.0	1 1	0.060 0.024
F. Rack Lifting Drive Erection/ Positioning/ Disassembly	<u>W/</u> CPCo	0.69 0.69	5 3	18 18	62.1 16.6	1 1	0.062 <u>0.017</u>

W Total of Task I 0.122
CPCo Total of Task I 0.759
Grand Total of Task I 0.881

3720 0251

PALISADES PLANT SPENT FUEL RACK REPLACEMENT
PERSONNEL EXPOSURE ESTIMATES

II. Removal of Existing NUS Racks

<u>Description of Task</u>	<u>Responsibility</u>	<u>Radiation Levels mr/hr</u>	<u>Number of Men</u>	<u>Task Hrs</u>	<u>Total Exp Per Task (Man-rem)</u>	<u># of Times Task Performed</u>	<u>Total Man-rem</u>
A. NUS Rack Lifting Rig Engaged	<u>W</u>	1.5	5	2	15.0	8	0.120
B. NUS Rack Decon & Hydrolase	<u>W</u>	1.5	5	8	60.0	8	0.480
C. NUS Rack Transfer to Cask Wash Down Area	<u>W</u>	0.69	4	2	5.52	8	0.044
	<u>CPCo</u>	0.69	2	2	2.76	8	0.022
D. Rack Packing & Loading onto Truck	<u>W</u>	0.69	4	2	5.52	8	0.044
	<u>CPCo</u>	0.69	3	2	4.14	8	<u>0.033</u>
						<u>W Total for Task II</u>	<u>0.688</u>
						<u>CPCo Total for Task II</u>	<u>0.055</u>
						<u>Grand Total for Task II</u>	<u>0.743</u>

3 7 2 0 0 2 5 2

PALISADES PLANT SPENT FUEL RACK REPLACEMENT
PERSONNEL EXPOSURE ESTIMATES

III. Installation of W Racks

<u>Description of Task</u>	<u>Responsibility</u>	<u>Radiation Levels mr/hr</u>	<u>Number of Men</u>	<u>Task Hrs</u>	<u>Total Exp Per Task (Man-rem)</u>	<u># of Times Task Performed</u>	<u>Total Man-rem</u>
A. Embedment Pad Elevation Measurements	<u>W</u>	1.5	4	9	54.0	6	0.324
B. <u>W</u> Rack Upending Transporting & Cleaning	CPCo	No Exposure					
C. <u>W</u> Rack Pre-level & Drag Test	<u>W</u>	No Exposure					
D. <u>W</u> Rack Transfer to Spent Fuel Building	CPCo	4	4	8	128	1	0.128
E. Rack Positioning	<u>W</u>	1.5	4	18	108	6	0.648
F. Rack Leveling	<u>W</u>	1.5	4	18	108	6	<u>0.648</u>
<u>W Total for Task III</u>							1.620
<u>CPCo Total for Task III</u>							0.128
<u>Grand Total for Task III</u>							<u>1.748</u>

3720 0253

ATTACHMENT 3

Consumers Power Company
Palisades Plant
Docket 50-255

SPENT FUEL POOL STORAGE CAPACITY EXPANSION

REFERENCED REPORTS

Shah, V N, Gilmore, C B, "Dynamic Analysis of a Structure with Coulomb Friction," ASME Paper No 82-PUP-18.

Gilmore, C B, "Seismic Analysis of Freestanding Fuel Racks," ASME Paper No 82-PUP-17.

Fritz, R J, "The Effects of Liquids on the Dynamic Motions of Immersed Solids," Journal of Engineering for Industry, February 1982.

DeSanto, D F, "Added Mass and Hydrodynamic Damping of Perforated Plates Vibrating in Water," Journal of Pressure Vessel Technology, May 1981.

July 24, 1986

3720
9254



The Society shall not be responsible for statements or opinions advanced in papers or in discussion at meetings of the Society or of its Divisions or Sections, or printed in its publications. Discussion is printed only if the paper is published in an ASME Journal. Released for general publication upon presentation. Full credit should be given to ASME, the Technical Division, and the author(s). Papers are available from ASME for nine months after the meeting.
Printed in USA.

DYNAMIC ANALYSIS OF A STRUCTURE WITH COULOMB FRICTION

V. N. Shah
Engineering Specialist
EG&G Idaho, Inc.
Idaho Falls, ID 83415
Mem. ASME

C. B. Gilmore
Senior Engineer
Westinghouse Electric Corporation
Pittsburgh, PA 15230
Mem. ASME

ABSTRACT

A modal superposition method for the dynamic analysis of a structure with Coulomb friction is presented. The finite element method is used to derive the equations of motion, and the nonlinearities due to friction are represented by a pseudo-force vector. A structure standing freely on the ground may slide during a seismic event. The relative displacement response may be divided into two parts: elastic deformation and rigid body motion. The presence of rigid body motion necessitates the inclusion of the higher modes in the transient analysis. Three single degree-of-freedom problems are solved to verify this method. In a fourth problem, the dynamic response of a platform standing freely on the ground is analyzed during a seismic event.

INTRODUCTION

Some components in nuclear power plants are not anchored to the ground and may slide when subjected to external forces. These components are designed to withstand hypothetical accidents resulting from an earthquake. In the seismic analysis of these components, it is necessary to model the sliding between the components and the ground. For instance, one such component is a fuel rack to store the spent fuel assemblies in a water filled pool. Generally the fuel racks are anchored to the floor of the pool; however, some applications do not permit the fuel racks to be anchored to the floor. The unanchored fuel racks, standing freely on the floor,

may slide and tip during a seismic event. In addition, a fuel rack may collide with other racks or with the pool walls during an earthquake. In the seismic analysis of the freestanding fuel racks, the possibilities of sliding, tipping, and collisions must be evaluated. The main purpose of this paper is to present a computationally economical method to perform a seismic analysis of a freestanding fuel rack.

The direct integration methods[1,2] are widely used for the nonlinear dynamic analyses, but their computer cost for the seismic analysis of a freestanding fuel rack is prohibitive. In order to reduce computer cost, the application of the modal superposition method to nonlinear analysis is considered.

In the modal superposition methods, two approaches are used to integrate the nonlinear equation of motion. In the first approach, referred to as the incremental approach[3], the equation of motion is converted to an incremental form and nonlinearities are treated by updating the natural frequencies and mode shapes. In the second approach[4,5,6], the nonlinear terms are represented as pseudoforce. In both approaches, the uncoupled modal equations are integrated analytically without introducing any artificial damping or phase distortion.

In the dynamic analyses of the nonlinear structures, such as spent fuel rack, the source of nonlinearities is restricted to a small portion of the structure. In the finite element analysis, a large portion of such nonlinear structure is modeled with linear elements, while the remaining small portion

3720
255

is modeled with nonlinear elements. The computational cost of the pseudoforce approach to analyze such nonlinear structures is lower than that of the incremental approach[5]. Therefore, the pseudoforce approach is developed for the subject analysis. Sliding of the structure is modeled with aid of Coulomb friction.

The modal superposition method using the pseudoforce approach was originally developed to analyze the structures subjected to single-point translational excitations. The nonlinearity due to impact between various structural components was permitted. Later, the scope of this method was expanded[7] to analyze the linear and nonlinear structures subjected to multiple support motions. Recently, this method has been further developed to analyze the structures with elastic-plastic material properties[8]. This method has now been expanded to analyze the structures with Coulomb friction which is the subject of this paper.

In the next section, an element representing Coulomb friction is described, followed by the discussion on the pseudoforce approach. Then the use of the friction element in the seismic analysis is discussed. The results of four test problems are presented to verify the subject method and to gain some insight in the use of the method. Gilmore[9] has applied the subject method to the seismic analysis of a freestanding fuel rack and reported a significant savings in the computer cost.

MODAL SUPERPOSITION METHOD

The discussion of the modal superposition method is divided into the following three topics:

1. Friction element
2. Pseudoforce approach
3. Seismic analysis.

Friction Element

Coulomb friction is used to represent the energy dissipation resulting from the sliding between two contact surfaces. The external force acting on the contact surfaces has two components: one acting normal to the contact surfaces and the other acting in the plane of contact. The latter component is referred to as shear force. A friction force exists between the contact surfaces and acts in a direction opposing the shear force. The magnitude of the friction force is equal to that of the shear force. As the magnitude of the shear force increases, the magnitude of the friction force increases until its magnitude becomes equal to the product of the normal force (P_N) and a static coefficient of friction (μ_s). Any further increase in the shear force will cause the two contact surfaces to slide along the direction of the force. During sliding, the friction force is equal to the product of the normal force and the dynamic coefficient of friction (μ_d).

The sliding between two contact surfaces takes place when the shear force becomes greater than the static friction force ($\mu_s P_N$). This ideal friction behavior is approximately simulated by the friction element. The friction element allows a small amount of relative displacement between two contact surfaces before the shear force becomes greater than the static friction force. The approximate friction behavior simulated by the friction element is shown in Figure 1.

The two-dimensional friction element is shown in Figure 2. Nodes I and J are located on each

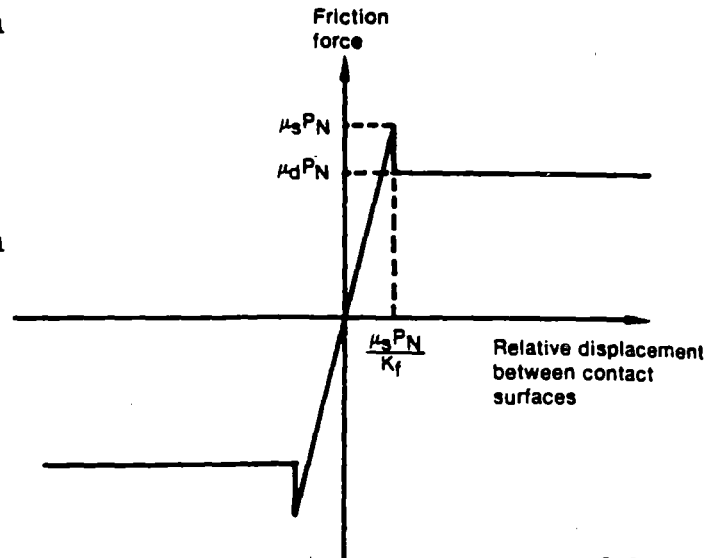


Fig.1 Approximate friction behavior simulated by friction element shown in Figure 2

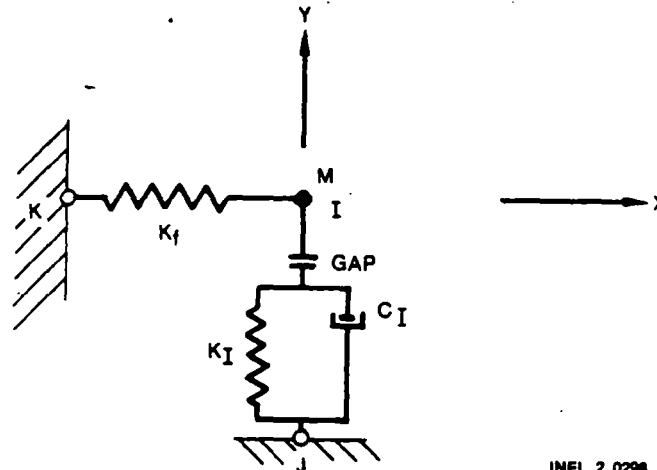


Fig.2 Friction element to represent approximate friction behavior shown in Figure 1

contact surface. Node K is fixed in the space. The direction K_I is along the direction of sliding. The friction spring (K_f) between nodes K and I simulates the friction behavior between two contact surfaces. The damper (C_f), spring (K_I) and the parameter GAP between two nodes I and J simulate the possibility of separation of and impact between two contact surfaces. In the absence of the friction spring, the friction element reduces to a gap element. In a gap element, the nonlinearity due to impact is represented by a pseudoforce as described in Reference[8]. In the following discussion, analysis of only sliding behavior is presented. When the force in the friction spring is greater than the static friction force $\mu_s P_N$, sliding takes place. At the initiation of sliding, the relative displacement between two surfaces in the direction of sliding is nonzero and is equal to $\mu_s P_N / K_f$. As the stiffness of the friction spring increases, the magnitude of the relative displacement decreases; and the behavior simulated by the friction element will be closer to the ideal behavior. The magnitude of K_f is selected such that the relative displacement $\mu_s P_N / K_f$ is a small fraction of the total displacement due to sliding.

Pseudoforce Approach

In this approach, the nonlinear dynamic analysis of a structure is divided into two parts: modal analysis and transient analysis. In the modal analysis, the nonlinear structure is linearized by treating the friction spring as a linear spring. Then, the mode shapes and the natural frequencies of the linearized structure are calculated. In the transient analysis, these mode shapes are used to uncouple the equation of motion. Mode shapes and the natural frequencies of the linearized structure are not updated during the transient analysis.

The equation of motion of a structure with Coulomb friction is

$$[M]\{\ddot{X}\} + [C]\{\dot{X}\} + [K_{nl}]\{X\} = \{F\} \quad (1)$$

where

$$\begin{aligned} [M] &= \text{mass matrix} \\ [C] &= \text{damping matrix} \\ [K_{nl}] &= \text{nonlinear stiffness matrix} \end{aligned}$$

Arrays $\{X\}$, $\{\dot{X}\}$, $\{\ddot{X}\}$, and $\{F\}$ are the displacement, velocity, acceleration, and applied force vectors, respectively.

Let

$$[K_{nl}] = [K] + [\bar{K}] \quad (2)$$

where

$$\begin{aligned} [K] &= \text{stiffness matrix representing the linearized structure} \\ [\bar{K}] &= \text{stiffness matrix representing the nonlinearity due to Coulomb friction.} \end{aligned}$$

Substitution of Equation (2) in Equation (1) gives

$$[M]\{\ddot{X}\} + [C]\{\dot{X}\} + [K]\{X\} = \{F\} - \{F_{nl}\} \quad (3)$$

where

$$\{F_{nl}\} = [\bar{K}]\{X\} = \text{pseudoforce vector.} \quad (4)$$

Initially, the pseudoforce vector is zero and it remains zero as long as the force in the friction spring is less than the static friction force. When the force in the friction spring exceeds the static friction force, the sliding initiates and the pseudoforce becomes nonzero. The resultant of the force in the friction spring and the pseudoforce is equal to a friction force acting on node I. Pseudoforce is a piecewise-linear function of displacement and velocity of node I relative to node J. Let $[\omega_j]$ and $\{\phi\}$ be the natural frequency and normalized mode shape matrix associated with the linearized, undamped structure. The transformation

$$\{X\} = \{\phi\}\{q\} \quad (5)$$

is substituted in Equation (3) premultiplied by $\{\phi\}^T$. Then, employing the orthogonality relations expressed by

$$\{\phi\}^T [M] \{\phi\} = [I]$$

$$\{\phi\}^T [C] \{\phi\} = [-2\zeta_j \omega_j -]$$

and

$$\{\phi\}^T [K] \{\phi\} = [\omega_j^2 -]$$

the resulting modal equations becomes

$$\ddot{\{q\}} + [-2\zeta_j \omega_j -]\dot{\{q\}} + [\omega_j^2 -]\{q\} = \{Q\} - \{Q_{nl}\} \quad (6)$$

where

$$\zeta_j = \text{percentage of the critical damping for the } j\text{th mode}$$

$$\{Q\} = \{\phi\}^T \{F\} = \text{generalized applied force vector}$$

$$\{Q_{nl}\} = \{\phi\}^T \{F_{nl}\} = \text{generalize pseudoforce vector.}$$

Arrays $\{q\}$, $\{\dot{q}\}$ and $\{\ddot{q}\}$ are the modal displacement, velocity and acceleration vectors, respectively. For a given time step, the pseudoforce is approximated by the first two terms of a Taylor series, provided the friction force is continuous during the previous time step. The pseudoforce is expressed as

$$\{Q_{nl}\} \Big|_t = \{Q_{nl}\} \Big|_T + \frac{d\{Q_{nl}\}}{dt} \Big|_T (t-T) \quad T < t < T + \Delta T \quad (7)$$

where

$$\frac{d\{Q_{nl}\}}{dt} \Big|_T = \frac{\{Q_{nl}\} \Big|_T - \{Q_{nl}\} \Big|_{T-\Delta T}}{\Delta T}$$

If the friction force is not continuous during the previous time step, then

$$\{Q_{nl}\} \Big|_t = \{Q_{nl}\} \Big|_T \quad T < t < T + \Delta T \quad (8)$$

For a given time step, Equation (6) is integrated analytically. Then, the displacements and velocities of the nodes associated with the friction elements are calculated. This information is used to calculate the generalized pseudoforce vector and its time derivative needed to integrate the modal equations during the next time step.

Seismic Analysis

In the seismic analysis of a structure subjected to single-point translational excitations[10], i.e., all supports are subjected to the same translational excitations; it is a normal practice to calculate the displacement response relative to a fixed point on the ground. If the structure is anchored to the ground, the displacement response

is calculated relative to its fixed base. The relative displacement response consists of the elastic deformation and can be simulated by the lower mode shapes of the structure. For a linear structure anchored to the ground, the number of mode shapes to be included in the analysis is determined by the frequency content of the seismic excitation.

If a linear structure is standing freely on the ground, its displacement response is calculated with respect to a point on the ground that is initially in contact with its base. If the structure slides during a seismic event, its relative displacement response consists of the elastic deformation superimposed on the rigid body motion of the structure. The presence of the rigid body motion influences the selection of the mode shapes.

The finite element model of a freestanding structure consists of friction elements between the base of the structure and the ground. The stiffness of the friction springs is kept high so that the base of the structure experiences little relative displacement before actual sliding takes place. In the modal analysis of a freestanding structure, the friction springs are treated as linear springs. In the lower mode shapes, these springs act like rigid members, while in some of the higher mode shapes the strain energy in the friction springs dominates the total strain energy. These higher mode shapes should be included in the analysis to simulate the rigid body motion. Thus, in the seismic analysis of a freestanding structure, the selection of the mode shapes depends upon the frequency content of the excitation and the stiffness of the friction springs.

Test Problems

The modal superposition method described in this paper is incorporated in the WECAN (Westinghouse Electric Computer ANalysis) computer program[8]. This program also has a direct integration method[2] to perform the transient dynamic analysis of a structure. Four test problems are solved to verify the modal superposition method in the WECAN program.

In the first two problems, respectively, free and forced vibrations of a spring-mass system with Coulomb friction are analyzed. In the third problem, forced vibrations of a spring-mass-damper system with Coulomb friction are analyzed. In the fourth problem, the seismic analysis of a platform supported freely on the ground is presented. The fourth problem is solved by the direct integration method and by the modal superposition method. The comparisons of the corresponding results and the computer costs are given.

The spring-mass system analyzed in the first two problems is shown in Figure 3. In the third problem, a viscous damper parallel to the spring is added to the system. The physical parameters of the spring-mass system are

Spring stiffness (K)	= 1000 lb/in. (1.751 x 10 ⁵ N/m)
Mass (M)	= 2.59 lb-sec ² /in. (1.1748 kg)
Natural frequency (ω_n)	= 3.1273 Hz
Static coefficient of friction (μ_s)	= 0.3

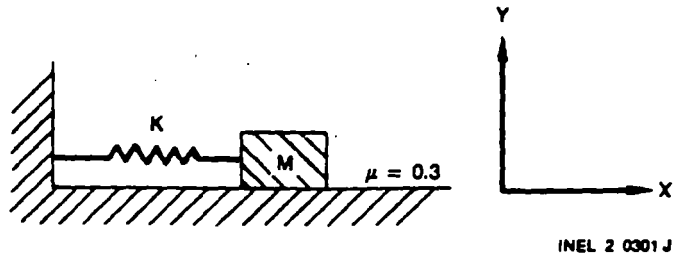


Fig. 3a Spring-mass system with Coulomb friction

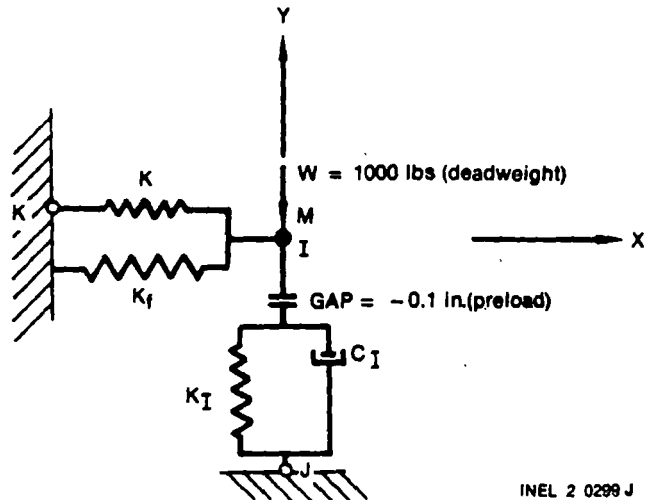


Fig. 3b Finite element model of a spring-mass system with Coulomb friction

Dynamic coefficient of friction (μ_d)	= 0.3
Normal spring stiffness (K_I)	= 10,000 lb/in. (1.75 x 10 ⁶ N/m)
Friction spring stiffness (K_f)	= 10,000 lb/in. (1.75 x 10 ⁶ N/m)
GAP	= -0.1 in. (-0.254 x 10 ⁻² m).

The deadweight of the mass M is 1000 lbs (4448.2 N) acting along the negative Y-direction. The deadweight is balanced by the preload in the normal spring. The transient displacement response of the mass M consists of only the X-component.

Test Problem 1. The free vibrations of the spring-mass system with Coulomb friction are analyzed in this problem. The initial conditions are

$$\begin{aligned} X &= 4.7 \text{ in. (0.1194 m)} \\ \dot{X} &= 0.0 \text{ in./s (0.0 cm/s)}. \end{aligned}$$

The pseudoforce acting on the sliding mass is given by one of the following four expressions.

For $\dot{X} < 0$ (mass sliding along negative X-axis)

$$F_{nl} = - [K_f X + \mu_d P_N] \quad X > 0$$

$$F_{nl} = - [K_f |X| - \mu_d P_N] \quad X < 0$$

For $\dot{X} > 0$ (mass sliding along positive X-axis)

$$= \pm 5.736 \text{ in.} \\ (\pm 0.1457 \text{ m}).$$

$$F_{nl} = - [K_f X - \mu_d P_N] \quad X > 0$$

$$F_{nl} = - [K_f |X| + \mu_d P_N] \quad X < 0$$

where

$$P_N = \text{dead weight} = 1000 \text{ lbs.}$$

The analytical result for the decay in amplitude of vibrations per half cycle is given by [11]

$$\text{Decay in amplitude per half cycle} = \frac{2 \times \text{friction force}}{K} \\ = 0.6 \text{ in. (0.01524 m).}$$

The decay in amplitude per half cycle is constant.

This problem is solved by the modal superposition method using two different time step sizes: $\Delta T = 0.01$ sec and $\Delta T = 0.005$ sec. Table 1 gives the decay in the amplitude of vibrations per half cycle using both time steps. The results show that for a smaller time step, the decay in the amplitude per half cycle is closer to the correct answer of 0.6 in. (0.01524 m) and is approximately constant during the analysis.

TABLE 1. DECAY IN AMPLITUDE PER HALF CYCLE DURING THE FREE VIBRATION RESPONSE OF A SPRING MASS SYSTEM WITH COULOMB DAMPING (1 in. = 0.0254 m).

	Decay in Amplitude per Half Cycle (in.)	
	$\Delta T = 0.1$ (sec)	$\Delta T = 0.005$ (sec)
First half cycle	0.73588	0.62674
Second half cycle	0.72421	0.61840
Third half cycle	0.74588	0.61798
Fourth half cycle	0.67863	0.61410
Fifth half cycle	0.64979	0.60568
Sixth half cycle	0.63398	0.606710

Test Problem 2. The forced vibrations of a spring-mass system with Coulomb friction are analyzed in this problem. The mass M is initially at rest and has zero displacement. The harmonic force $P \sin \omega t$ is acting on the mass in the X-direction. The two cases considered are

Case 1:	P	=	2100 lbs (9341 N)
	ω	=	2.50184 Hz
Case 2:	P	=	2100 lbs (9341 N)
	ω	=	3.1273 Hz ($= \omega_n$)

Case 1. The analytical results for the steady state amplitude are given by [12]

$$\text{steady state amplitude} = A = \frac{P}{K} \frac{\sqrt{1 - (4F/\pi P)^2}}{1 - \omega^2/\omega_n^2}$$

The dynamic response of the mass M calculated by the modal superposition method is shown in Figure 4. The amplitude of the steady state displacement response varies from 5.6367 in. (0.1432 m) to 6.048 in. (0.1536 m). The average frequency content of the response over the last three cycles is 2.5042 Hz--approximately equal to the excitation frequency of 2.5018 Hz.

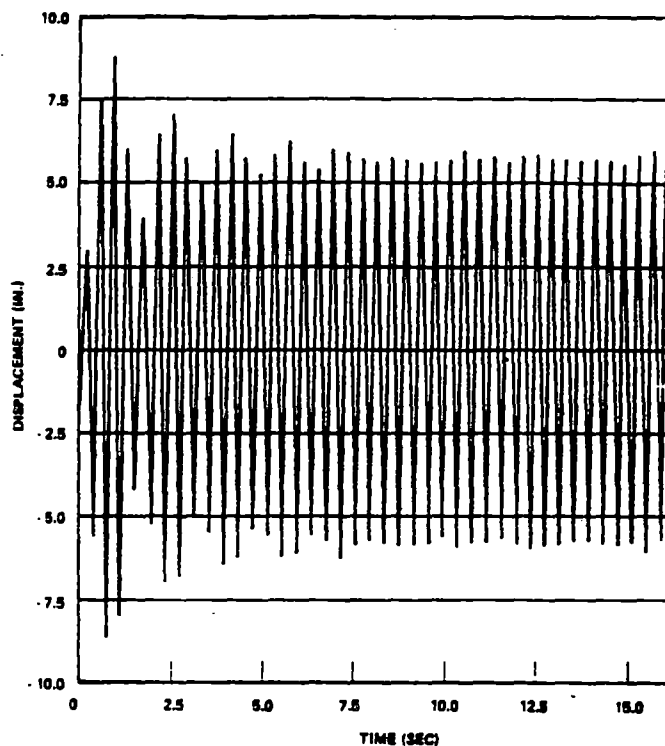


Fig. 4 Displacement response of a spring-mass system with Coulomb friction, subjected to sinusoidal forcing function $P \sin \omega t$, $\omega = 2.50184$ Hz (1 in. = 0.0254 m)

Case 2. The ratio of the friction force (F) over the applied force (P) is less than $\pi/4$. During resonance, as explained in Reference [12], the amplitude of the displacement response is unbounded. The results calculated by the modal superposition method are shown in Figure 5. The frequency content of the displacement response is 3.1250 Hz--approximately equal to the resonance frequency of 3.1273 Hz.

Test Problem 3. The forced vibrations of a spring-mass-damper system with Coulomb friction are analyzed in this problem. The spring-mass system shown in Figure 3 is modified by adding a viscous damper (modal damping coefficient = ζ) in parallel to a spring between nodes I and K. The mass is initially at rest and has zero initial displacement. It is subjected to a harmonic force $P \sin \omega t$.

Den Hartog [13] has given a complete analytical solution of this problem. The numerical results for the amplitude (A) of the forced vibrations are plotted in the amplitude diagrams. The horizontal axis represents the frequency ratio (ω/ω_n) and the vertical axis represents the magnification factor

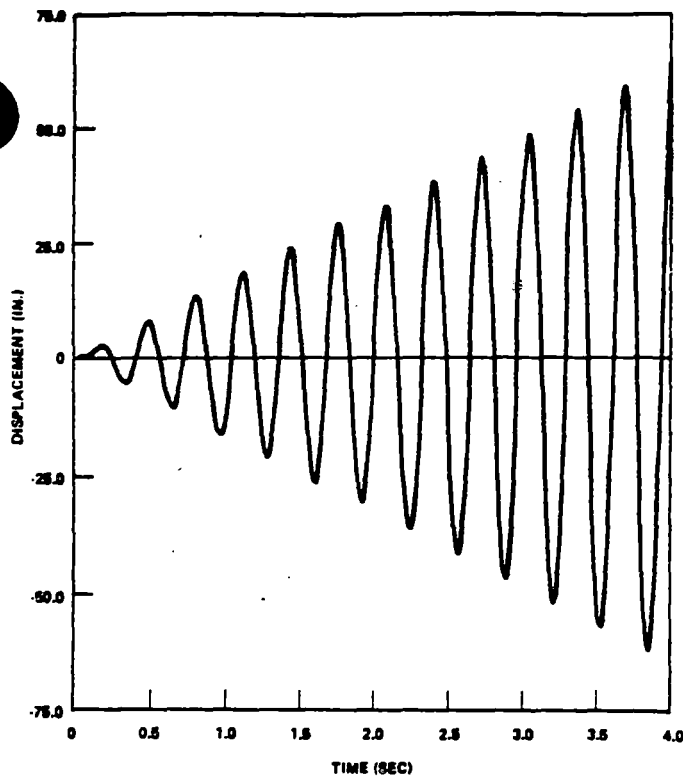


Fig. 5 Displacement response of a spring-mass system with Coulomb friction subjected to sinusoidal forcing function $P\sin\omega t$, $\omega = 3.1273$ ($= \omega_n$ system frequency) (1 in. = 0.0254 m)

($A \cdot K/P$). In each of the amplitude diagrams, several curves are plotted for a constant value of the modal damping coefficient. Along each curve the ratio of the friction force (F) over the amplitude of the applied force (P) is constant. These diagrams are used to calculate the amplitude of vibrations for the following two cases, and the results are compared with the corresponding results from the modal superposition analysis.

- | | | | |
|---------|----------|---|-------------------|
| Case 1: | P | = | 1500 lbs (6672 N) |
| | ω | = | 2.50184 Hz |
| | ζ | = | 0.1 |
| Case 2: | P | = | 250 lbs (1112 N) |
| | ω | = | 2.50184 Hz |
| | ζ | = | 0.5 |

The magnitude of the remaining physical parameters remain unchanged from those defined in Test Problem 1, except in Case 2 where coefficients of friction are reduced from 0.3 to 0.1 and the stiffness of the friction spring is increased from 10,000 lb/in. (1.75×10^6 N/m) to 100,000 lb/in. (1.75×10^7 N/m).

The natural frequency of a spring-mass system is increased due to the presence of the friction spring. This increased frequency is used in the transient analysis. Therefore it is necessary to modify the modal damping coefficient ζ . The modified modal damping coefficient ζ_m is calculated from

$$\zeta_m = \frac{K}{K + K_f} \cdot \zeta \quad (9)$$

- = 0.0301513 (Case 1)
- = 0.0497519 (Case 2).

Equation (9) gives the modified modal damping coefficient for a single degree-of-freedom problem. The modified damping coefficients for a multidegree-of-freedom system may be calculated as follows. In the modal analysis of a system, the presence of the friction springs may or may not modify the original natural frequency of a mode shape. If the natural frequency is not modified, then the modal damping coefficient need not be modified. If the natural frequency of the i th mode shape is modified, then the modified damping coefficient $\zeta_{m,i}$ may be calculated from

$$\zeta_{m,i} = \frac{\omega_i^2}{\omega_{m,i}^2} \cdot \zeta_i \quad (10)$$

where

- ω_i = original natural frequency
- $\omega_{m,i}$ = modified natural frequency
- ζ_i = modal damping coefficient.

Case 1. For this case, the frequency ratio $\omega/\omega_n = 0.8$, and the force ratio $F/P = 0.2$. From the amplitude diagram for $\zeta = 0.1$ (Figure 8 in Reference [13]), the magnification factor is 2.26. The amplitude A of the steady state response is given by

$$A = 2.26 \cdot \frac{P}{K} = 3.39 \text{ in. (0.08611 m)}$$

The displacement response of the mass M calculated by the modal superposition method is shown in Figure 6. During the last four cycles, the amplitude of the steady state displacement response varies from 3.3927 in. (0.08617 m) to 3.2952 in. (0.08370 m). The frequency content of the response is 2.5047 Hz—approximately equal to the excitation frequency of 2.5018 Hz.

Case 2. For this case, the frequency ratio ω/ω_n is equal to 0.8 and the force ratio $F/P = 0.4$. From the amplitude diagram for $\zeta = 0.5$ (Figure 12 in Reference [13]), the magnification factor is 0.6. The amplitude A of the steady state response is given by

$$A = 0.6 \cdot \frac{P}{K} = 0.15 \text{ in. (0.00381 m)}$$

The displacement response of the mass M calculated by the modal superposition method is shown in Figure 7. During the last cycle, the amplitude of the steady state displacement response varies from 0.1448 in. (0.00368 m) to 0.1455 in. (0.00369 m). The frequency content of the response is 2.4956 Hz. It should be noted that during each cycle, the response curve has a flat portion near its peaks. No sliding takes place in this flat portion. This

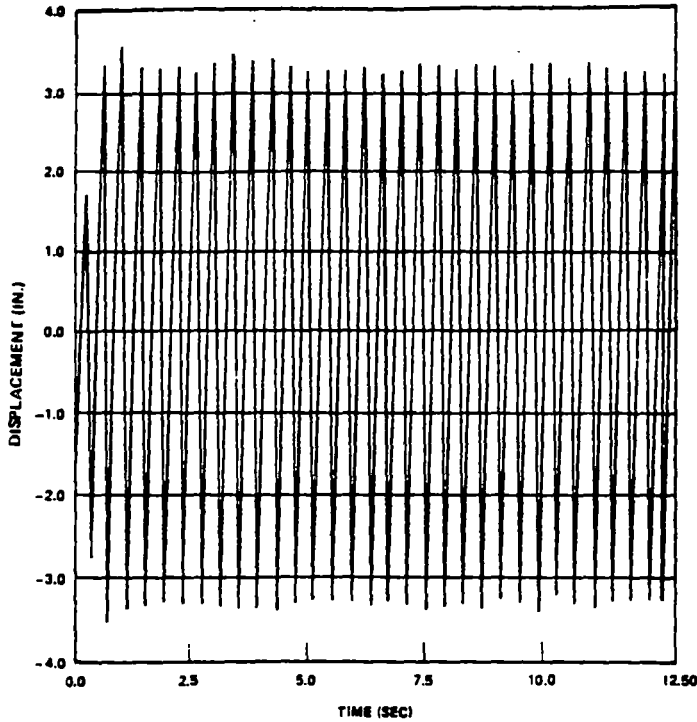


Fig.6 Displacement response of a spring-mass system with combined Coulomb and viscous damping, $\omega/\omega_n = 0.8$, $F/P = 0.2$ and $\zeta = 0.1$ (1 in. = 0.0254 m)

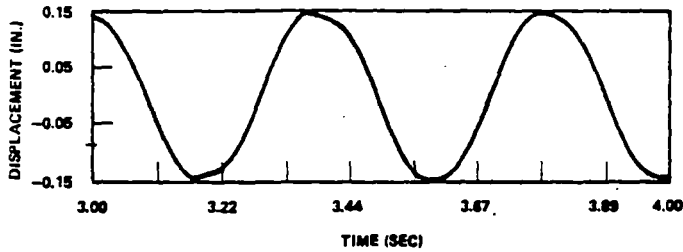


Fig.7 Displacement response of a spring-mass system with combined Coulomb and viscous damping $\omega/\omega_n = 0.8$, $F/P = 0.4$ and $\zeta = 0.5$ (1 in. = 0.0254 m)

particular characteristic of the displacement response is also predicted in Reference [13].

Test Problem 4. The transient dynamic response of a long platform supported freely on the ground and subjected to seismic excitation is analyzed in this problem. The platform is supported at both ends as shown in Figure 8. The platform is representative of the base of a spent fuel rack and its supports are representative of the support pads of the rack. A concentrated mass, m , is located at the center of the platform. There is a clearance between the mass and the platform along the horizontal direction, and the mass is free to move relative to the platform. During a seismic event, the mass may collide with the platform. The impact between the mass m and the platform is a simplified representation of the impact phenomena between the fuel assemblies and storage cells in a spent fuel storage rack.

This problem is solved by the direct integration and the modal superposition methods present in the WECAN program. Both methods use different friction elements. In the direct integration method,

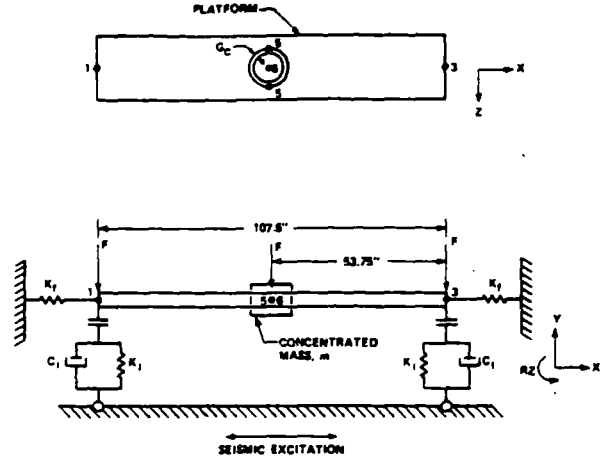


Fig.8 Finite element model of a long, freestanding platform. $F = 1288$ lbs, (5729.3 N), (1 in. = 0.0254 m)

the nonlinearity due to friction is handled by modifying the stiffness matrix. In the modal superposition method, the nonlinearity due to friction is handled by the pseudoforce approach as described in this paper. The impact between the mass m and the platform is modeled by a gap element [5,8] and is used with both methods. The platform properties are

Modulus of elasticity	=	2.8×10^7 lb/in. ²	(19.3×10^{10} Pa)
Length	=	107.50 in.	(2.731 m)
Cross-sectional area	=	60.6275 in. ²	(0.0391 m ²)
Area moment of inertia	=	5.70 in. ⁴	(0.237×10^{-5} m ⁴)
Density	=	1.5343×10^{-3} lb-s ² /in. ⁴	(42.47 kg/m ³).

The friction element properties used with the modal superposition method are

Normal spring stiffness (K_I)	=	8.351×10^5 lb/in.	(1.46×10^8 N/m)
Friction spring stiffness (K_f)	=	8.351×10^7 lb/in.	(1.46×10^{10} N/m)
GAP	=	1.0×10^{-6} in.	(-0.254×10^{-7} m)
Mass (M)	=	0.0 lb-s ² /in.	
Coefficient of friction ($\mu_s = \mu_d$)	=	0.8.	

The friction element used with the direct integration method has the same properties except the normal spring stiffness is 8.351×10^7 lb/in. (1.46×10^{10} N/m).

The magnitude of the concentrated mass, m , at the center of the platform is equal to 4.0 lb-s²/in. (1.8144 kg). The initial clearance G_c between the mass m and the platform is equal to 0.2145 in. (0.005448 m). The energy loss due to impact between

mass m and the platform is neglected. In the detailed documentation of this problem[14], the energy loss due to impact is taken into account. The deadweight of the platform is modeled by three concentrated forces acting at the Nodes 1, 3, and 5. The magnitude of each force is 1288.0 lbs (5729.3 N). The transient displacement response of the platform consists of only the x-component.

The platform is modeled with two two-dimensional beam elements. The finite element model has ten degrees of freedom; nine are associated with the platform and the tenth is associated with the concentrated mass m . The modal analysis of the platform gives ten natural frequencies and mode shapes. The first frequency is 0.0 Hz and is associated with the concentrated mass. The next six frequencies represent the bending mode shapes of the platform. The three highest frequencies are 990.9 Hz, 1323.0 Hz, and 1836.0 Hz and represent the axial mode shapes of the platform. A rigid body motion of the platform can be represented by the linear superposition of these three mode shapes.

Seismic excitation applied to the platform along the X-direction is shown in Figure 9. The platform may slide during the seismic analysis, and its displacement response consists of the rigid body motion superimposed on the elastic deformation. As explained earlier, the three axial mode shapes must be included in the modal superposition analysis to represent the rigid body motion.

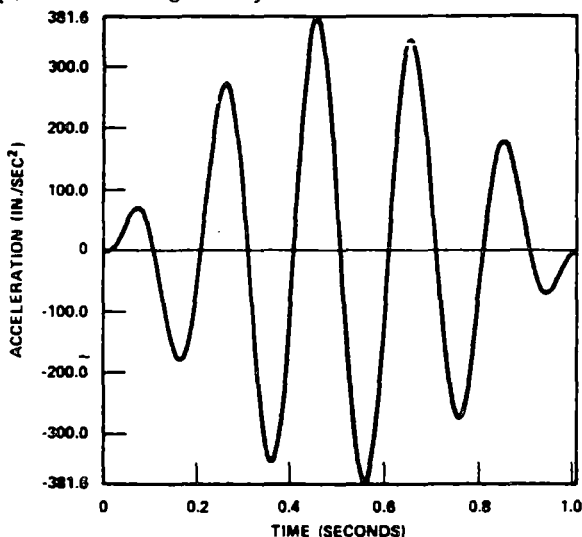
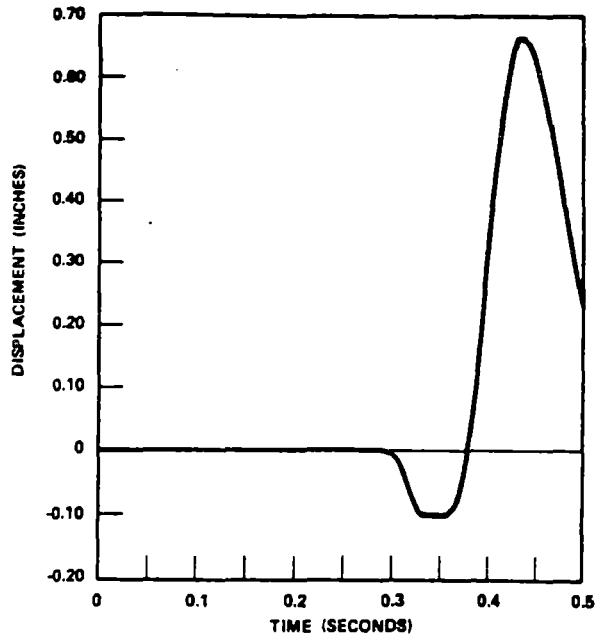
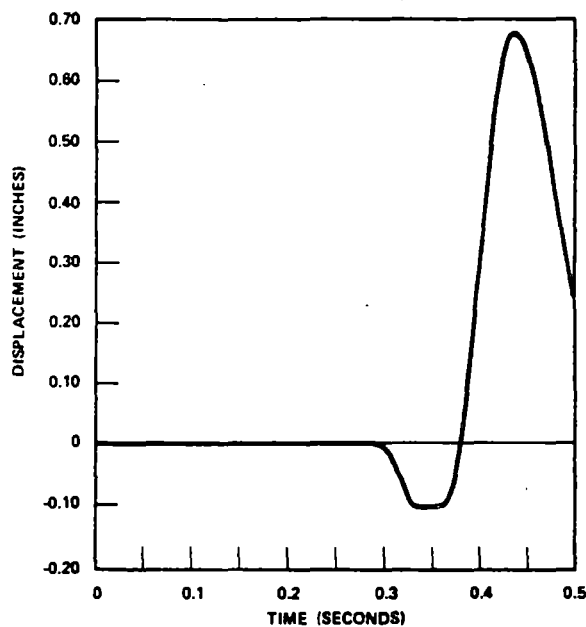


Fig.9 Acceleration time history applied to the freestanding platform in X-direction ($1 \text{ in}/\text{sec}^2 = 0.0254 \text{ m}/\text{sec}^2$)

Results of the modal superposition and the direct integration analyses are presented in Figures 10 to 13. All the mode shapes are included in the modal superposition analysis. The displacement response of Nodes 1 and 6 respectively, along the X-direction is shown in Figures 10 and 11. The time history of the friction force at Node 1 is presented in Figure 12. The time history of the impact force between mass M and the platform is shown in Figure 13. The comparison of time history results in Figures 10 to 13 show that the modal superposition method and the direct integration method give approximately the same results. The computer cost of using modal superposition method is found to be four times less than that of using the direct integration method[14].



(a) Modal superposition

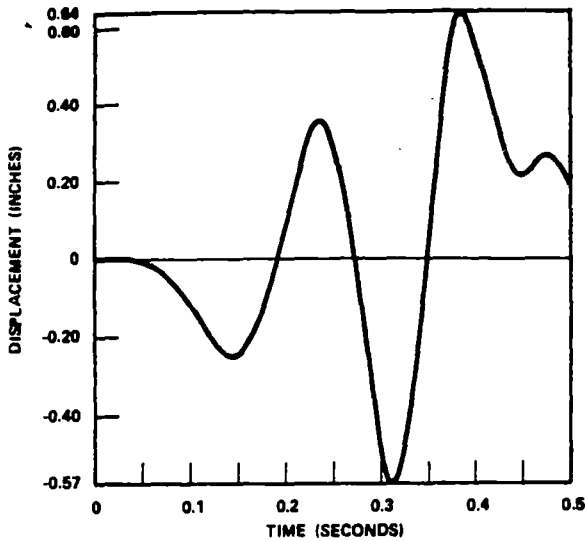


(b) Direct integration

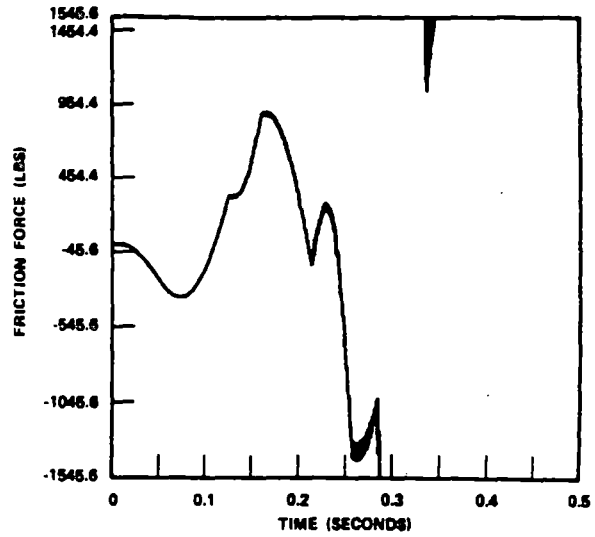
Fig.10 Displacement response of Node 1 along X-direction, Test Problem 4. ($1 \text{ in.} = 0.0254 \text{ m}$)

CONCLUSION

1. The modal superposition method may be used to analyze a structure with Coulomb friction.
2. The dynamic analysis of a structure with Coulomb friction requires that the mode shapes with higher frequencies be included so that the rigid body motion due to sliding of the structure is correctly represented.



(a) Modal superposition



(a) Modal superposition

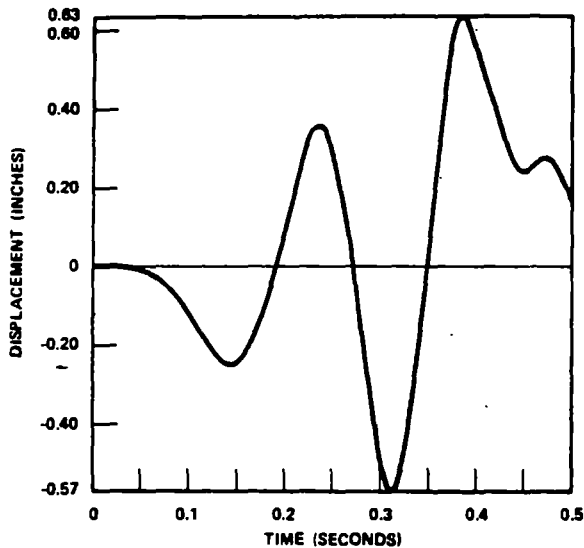


Fig.11 Displacement response of the concentrated mass m at Node 6 along X-direction (1 in. = 0.0254 m)

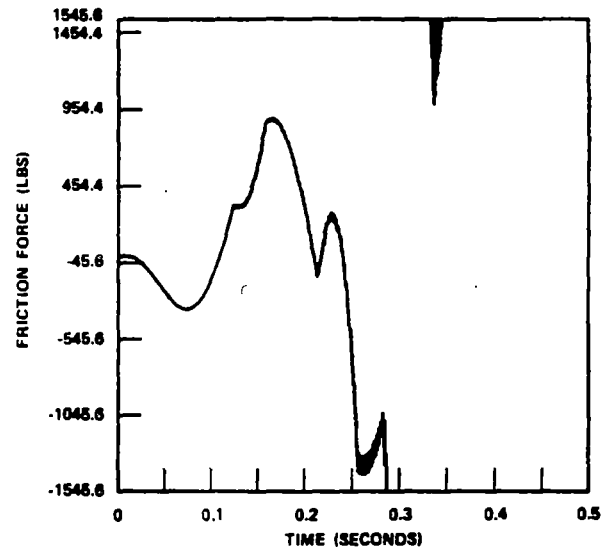


Fig.12 Transient response of the friction force at the left support of platform, element 1 (1 lb = 4.448 N)

3. The computer cost of using the modal superposition method is less than that of using the direct integration method to analyze a structure with Coulomb friction.

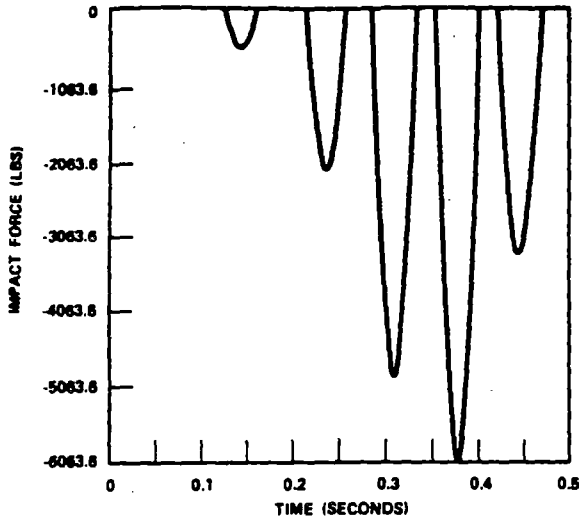
ACKNOWLEDGMENT

The authors wish to thank D. F. Miller for providing encouragement on this project and for suggesting Reference [13]. A. J. Kuenzel's assistance in solving the fourth test problem is also acknowledged.

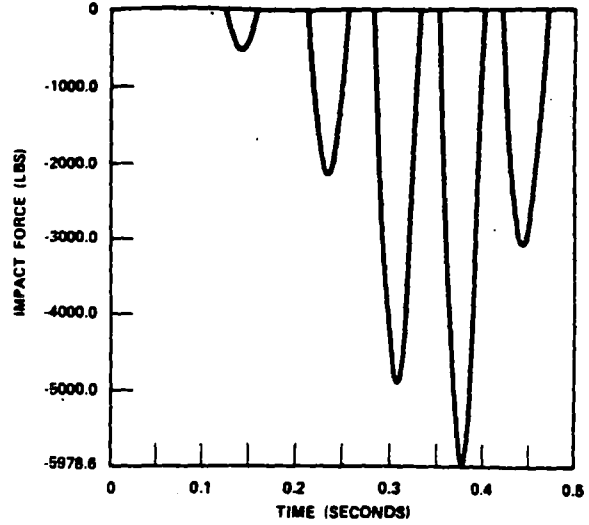
REFERENCES

Houbalt, J. C., "A Recurrence Matrix Solution for the Dynamic Response of Elastic Aircraft," Journal of Aeronautical Science, Vol. 17, 1950, pp. 540-550.

2. Chan, S. P., Cox, H. L., and Benfield, W. A., "Transient Analysis of Forced Vibrations of complex Structural-Mechanical Systems," Journal of the Royal Aeronautical Society, 66, 1962, pp. 457-460.
3. Nickle, R. E., "Nonlinear Dynamics by Mode Superposition," Computer Methods in Applied Mechanics and Engineering, 7 1976, pp. 107-129.
4. Stricklin, J. A., and Heisler, W. E., "Formulations and Solutions Procedures for Nonlinear Structural Analysis," Computers and Structures, No. 7, 1977, pp. 125-136.
5. Shah, V. N., Bohm, G. J., and Nahavandi, A. N., "Modal Superposition Method for Computationally Economical Nonlinear Structural Analysis," ASME Journal of Pressure Vessel Technology, Vol. 101, May 1979, pp. 134-141.
6. Molnar, A. J. Vashi, K. M., and Gay, C. W., "Application of Normal Mode Theory and



(a) Modal superposition



(b) Direct integration

Fig.13 Transient response of impact force on the concentrated mass m (1 lb = 4.448 N)

7. Pseudoforce Methods to Solve Problems with Nonlinearities," ASME Journal of Pressure Vessel Technology, May 1976, pp. 151-156.

8. Shah, V. N., and Hartmann, A. J., "Nonlinear Dynamic Analysis of a Structure Subjected to Multiple Support Motions," ASME Journal of Pressure Vessel Technology, Vol 103, February 1981, pp. 27-32.

9. WECAN User's Manual, ed. A. W. Filstrup, Westinghouse Research Laboratories.

10. Gilmore, C. B., "Seismic Analysis of Freestanding Fuel Racks". Submitted for presentation at 1982 Orlando Pressure Vessel and Piping Conference.

10. Biggs, J. M., Introduction to Structural Dynamic, McGraw-Hill, N.Y., 1964, pp. 245-248.

11. Tse, F. S., Morse, I. E., and Hinkle, R. T., Mechanical Vibrations, Prentice-Hall, 1963, pp. 175-178.

12. Timoshenko, S., and Young, D. H., Vibration Problems in Engineering, 3rd Edition, D. VanNostrand, 1955, pp. 92-95.

13. Den Hartog, J. P., "Forced Vibrations with Combined Coulomb and Viscous Friction", ASME Transactions, Vol. 53, 1931, pp. 107-115.

14. "WECAN, Westinghouse Electric Computer Analysis, Verification Manual," Westinghouse Research Laboratories.



The Society shall not be responsible for statements or opinions advanced in papers or in discussion at meetings of the Society or of its Divisions or Sections, or printed in its publications. Discussion is invited only if the paper is published in an ASME Journal. Requests for general publication upon presentation. Full credit should be given to ASME, the Technical Division, and the author(s). Papers are available from ASME for three months after the meeting.

SEISMIC ANALYSIS OF FREESTANDING FUEL RACKS

C.B. Gilmore

Senior Engineer

Nuclear Technology Division
Westinghouse Electric Corporation
Pittsburgh, Pennsylvania
Mem. ASME

ABSTRACT

This paper presents a nonlinear transient dynamic time-history analysis of freestanding spent fuel storage racks subjected to seismic excitation. This type of storage rack is structurally unrestrained and submerged in water in the spent fuel pool of a nuclear power complex, holds (spent) fuel assemblies which have been removed from the reactor core. Nonlinearities in the fuel rack system include impact between the fuel assembly and surrounding cell due to clearances between them, friction due to sliding between the fuel rack support structure and spent fuel pool floor, and the lift-off of the fuel rack support structure from the spent fuel pool floor. The analysis of the fuel rack system includes impacting due to gap closures, energy losses due to impacting bodies, Coulomb damping between sliding surfaces, and hydrodynamic mass effects. Acceleration time history excitation development is discussed. Modeling considerations, such as the initial status of nonlinear elements, number of mode shapes to include in the analysis, modal damping, and integration time-step size are presented. The response of the fuel rack subjected to two-dimensional seismic excitation is analyzed by the modal superposition method, which has resulted in significant computer cost savings when compared to that of direct integration.

INTRODUCTION

Various structures, systems, and components important for safety in nuclear power plants are designed to withstand the effects of earthquakes (seismic events) without loss of capability to perform their functions. In this paper, a seismic

analysis of one of these components, i.e., freestanding spent fuel storage rack, is presented. The primary functions of the freestanding spent fuel storage rack are to contain the spent fuel assemblies in a water-filled pool and protect the fuel assemblies from excessive mechanical loads.

The spent fuel storage rack consists of an array of individual storage cells made of stainless steel. The top of the storage cell is flared to facilitate insertion of the fuel assembly into the storage cell and precludes placing the fuel assembly in an inappropriate location. The inside dimension of the cell is such that clearance (a gap) exists between the fuel assembly and cell. The cells within a spent fuel storage rack are interconnected by top and bottom grid structures to form an integral module. The bottom grid structure is connected to a support plate which provides the level support surface required for the fuel assembly. Support screws (pads) attached to the support plate, via leveling pads, raise the rack above the pool floor, yet provide contact with it. The support pads also transmit loads from the fuel rack module to the pool floor. For some applications, the support pads are anchored to the pool floor by bolts which react to the seismic loads. Other applications require the fuel rack modules to be neither anchored to the pool floor nor braced to the pool walls; thus, giving rise to the "freestanding" fuel rack terminology. A typical freestanding spent fuel storage rack module is shown in Figure 1.

In the analysis of freestanding spent fuel storage racks, hereafter referred to as fuel storage rack(s), various factors are considered. First, the effects of water, in terms of frequency and forces,

3720
265

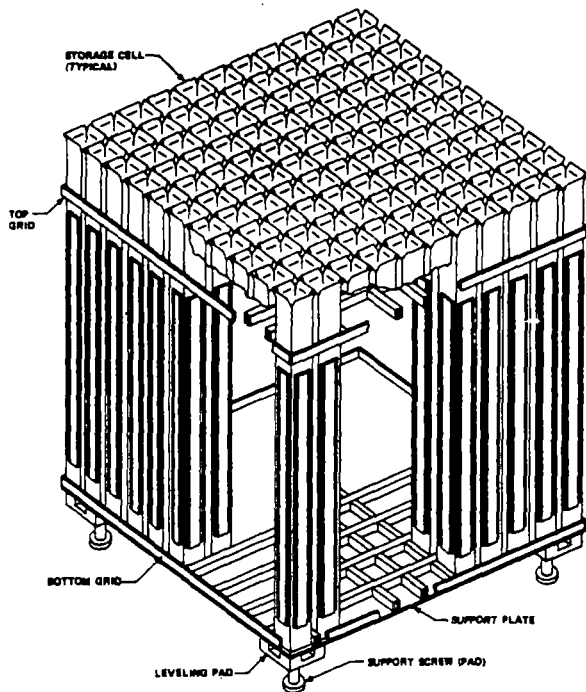


Figure 1 Typical Freestanding Spent Fuel Storage Rack Module

must be considered. During seismic excitation, the fuel assembly and cell respond, accelerating the surrounding fluid. The accelerating fluid in return induces an added mass effect on the two structures. Secondly, the presence of nonlinearities in the fuel rack system (fuel rack structure and fuel assembly) are considered. Sources of nonlinearities in the fuel rack system include geometrical nonlinearities (impact) and a combination of material (friction) and geometrical nonlinearities (impact). These nonlinearities are located at the fuel assembly grid/nozzle-cell interface (impact) and rack support pad-pool floor interface. The nonlinearities at the later interface consists of Coulomb or friction damping due to sliding and impact due to support pad lift-off. The possible sliding and impact phenomena which may occur at the support pad-pool floor interface result from coupled, horizontal, and vertical fuel rack system response.

Due to the highly nonlinear characteristics of the fuel rack system, a nonlinear, transient, dynamic, time-history analysis is required. For nonlinear analysis, direct integration methods are widely used; however, the computer cost for seismic analysis of structures employing large finite element models is very high. To reduce the computer cost, the modal superposition method found in WECAN(1) is applied. The nonlinear behavior due to impacting of fuel assembly and cell is modeled using a gap element(2). The friction element presented in Reference (3) is used to model the nonlinear behavior due to lift-off and/or sliding of the support pad relative to the pool floor. Verification of the modal superposition method for structural problems with nonlinearities due to impacting components and Coulomb friction is demonstrated in References (2) and (3).

The methods described herein include analytical techniques used for determination of hydrodynamic mass and acceleration time-history excitation. Dynamic modeling considerations, i.e., initial status of nonlinear elements, number of mode shapes to include in the analysis, modal damping, and integration time-step, are discussed. The nonlinear response of the fuel rack system subjected to two-dimensional seismic excitation is presented. The use of the modal superposition method has resulted in significant computer cost savings when compared to that of the direct integration method.

FUEL RACK SYSTEM DEFINITION

The data required to formulate the finite element model of the fuel storage rack consists of structural mass, structural stiffness, and hydrodynamic mass properties of the fuel rack system. The structural mass and stiffness properties of the fuel rack system are determined using well-known analytical techniques. Discussion concerning derivation of hydrodynamic mass for the fuel rack system is found as follows:

Fuel Rack System Hydrodynamic Mass

For this application, the fluid motion is considered to be described by incompressible potential flow, so that the dynamic fluid effect on the fuel rack system can be accounted for by hydrodynamic mass. Various sources for hydrodynamic mass can be found in the literature(4,5,6,7). Many of these sources have experimental data to substantiate the potential flow theory results. However, the cross-sectional geometry and/or bodies for which hydrodynamic mass is available, are quite simple. Due to the complexity of the fuel assembly geometry (an array of $N \times N$ rods), the finite element method discussed by Yu(8) is used to determine fuel assembly hydrodynamic mass.

The finite element model used to determine the fuel assembly hydrodynamic mass is shown in Figure 2. The 45-degree segment model shown in Figure 2 is for a 15×15 (rod array) fuel assembly. Because of the large number of elements involved in this model, substructure technique is used to generate the full model. The results obtained from this model include a full matrix (452 x 452 mass matrix) and a reduced matrix (2 x 2 mass matrix). The elements of the full mass matrix are the hydrodynamic mass coefficients and represent the inertia coefficients that give the forces on each body (225 rods and 1 cell) when the accelerations in two directions of each body are specified; namely, 452 degrees of freedom (DOF). The 2 x 2 matrix represents the hydrodynamic mass for two-body (fuel assembly and cell) motion in one direction with fluid coupling and is based on identical motion of all fuel rods in the fuel assembly rod array, relative to the cell.

The 2 x 2 hydrodynamic mass matrix is implemented in the fuel rack system model using a general, mass matrix, element. This technique models hydrodynamic mass effect on both frequency and force response of the fluid coupled bodies, as discussed by Fritz(9), and Stokey and Scavuzzo(10). System modeling of fuel storage rack module hydrodynamic mass coupling with the pool wall follows the method used for the fuel assembly. Hydrodynamic mass coupling between adjacent cells was found to have an insignificant effect on the response of the

3 7 2 0 2 6 6

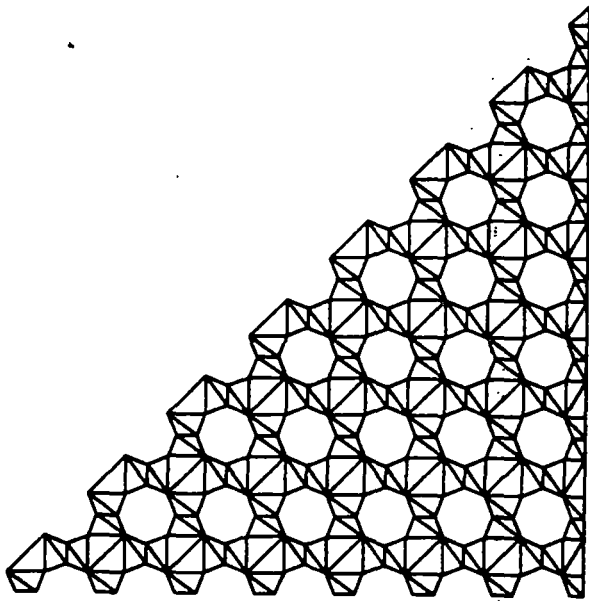


Figure 2 Finite Element Model (45 degrees segment) of 15x15 Fuel Assembly Used to Determine Fuel Assembly Hydrodynamic Mass

rack module. However, the mass of water between adjacent cells was taken as part of the structural mass of each cell.

ACCELERATION TIME HISTORY EXCITATION

The acceleration time history seismic excitation used in this analysis is developed using the design response spectra and damping values given in Regulatory Guides 1.60⁽¹¹⁾ and 1.61⁽¹²⁾, respectively. The seismic excitation is synthesized using spectrum amplification and suppression techniques per Reference (13). The 1940 El Centro earthquake record is the basis for the synthesized time-history excitation. The spectral characteristics of the synthesized time-history is similar to the original El Centro earthquake record. Consequently, statistical characteristics of the El Centro earthquake are maintained in the synthesized time-history excitation. The synthesized horizontal and vertical acceleration time-history excitation is shown in Figures 3 and 4, respectively.

FINITE ELEMENT MODEL OF FUEL RACK SYSTEM

The finite element model of the fuel rack system is shown in Figure 5. The fuel rack system model is composed of three-dimensional beams, three-dimensional springs, two-dimensional rotary springs, general matrix elements, gap elements, and friction elements. These elements are discussed in Reference (1).

The gap element^(1,2) is used to model the nonlinear behavior due to impacting of the fuel assembly and cell. The gap element is a combination of a spring and a dashpot (damper) in parallel, coupled to a gap in series. The friction element^(1,3) is used to model the friction interface (two surfaces) between the fuel rack support

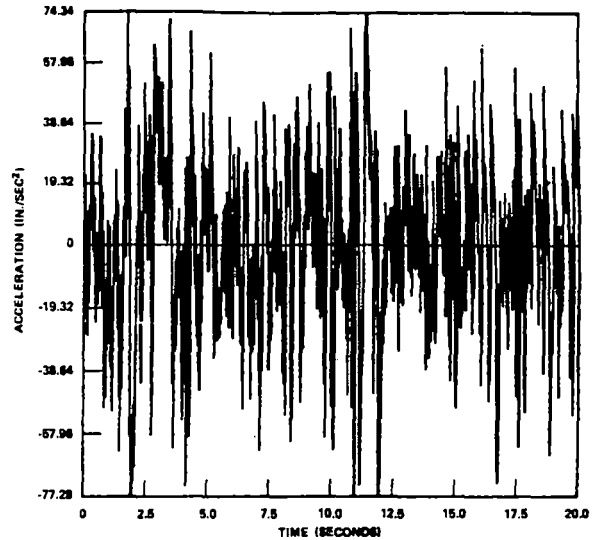


Figure 3 Synthesized Horizontal Acceleration Time History (1 In/Sec² = 25.4 mm/Sec²)

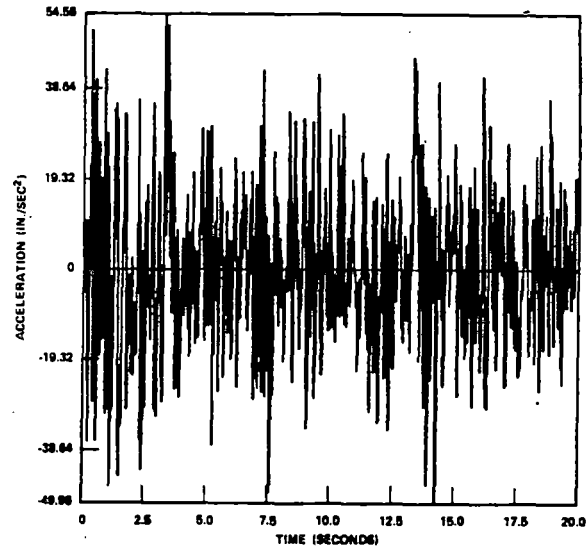


Figure 4 Synthesized Vertical Acceleration Time History (1 In/Sec² = 25.4 mm/Sec²)

pad and spent fuel pool floor. These two surfaces may slide relative to each other, separate from each other, and impact during the seismic event. The friction behavior is represented by a linear spring, hereafter referred to as friction spring. The purpose of the friction spring is to calculate the shear force at the friction interface.

The fuel rack system model shown in Figure 5 consists of 119 elements (99 linear elements and 20 nonlinear elements) and 60 unique nodes, which results in 339 gross DOF. Boundary conditions are imposed on 206 DOF. The remaining DOF's are specified in the ensuing modal and time-history analysis. The imposed boundary conditions are on all DOF's associated with the spent fuel pool wall, floor, and U_z, R_x, and R_y fuel rack system structural motion. Thus, the fuel rack module or system can slide only in the X-direction and respond

263

3720

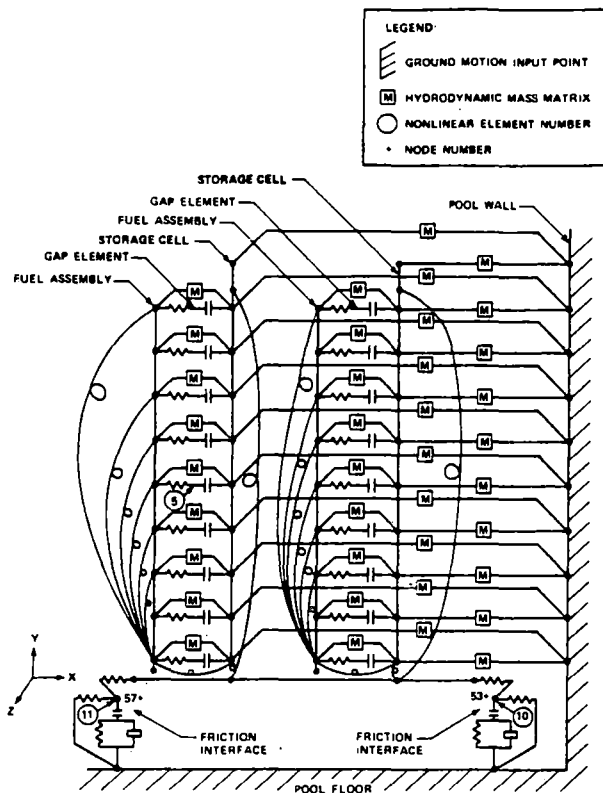


Figure 5 Finite Element Model of Fuel Rack System

two-dimensionally in the X-Y plane. The seismic excitation shown in Figures 3 and 4, which represents the motion of the pool wall and floor, is transmitted to the fuel rack structure via the friction and mass matrix (hydrodynamic mass coupling) elements.

To ensure that the spent fuel storage rack modules function during a seismic event, design requirements stipulate, in part, that the rack modules must be analyzed for any possible fuel assembly loading configuration. To satisfy this requirement, analysis is performed to simulate full, partially filled (half-full), and empty fuel assembly rack module loadings. The analysis to simulate the full fuel assembly rack module loading is based on the fuel rack system model shown in Figure 5. This model is a two-cell representation of a fully loaded rack module. The partially filled and empty fuel assembly loading configuration system model is derived from the model shown in Figure 5 by removing one and two fuel assemblies, respectively. This analysis also encompasses variations in friction coefficient μ_{\min} (0.2) $\leq \mu \leq \mu_{\max}$ (0.8) between rack module support pads and pool floor.

MODELING CONSIDERATIONS

In determining the transient dynamic response of a structure when using the modal superposition method in Reference (1), consideration must be given to the initial status of nonlinear elements, modal damping, mode shape selection, and integration time step. These considerations are discussed in detail in the following sections.

Initial Status of Nonlinear Elements

The status of the nonlinear elements, i.e., "open" or "closed", in a finite element model should be such that initially it represents the linear, reference state of the structure, as implied by Shah, et al.⁽²⁾ For some structures, with various preloads and nonlinearities, determination of the reference state may require a nonlinear static (iterative) analysis. However, for this application, the reference state of the fuel rack system is determined by inspection.

Prior to the seismic event, the fuel rack system is in static equilibrium, resting on the spent fuel pool floor. The support pads are preloaded due to weight of fuel assemblies and module, including buoyant effects. Clearance exists between the fuel assembly and cell since external forces are not acting on the system. Therefore, the initial state of the nonlinear friction and gap elements is "closed" and "open", respectively. Having defined the reference state of the fuel rack system, the natural frequencies and mode shapes associated with the linear system are calculated. As the nonlinear elements change status during the time-history analysis, changes in the natural frequencies and mode shapes associated with the linear system are represented by pseudoforces, as discussed in References (2) and (3).

Modal Damping

Different values of damping are specified for the elements which define the fuel rack system. Since the damping is not uniform in the system for a given natural frequency, it is called nonproportional damping⁽¹⁴⁾. For nonproportional damping, an additional computation is required to calculate equivalent modal damping coefficients to be used in the time-history analysis.

For this application, modal damping is assumed to be proportional to the strain energy in each element. This type of damping is used to represent the energy loss due to structural damping. The method presented by Whitman⁽¹⁵⁾ is used to calculate equivalent modal damping coefficients.

Mode Shape Selection

For the fuel storage rack system, consideration was given to the number of mode shapes to include in the analysis to achieve the correct deadweight and sliding (rigid body) solution. In the fuel rack system model, the weight is distributed uniformly throughout the structure (represented by mass times acceleration due to gravity). Thus, a portion of the structural weight (mass) is associated with each node in the system model. Since the vertical frequencies associated with these nodes are generally high, the higher mode shapes should be included to achieve the correct static equilibrium solution. To support this reasoning, a study was performed to determine the number of mode shapes required to achieve static equilibrium. The results of this study showed that 95 percent of the system mode shapes are required to achieve the correct static equilibrium support pad load.

In modeling the friction interface between the support pad and pool floor, the value for the friction spring stiffness is set high such that: a) small elastic deformation occurs in the friction spring prior to rigid body motion; and b) the lateral frequency response of fuel rack system is

not affected significantly (lowered) due to the friction spring (which is a flexibility between the support pads of the rack module and the pool floor and is included in the modal analysis of the fuel rack system). Note that the friction spring stiffness is not set so high that it governs the integration time-step used in the analysis. Since the mode shapes associated with the friction springs possess high strain energy and frequencies, these mode shapes must be included in the analysis to obtain the correct rigid body solution, as discussed by Shah and Gilmore⁽³⁾. Therefore, based on dead-weight and rigid body motion considerations, all mode shapes are included in the analysis.

Integration Time-Step

Using the time history excitation shown in Figures 3 and 4, with acceleration due to gravity added (superposed) to the vertical excitation, a study was performed to determine the integration time step required for converged results. This study utilized the partially filled fuel rack system model. This configuration was chosen because it is more sensitive to an integration time-step (due to stability considerations), as compared to the full and empty fuel rack system models.

Based on previous analyses, an integration time-step of $2.000 \cdot 10^{-4}$ sec. was used to calculate the rack response during the time interval $0.00 \text{ sec} < t < 1.95 \text{ sec}$. The rack response was calculated during this time interval to provide for: a) time for the fuel rack system to respond to the initial portion of the seismic event; and b) initial conditions for calculating rack response due to strong motion excitation ($1.95 \text{ sec} < t < 3.90 \text{ sec}$). Using the restart capability in Reference (1) from this point in the time-history excitation (1.95 sec), the integration time-step study is performed using integration time-steps of $\Delta T/6$ ($8.333 \cdot 10^{-4}$ sec), $\Delta T/8$ ($6.250 \cdot 10^{-4}$ sec), $\Delta T/12$ ($4.167 \cdot 10^{-4}$ sec), $\Delta T/25$ ($2.000 \cdot 10^{-4}$ sec), and $\Delta T/50$ ($1.000 \cdot 10^{-4}$ sec). ΔT is the time interval (0.005 sec) between successive points in the time history data.

Based on a comparison of support pad and fuel assembly force response versus integration time-step, the results indicate a converged solution is achieved (within 7 percent) using an integration time step of $2.000 \cdot 10^{-4}$ sec. Thus, the integration time-step of $2.000 \cdot 10^{-4}$ sec is used in the full, partially filled, and empty fuel rack system analyses.

FUEL RACK SYSTEM DYNAMIC RESPONSE

The fuel rack system dynamic response consists of spent fuel pool floor loads, fuel assembly-cell impact loads, and rack module displacements. As mentioned previously, the seismic analysis of the fuel rack system includes all possible fuel assembly loading configurations, as well as variations in friction coefficient, $\mu_{\min} < \mu < \mu_{\max}$. The results of this analysis indicate the maximum spent fuel pool floor loads, i.e., vertical and friction load, and fuel assembly-cell impact loads are derived from the full fuel assembly loading configuration, with maximum friction coefficient, μ_{\max} . The maximum rigid body, or sliding motion of the rack module was also determined from the full fuel assembly loading configuration; however, with minimum friction coefficient, μ_{\min} .

Figures 6 through 12 show plots of the typical fuel rack system response due to the two-dimensional seismic excitation. The response in these figures is obtained from the partially filled fuel rack system model during the time interval $9.75 \text{ sec} < t < 11.70 \text{ sec}$. The partially filled fuel rack system model is derived by removing the fuel assembly on the right side of the full fuel rack system model, shown in Figure 5.

Figure 6 shows the impact force response of element 5. Element 5 represents the interaction between the fuel assembly and cell. This element is located at the center of the fuel assembly and cell. The maximum impact force for this element is -260.3 lb (-1157.8 N), which occurs at 11.48 sec.

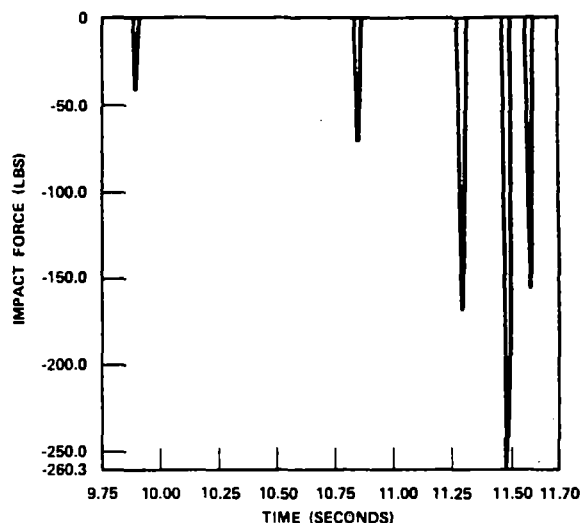


Figure 6 Fuel Assembly Impact Force at Element 5 for Time Interval $9.75 \text{ sec} < t < 11.70 \text{ sec}$ ($1 \text{ lb} = 4.448 \text{ N}$)

A plot of the vertical force on the pool floor from element 10 is shown in Figure 7. Element 10 represents the support pad on the right side of the fuel rack module. The minimum vertical force response for this element is 0.0 lb (0.0 N), which occurs during the time interval $11.50 \text{ sec} < t < 11.54 \text{ sec}$. The value of 0.0 lb (0.0 N) for the vertical force of this element indicates that this support pad lost contact (lift-off) with the pool floor. The vertical force on the pool floor from the support pad on the left side of the fuel rack module, element 11, is shown in Figure 8. The maximum and minimum vertical force response for this support pad is -2023.2 lb (-8999.2 N) and -830.7 lb (-3694.5 N), respectively. The minimum vertical force for element 11, -830.7 lb (-3694.5 N), indicates that this support pad does not lift off the pool floor. The maximum vertical force for element 11, -2023.2 lb (-8999.2 N), occurs at time $t = 11.52 \text{ sec}$, the time at which the support pad on the right side of the rack module has no contact with the pool floor. The vertical force response for the right (element 10) and left (element 11) support pads are out of phase with each other and are centered about the static equilibrium position of -570.0 lb (-2535.4 N) and -1400.0 lb (-6227.2 N), respectively.

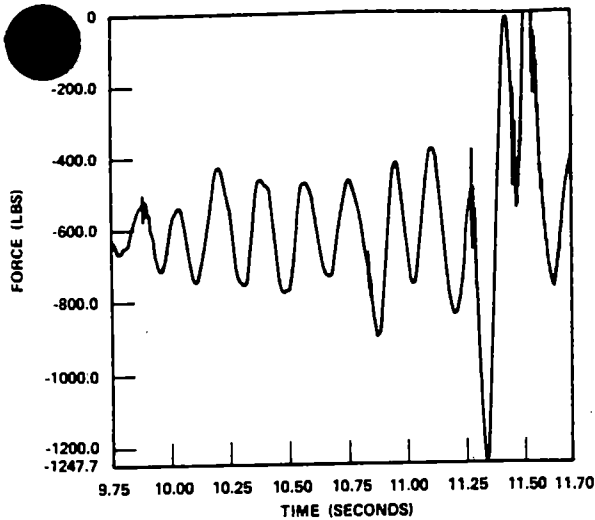


Figure 7 Vertical Force on Pool Floor from Support Pad, Element 10, During Time Interval 9.75 sec $< t < 11.70$ sec (1 lb = 4.448 N)

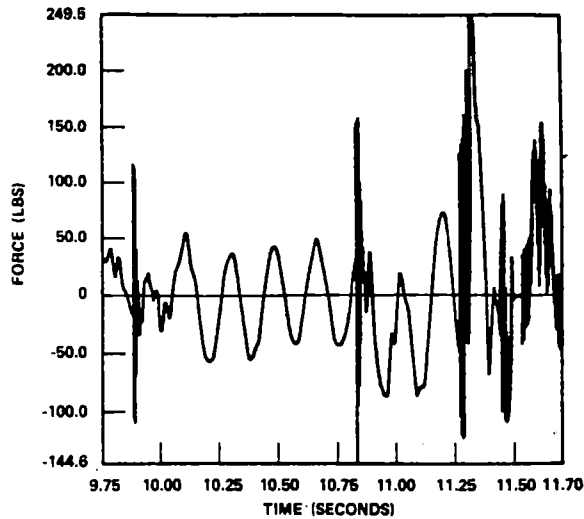


Figure 9 Friction Force on Pool Floor from Support Pad, Element 10, During Time Interval 9.75 sec $< t < 11.70$ sec (1 lb = 4.448 N)

the U_x response of node 53 indicate no sliding and sliding motion, respectively. Figure 10 shows that sliding motion of the support pad is initiated at times $t = 10.80, 11.27, 11.32, 11.38,$ and 11.52 sec. During the time interval shown in Figure 10,

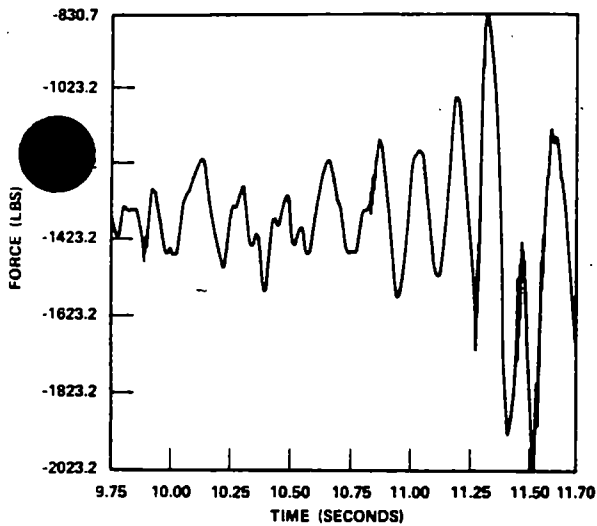


Figure 8 Vertical Force on Pool Floor from Support Pad, Element 11, During Time Interval 9.75 sec $< t < 11.70$ sec (1 lb = 4.448 N)

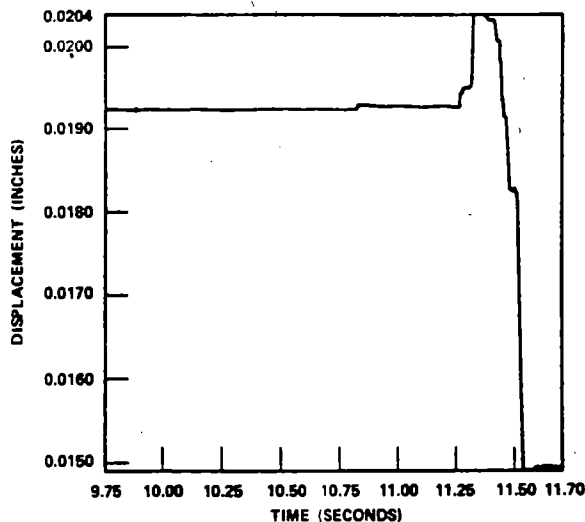


Figure 10 Lateral (U_x) Displacement of Support Pad, Node 53, During Time Interval 9.75 sec $< t < 11.70$ sec (1 In. = 25.4 mm)

The friction force on the pool floor from the support pad on the right side of the rack module, element 10, is shown in Figure 9. The maximum and minimum friction load on the pool floor is 249.5 lb (1109.7 N) and -144.6 lb (-643.2 N), respectively. During the time interval 11.50 sec $< t < 11.54$ sec, the friction force for this element is 0.0 lb (0.0 N). This follows from Figure 7, which shows the vertical force for element 10 to be 0.0 lb (0.0 N) during this time interval.

Figure 10 shows the lateral (U_x) displacement of node 53. Node 53 represents the support on the right side of the rack module (Figure 5). In Figure 10, horizontal and vertical lines for

the right support pad experiences maximum sliding motion of 0.0055 in. (0.1397 mm), from 0.0204 in. (0.5182 mm) to 0.0149 in. (0.3785 mm). The U_x displacement plot for node 57 is shown in Figure 11. Node 57 represents the support pad on the left side of the rack module (Figure 5). A comparison of Figures 10 and 11 shows nodes 53 and 57 to be in phase. The phase relationship between nodes 53 and 57 indicates that the rack module experiences rigid body sliding motion during the time interval shown.

A review of Figure 6 indicates that the fuel assembly impacts the cell at times $t=9.90, 10.85, 11.29, 11.48,$ and 11.61 sec. The impact of the fuel assembly with the cell at these times is indicated in the vertical and friction force response of the support pads as shown in Figures 7 through 9. Specifically, the impact between the fuel assembly and cell at time $t = 11.48$ sec results in lift-off of the support pad from the pool floor at time 11.55 sec. Comparison of Figures 6 and 10 indicates that rigid body motion of the support pad occurs as a result of the fuel assembly-cell impact. Thus, the results indicate that the fuel rack system response is significantly influenced by the structural interaction (impact) between the fuel assembly and cell.

COMPUTER COST

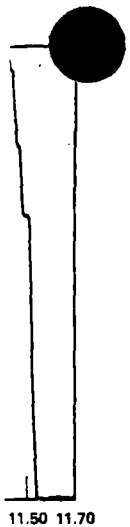
The response of the partially filled fuel rack system model (with rms wave front equal to 96.7) was calculated using the direct integration method⁽¹⁾. The computer cost, i.e., cost per integration time-step, of this analysis was compared to that of the modal superposition method, which included all (103) mode shapes in the solution. An integration time-step of $2.0 \cdot 10^{-4}$ sec was used for both analyses. The comparison showed the modal superposition method to cost less by a factor of 22.1 than that of the direct integration method. Only 0.8 percent of the modal superposition cost is associated with the modal analysis; i.e., calculation of natural frequencies and mode shapes. The cost advantage of the modal superposition method reported here makes use of the option in WECAN to bypass the calculation of the forces in the linear elements^(1,2).

CONCLUSIONS

1. The modal superposition method can be used to determine seismic response of detailed structures which have nonlinearities due to gap closure and Coulomb damping or dry friction between two sliding surfaces.
2. Mode shapes with high frequencies must be included in the analysis to represent static equilibrium (deadweight) and rigid body motion of the fuel rack system.
3. The maximum spent fuel pool floor loads and rigid body (sliding) rack module displacement result from the full fuel assembly loading configuration.
4. The fuel rack system response is significantly influenced by the structural interaction between the fuel assembly and cell.
5. Significant reduction in computer cost has been realized by using the modal superposition method in lieu of the direct integration method to determine dynamic response of freestanding spent fuel storage racks subjected to seismic excitation.

ACKNOWLEDGEMENTS

The author wishes to express his appreciation to Dr. V. N. Shah for his valuable comments in using WECAN Modal Superposition Method. Ms. C. Culbertson assisted in model development for determination of fuel assembly hydrodynamic mass. Mr. T. P. Murphy



Support Pad Vertical Force
 Peak Value: 9.75
 (.4 mm)
 Cause for
 Rack
 The maximum
 pad is
 for this
 pad has
 of Figures
 ical
 se.
 and lift-off
 the support



Support Pad Vertical Force
 Peak Value: 9.75
 (.4 mm)

of Hydrodynamic
ite Element
80-CP-117.

of [redacted] on the
ds," ASME, Journal
. 94, 1972, pp.

uzzo, R. J., "Normal
oncentric
No. 77-PVP-37.

ission, Directorate
ory Guide 1.60,
smic Design of
1, Dec., 1973.

ission, Directorate
ory Guide 1.61,
gn of Nuclear Power

rum-Compatible
CE J. Engr. Mech.
, (No. EM 2).

of Vibration with
Tewood Cliffs, N.J.,

ucture Interaction,"
Plants, (R. J.
ridge, Mass., 1970,



R. J. FRITZ
 Consulting Engineer,
 General Electric Co.,
 Schenectady, N. Y.
 Mem. ASME

The Effect of Liquids Motions of Immersed

It is known that the presence of liquids can immersed solids. This paper proposes a the dynamic analysis of moving systems in in incompressible, frictionless fluids. A u whether a fluid system may be considered j ment is also discussed. Experimental dai Formulas for hydrodynamic masses are tai

3 2 7 3

Introduction

WHENEVER solids move in contact with liquids, the liquids must be displaced to accommodate these motions. Fluid pressures are generated as a result. Fluid forces occur on these solids due to the integrated effect of these pressures. In this paper the case of moving solids completely immersed in frictionless, incompressible liquids is considered. In this case, the fluid force is usually proportional to the relative accelerations of the moving solids, and therefore gives rise to an effective or hydrodynamic mass. Where the liquids must flow dynamically in small passages, the hydrodynamic masses may be many times larger than the solid masses, even though the solids may be of large specific gravity. For such systems, dynamic analyses of the solid motions must consider the presence of the liquids in order to provide meaningful results. It is expected that the results of this paper would be found useful in the dynamic analysis of nuclear reactor and steam generator internals subjected to seismic shock as well as in the dynamic analysis of some fluidic devices, including fluidic shock absorbers.

The concept of the hydrodynamic mass has been described by Stokes [1], Lamb [2], Birkhoff [3], Patton [4], and others. These reports have generally considered the motion of a single body in a fluid. In this paper, existing information, particularly from Lamb [2], is applied to the dynamic analysis of systems with more than a single solid completely immersed in a liquid. The plan of presentation will be: (a) analysis of two-body motions with liquid coupling, (b) theory of multiple-body motion with liquid coupling, (c) experimental data on two-body motions

with liquid coupling degrees-of-freedom n

Two-Body Motions

Consider the case by a liquid annulus, surrounded by an outer radius b . The length l is greater than b . The inner cylinder is of radius a . The inner cylinder is assumed small compared to the outer cylinder (similar to motion):

$$V_r$$

where

$$V_r = \text{radial fluid velocity}$$

$$V_\theta = \text{tangential fluid velocity}$$

The fluid is considered incompressible and the cylinders are at rest. The potential ϕ will be

$$-\frac{\partial \phi}{\partial t}$$

$$-\frac{\partial \phi}{\partial t}$$

The continuity equation

A form of solution

Numbers in brackets designate references at end of paper. Contributed by the Design Engineering Division and presented at the Vibrations Conference, Toronto, Canada, September 8-10, 1971, of THE AMERICAN SOCIETY OF MECHANICAL ENGINEERS. Manuscript received at ASME Headquarters, June 11, 1971. Paper No. 71-Vibr-100.

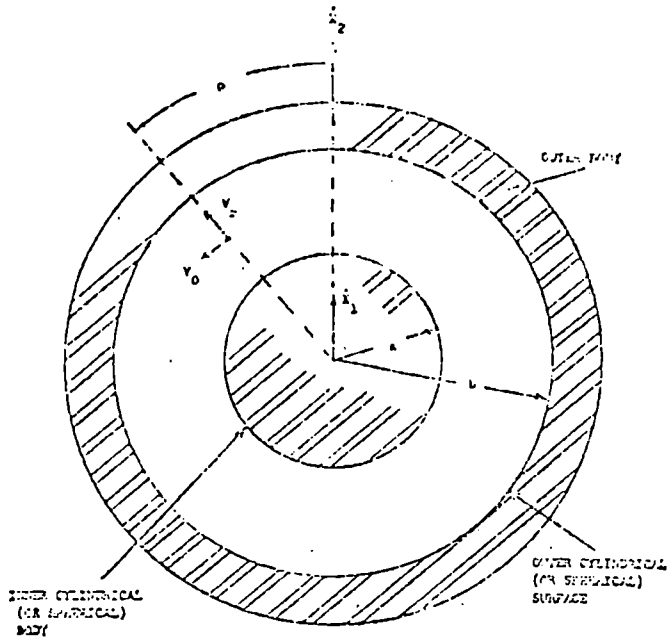


Fig. 1 Two-body motions with fluid coupling

From equations (4) and (5)

$$r^2 f'' + r f' - f = 0 \quad (6)$$

where the prime indicates differentiation with respect to r .

The solution of this equation is reasonably straightforward. The final solution is

$$V_r = \left(\frac{B}{r^2} - A \right) \cos \theta \quad (7)$$

$$V_\theta = \left(\frac{B}{r^2} + A \right) \sin \theta \quad (8)$$

where

$$B = \frac{b^2 a^2}{b^2 - a^2} (\dot{x}_1 - \dot{x}_2) \quad (9)$$

energy and may be called an inertial Lagrangian system. The fluid reaction force F_{ji} in such a system is given by Lagrange's equation

$$F_{ji} = - \frac{d}{dt} \frac{\partial T_f}{\partial \dot{x}_i} + \frac{\partial T_f}{\partial x_i} \quad (11)$$

where x_i are the generalized coordinates of motion and T_f is the fluid kinetic energy. In this paper x_i will generally be the translational motion of a solid body (body i), and F_{ji} will be the fluid reaction force on that solid body.

It is reasonable to neglect the contribution of the last term in equation (11) if the solid motions are assumed to be small with respect to fluid channel thicknesses. Such an assumption is made in this paper. Lamb [2] considers a few cases of single-body motion including the last term. Neglecting the last term of equation (11), the fluid reaction force is

$$F_{ji} = - \frac{d}{dt} \left(\frac{\partial T_f}{\partial \dot{x}_i} \right) \quad (\text{approximately}) \quad (12)$$

The fluid kinetic energy is

$$T_f = \int_a^b \int_0^{2\pi} \frac{1}{2} \rho r l dr d\theta (V_r^2 + V_\theta^2) \quad (13)$$

From equations (7), (8), (12), and (13)

$$F_{j1} = -M_{11} \dot{x}_1 + (M_1 + M_H) \ddot{x}_1 \quad (14)$$

$$F_{j2} = (M_1 + M_H) \dot{x}_1 - (M_1 + M_2 + M_H) \ddot{x}_1 \quad (15)$$

where F_{j1} and F_{j2} are the fluid reaction forces on the inner and outer cylinders, respectively, and

$$\begin{aligned} M_1 &= \pi a^2 l \rho = \text{mass of fluid displaced by the inner cylinder} \\ M_2 &= \pi b^2 l \rho = \text{mass of fluid that could fill the outer cylindrical cavity in the absence of the inner cylinder} \end{aligned} \quad (16)$$

$$M_H = M_1 \frac{b^2 + a^2}{b^2 - a^2}$$

For the case of concentric spheres separated by a frictionless, incompressible fluid (see Fig. 1), the fluid forces that result from a similar analysis are also given by equations (14) and (15) where F_{j1} and F_{j2} are the fluid reaction forces on the inner and outer spheres, respectively, and

$$M_1 = \frac{4}{3} \pi a^3 \rho = \text{mass of fluid displaced by inner sphere} \quad (17)$$

$$M_2 = \frac{4}{3} \pi b^3 \rho = \text{mass of fluid that could fill the outer spherical cavity in the absence of the inner sphere} \quad (17)$$

$$M_H = \frac{M_1 b^3 + 2a^3}{2(b^3 - a^3)}$$

Synthesis of Fluid Forces for Two-Body Problem

Equations (14) and (15) may be developed in a more general way. Consider the case where fluid motion is determined by the motion of immersed solids. Similar to Lamb [2, p. 158], the fluid kinetic energy is taken as a quadratic function

(10) the fluid kinetic energy may be considered as a quadratic function of \dot{x}_i . For the two-body problem

$$2T_f = A_{11} \dot{x}_1^2 + 2A_{12} \dot{x}_1 \dot{x}_2 + A_{22} \dot{x}_2^2 \quad (20)$$

From equations (12) and (20)

$$F_{j1} = -A_{11} \dot{x}_1 - A_{12} \dot{x}_2 \quad (21)$$

$$F_{j2} = -A_{12} \dot{x}_1 - A_{22} \dot{x}_2 \quad (22)$$

where again, F_{j1} and F_{j2} are the fluid reaction forces on solid bodies 1 and 2. The coefficients A will now be determined. Assume for this example that body 2 surrounds body 1, similar to the condition of the problem above for the cylinders and spheres. Now equations (21) and (22) are generally true for all values of \dot{x}_1 and \dot{x}_2 . If $\dot{x}_1 = \dot{x}_2$, then the fluid acceleration is \ddot{x}_i at every point in an incompressible fluid and a pressure gradient exists throughout the fluid due to the fluid inertia,

$$-\frac{\partial p}{\partial x_i} = \rho \ddot{x}_i \quad (23)$$

The pressure distribution gives rise to a buoyancy force of an Archimedes type, so that

$$F_{B1} = -(A_{11} + A_{12})\ddot{x}_1 = M_1\ddot{x}_1 \quad (24)$$

$$F_{B2} = -(A_{21} + A_{22})\ddot{x}_2 = -M_2\ddot{x}_2 \quad (25)$$

from which

$$A_{11} + A_{12} = -M_1 \quad (26)$$

$$A_{21} + A_{22} = M_2 \quad (27)$$

and

M_1 = the mass of fluid displaced by the inner body

M_2 = the mass of fluid that would fill the body 2 in the absence of the inner body

Equations (26) and (27) provide two relations. To evaluate the three unknowns A_{11} , A_{12} , A_{21} , a third relation is needed. Assume the containing body 2 to be static, $\ddot{x}_2 = 0$. From equation (21)

$$F_{B1} = -A_{11}\ddot{x}_1 = -M_H\ddot{x}_1 \quad (\text{defines } M_H) \quad (28)$$

As indicated, equation (28) defines the term M_H . M_H may be evaluated by assuming the body 1 to have a velocity \dot{x}_1 and by the continuity of flow, the fluid velocity distribution may also be evaluated. The fluid force may be evaluated using the conservation of momentum or by using equation (12), which results in

$$M_H = \frac{2T_f}{\dot{x}_1^2} \quad (\text{for } \ddot{x}_1 = 0) \quad (29)$$

where T_f is the fluid kinetic energy. Since the momentum relation will give the fluid pressure which must be integrated to obtain a fluid force on an immersed body, the use of equation (29) is usually simpler. From equations (21), (22), (26), (27), and (28), equations (14) and (15) follow. Thus, these relations which were derived from basic fluid mechanics are also obtainable by the method of synthesis described above.

The data in Table 1 are typical of some available information giving hydrodynamic mass relations where a single body is in motion and is surrounded either by an unbounded fluid initially at rest or by a static container. By use of the above procedure, these tabulated data are transformable into hydrodynamic mass relations where the single body is either surrounded by a moving container whose dimensions are large compared to the single body for the cases where a single body is shown in Table 1 or where the outer surface for Cases 8, 9, 10, 11, and 14 may be considered in motion.

The reader may note in equation (14) that when $\ddot{x}_1 = \ddot{x}_2$, the hydrodynamic mass M_1 is the displaced mass arising from buoyancy. The hydrodynamic mass M_H in equation (14) is associated with relative motion and may be considered an inertial squeeze-film effect. In general, the hydrodynamic mass can be considered to consist of these buoyancy and inertial squeeze-film components.

Multiple-Body Motions With Fluid Coupling

Where many bodies are immersed in a frictionless, incompressible liquid and are coupled by this liquid, the method of synthesis described above for the two-body problem should facilitate the determination of the hydrodynamic forces. This method is summarized for the multiple-body problem. From equations (19) and (22)

$$-F_f = AP \quad (30)$$

where F_f and P are $(n \times 1)$ column vectors and A is a square symmetric matrix $(n \times n)$. F_{fj} is the vector component of fluid force on each solid body where \ddot{x}_j is the instantaneous acceleration of the j th solid body. To determine the component of A , we observe that since equation (30) must be generally true, it must apply for any n -valued input vector P . We now assume first that

all \ddot{x}_j 's are equal. For this condition the fluid forces are usually easily determinable, similar to the two-body case already described. With these fluid forces determinable, n equations are established involving the components of A . There are $n(n+1)/2$ components of A which must be determined. The remaining equations may be established by setting all $\ddot{x}_j = 0$ except one, \ddot{x}_j , and letting $j = 1$ to n . The values of the fluid forces are most easily determined if only one body at any one time is allowed to move. It is suggested that these fluid forces would be determined from the continuity of flow and by use of equation (12). Although it is difficult to predict all the possible configurations that may be met in practice, it is suggested that in solving the continuity equation, some method of series and parallel flow impedances might be considered, analogous to an electric network analysis. Following this prescription, the components of the fluid mass matrix A in equation (30) are determined. These fluid forces are then considered along with other forces present, to arrive at the complete dynamic solution.

For the multiple-body problem the analyst may find it more convenient to synthesize the dynamic problem by considering the response of single channels. The pressure distribution of these channels can be written in terms of entrance and exit fluid velocities and channel wall motions determined by the motion of immersed solids. By considering continuity and momentum or continuity and Lagrange's equation, a series of equations result. The pressure distributions are then considered as elements of dynamic force generation in the equations of motion of the solids. An eigenvalue problem results, which can be solved to develop the solution for frequency and deflectional responses, given the necessary boundary conditions. In many cases, it may be necessary for a fluid specialist to work with the dynamics specialist to develop the solution for the complex fluid-solid problem.

In some cases, fluid compressibility acts in conjunction with fluid inertia or hydrodynamic mass to cause frequency modes largely due to the fluid. An example is a Helmholtz resonator formed by a tub sheet vibrating relative to an adjacent plenum. Oscillation of the tub-sheet must be accompanied by displacement of the fluid. This displacement can be accommodated by the compressibility of the adjacent fluid and by the flow through the tubes which causes an inertia effect. The author developed equations of motion for such systems by first assuming that compressibility was so low that only tube flow was important. The methods of analysis of this paper were then used to develop dynamic equations. Then, the tube flow impedance was assumed to be so high that compressibility effects predominated. In such a case it was easy to write the equation for a fluid spring. It was then an easy step to write a continuity requirement considering both effects. Another example of such a Helmholtz resonator which interacts with the mechanical system occurs in the analysis of violins.

The Effect of Fluid Damping

The preceding analysis assumes a frictionless fluid. The engineering designer must have some guidance to judge when a fluid may be considered frictionless. Some guidance is presented here.

The frictional pressure drop is assumed to be based on the Darcy friction factors, obtained from steady-flow data,

$$\Delta P = \frac{fL}{D_H} \frac{V^2}{2} \rho \quad (31)$$

where

ΔP = frictional pressure drop

f = Darcy friction factor

L = length of channel

V = channel velocity, assumed uniform in channel

ρ = fluid mass density

The effective linear damping coefficient b may be determined by setting $E_b = E_f$, with the result

$$b = \frac{2}{3\pi} \frac{fV_0 \rho L A}{c} \quad (36)$$

A parameter 2ξ may be defined where

$$2\xi = \frac{b}{M_f \omega} \quad (37)$$

and $M_f =$ fluid mass. 2ξ is the ratio of the damping impedance to the inertial impedance. ξ is similar to a fraction of critical damping for a one-degree-of-freedom system with linear damping b , mass M_f , and natural frequency ω . From equations (36) and (37) and with $M_f = \rho L A$,

$$2\xi = \frac{2}{3\pi} \frac{fV_0}{\omega c} \quad (38)$$

Further, if $V_0 = \omega r_0$, from equation (38)

$$2\xi = \frac{2}{3\pi} \frac{f r_0}{c} \quad (\text{turbulent flow}) \quad (39)$$

Equation (39) defines a dimensionless number, a damping parameter, that should provide a reasonable measure of the ratio of fluid friction to fluid inertia. We recall that in equation (39)

- 1 $f =$ the Darcy friction factor for turbulent flow
- 2 $r_0 =$ the distance that the fluid moves in an oscillatory cycle (amplitude of sinusoidal motion)
- 3 $c =$ the fluid channel spacing

A similar analysis for laminar flow through a parallel plate channel gives the result

$$2\xi = \frac{12\nu}{\omega c^2} \quad (\text{laminar flow}) \quad (40)$$

where

- 1 $\nu =$ fluid kinematic viscosity
- 2 $\omega =$ angular frequency of oscillatory motion
- 3 $c =$ fluid channel spacing

If the concept of this damping parameter 2ξ is reasonable, then the assumption of a frictionless fluid must require that 2ξ must be much smaller than 1. The quantity 2ξ will later be calculated for some test cases.

Fluid Compressibility

The preceding analysis assumed an incompressible fluid. Where the possibility of a fluid spring is present, it is usually a straightforward calculation to determine if the volume storage of a fluid spring will affect the continuity balance. The application of this paper is further restricted to cases of small Mach number (less than about 10 percent) and cases where the flow channel length is small compared to the wave length for propagating vibratory disturbances (less than about 10 percent), in order to avoid the possibility of standing-wave effects.

Comparison to Test Data

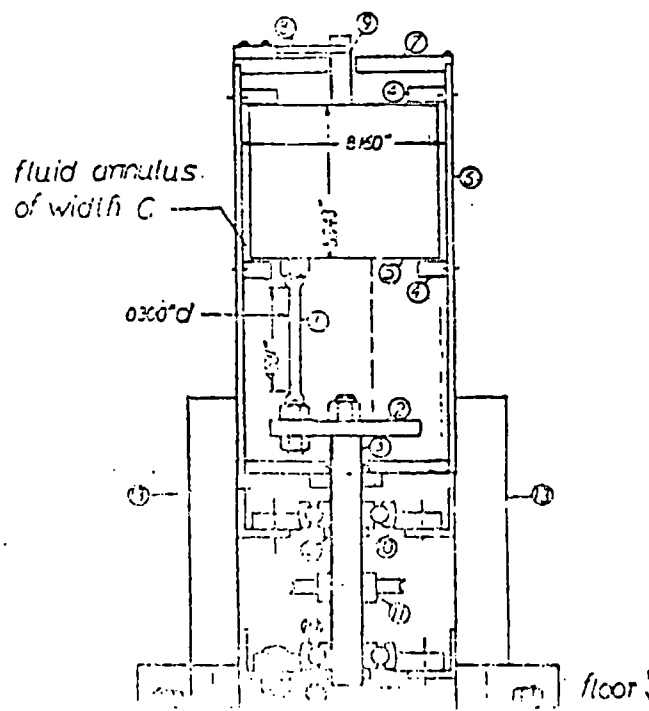
Keane's data. Keane [6] vibrated a circular cantilever tube surrounded by an annular cavity. The empty space was filled with a fluid, which made the test consistent with item 8 of Table 1 (due originally to Fisher [1]). Keane examined flexural vibrations and analyzed the cantilever beam with the added hydrodynamic mass. For one set of test, Keane's beam length-to-diameter ratio was 17 and b/a (in Fig. 9, Table 1) ranged

seemed to agree exactly with prediction. For other points of his graphed data, the variation between measured natural frequency and predicted natural frequency was typically less than 2 percent.

For $b/a = 1.2$ and a frequency of 29 cps, the maximum value of the Reynolds number during the vibratory cycle is estimated from Keane's data to be 24,000. Turbulence may be assumed to occur if the Reynolds number is greater than 3000. Thus, the water surrounding the beam can be considered turbulent. Relation (39) gives a value of 2ξ of 0.03, using a friction factor of 0.025. This friction factor is taken from Moody [7]. Since $2\xi = 0.03$ is much smaller than 1, the concept of this damping parameter would imply that the fluid could be considered essentially frictionless. The fact that the data on natural frequency agreed so well with theory would tend to validate the assumption of a frictionless fluid. The amplification in Keane's test was about 15 at resonance, which can also be considered as evidence that the overall inertial impedance is considerably greater than the overall damping impedance.

Data of Fritz and Kiss. Fritz and Kiss [8] reported the results of a test on a solid aluminum cylinder flexibly supported within a rigid cylindrical container. The equipment was vibrated on a shaker-table. The length-to-diameter of the cylinder was about 1.0. The cylinder was surrounded by a thin annular fluid which was free to flow axially as well as circumferentially. The natural frequency was taken as the frequency at which the vibrational amplitude of the cylinder reached its maximum value with a constant table amplitude. The axial and circumferential hydrodynamic masses were combined as shown in item 10 of Table 1. The natural frequency of the cylinder in air was 35.5 cps. With water surrounding the cylinder, the frequency was reduced to 17.0 cps, which gave very satisfactory agreement with the prediction of 16.9 cps.

In reference [8] the Reynolds number was estimated to be 4800 which was considered turbulent. The value of 2ξ is calculated from equation (38) to be 0.03, using the data from reference [8]: $f = 0.04$, $V_0 = 3.2$ fps, $\omega = 2\pi$ (17 cps), $c = 0.090$ in. Since 2ξ is much less than 1, the assumption of a frictionless fluid should be valid. This is validated in that the use of the hydrodynamic mass concept in reference [8] provided a very



accurate estimate of the natural frequency in the presence of the liquid.

Free Vibration of a Concentric Cylinder. A concentric cylinder assembly shown in Fig. 2 was available for test. An aluminum cylinder (part 5) is flexibly supported by column struts (part 1). The cylinder is surrounded by an annulus. Fluid leakage from the annulus is limited by close-clearance metal seals, parts 4. The motion of the cylinder was measured by use of a cantilever displacement gage, fitted with strain gages, part 8. The fluid annulus width c was varied by machining the cylinder diameter. Table 2 shows some numerical data from these tests. Fig. 3 shows some typical oscillograph records of the free vibrations taken during these tests. The vibrations with air and the glycerol solution were created by velocity-shocking the cylinder with a large mallet. The vibrations with water and oil were created by causing an initial large deflection.

The hydrodynamic weight was calculated from item 8, Table 1. The hydrodynamic weight was also calculated from the test frequencies. Due to the nature of the equipment it was felt that there was a small amount of leakage past the end seals which would cause the actual hydrodynamic weight to be smaller than the theoretical value. Even though the value of 2ξ was as high as 0.7, the calculated hydrodynamic weight was felt to be in reasonable agreement with the test values.

It is noted that this apparatus was also used to measure the hydrodynamic mass of a thin annulus around a rotating cylinder. The results were published in [11].

General Comments on These Comparisons to Test Data. The above comparisons to test data apply to the effect of the inertial squeeze film and the use of the damping parameter 2ξ . The phenomenon of the inertial squeeze film or, in other words, the virtual mass effect, was first predicted by Stokes [1], and has since been widely accepted. Therefore, confirmation of this effect is not new. However, both references [6] and [8] involve annular fluid spaces where the outer and inner boundaries of the fluid annulus both move. Both references [6] and [8] report forms of fluid motion equations (cf. equation (4.2.15) of [6] and equa-

Table 2 Calculations of 2ξ , relations (39) or (40), for equipment shown in Fig. 2

Radius in.	Annulus Clearance in.	Dynamic Frequency ω 10^{-3} in sec^{-1}	Liquid	Natural Frequency cps	ω_{22} (11)	ξ	2ξ	Actual Weight lbs.	Calculated Hydrodynamic Weight lbs.	Agreement to 100 %
1.0	.16	1.37	Water	770	10,000	.076	.15	70	100	100
1.0	.10	1.37	Water	570	43,000	.109	.22	75	100	75
1.0	.05	1.37	Water	475	30,000	.133	.27	80	100	67
1.0	.05	0.2	Glycerol solution	770	6,000	.126	.25	10	100	100
1.0	.05	1.37	Oil	570	260	0.22	.44	20	100	200

(1) $\omega_{22} = \text{Natural Frequency} = \sqrt{\frac{M_0 \omega_0^2}{M_0 + M_{22}}}$ where the cylinder deflection is $\frac{1}{2}$ and the fluid displacement is $\frac{1}{2} \left(\frac{c}{r} \right)$ at the angular frequency.

(2) Formula: $2\xi = \frac{2\gamma}{\omega} \frac{c}{r} \frac{1}{\omega_0} = \frac{2\gamma}{\omega} \frac{c}{r} \frac{1}{\omega_0} = 2(2) \xi = \text{Friction factor taken from L.P. Moody}^1 \text{ for smooth pipe}$
 Formula: $2\xi = 12 \nu / \omega c^2$

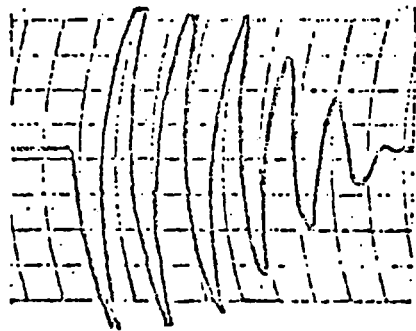
tion (1) of [8]) that are consistent with equation (14) of this paper. These equations for two-body motions presented in this paper connect buoyancy and inertial squeeze-film effects. Therefore, references [6] and [8] are consistent with the model presented in this paper. In references [6] and [8] the buoyancy term implied negligible effects on natural frequency, but did imply a significant effect on the predicted amplifications. This effect on amplification was specifically noted in reference [8].

References [6] and [8] do result in some confirmation of the models proposed in this paper. Admittedly, more confirmation is desirable. However, since the information of this paper is based on basic principles, it is expected that the equations will be accurate for the specified conditions.

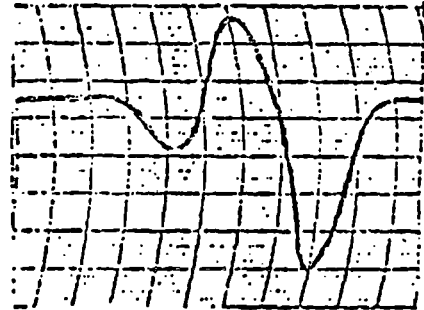
Comments of Multi-Degree-of-Freedom Dynamic Analysis

A salient feature of the most widely used multi-degree-of-freedom dynamic analyses of linear systems which are excited by some arbitrary base motion is the transformation of an arbitrary configuration of dynamic components into a decoupled array of simple oscillators which are excited by the base motion.

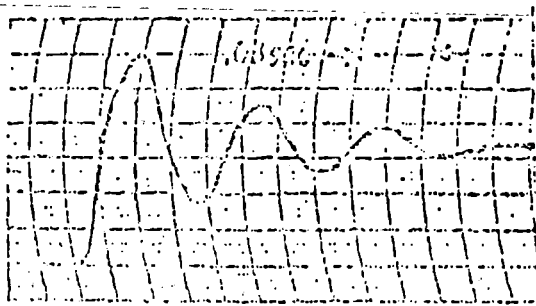
3 7 2 0 2 7 3



Air; $F = 266$ cpm



Glycerol solution; $F = 390$ cpm



Water; $F = 425$ cpm



10W-50 oil; $F = 330$ cpm

Fig. 3 Oscillograph records of free vibrations of inner cylinder $R = 6.0$ in., annulus clearance $C = 0.1$ in.

The motion of the complex array is then related to the motion of the simple oscillators. Many forms of this transformation have been reported in the literature in equations which are in cases applicable without dynamic coupling, that is, for the case where the mass matrix is diagonal in the dynamic equations. Correct transformations to be used for the case of dynamic coupling, where the mass matrix is nondiagonal, is given by McCalley in reference [9]. The methods of hydrodynamic analysis of this paper generally result in dynamic coupling and should therefore use McCalley's relations (or equivalent) when treating fluid effects in a multi-degree-of-freedom analysis.

SUMMARY

Some available relations are given in Table I for hydrodynamic masses for motions of a single solid body fully immersed in a frictionless incompressible fluid. This paper proposes a method of using these results for two-body motions. Where a single body is shown in Table I, the second body is considered large compared to the single body. For cases 8, 9, 10, 11, and 14 the outer surfaces may be considered in arbitrary motion. Some guidelines are proposed to establish the conditions of frictionless, incompressible flow. The case of motions of multiple immersed solids is considered. Comparisons to test data indicated favorable agreement.

References

- 1 Stokes, G. G., "On Some Cases of Fluid Motion," *Proceedings Cambridge Philosophical Soc.*, Vol. 8, May 1843, pp. 105-137.

- 2 Lamb, H., *Hydrodynamics*, 6th ed., Dover, 1933, ch. 6.
- 3 Birkhoff, G., *Hydrodynamics, A Study in Logic, Fact, and Similitude*, Princeton University Press, 1960, ch. 6.
- 4 Patton, K. T., "Tables of Hydrodynamic Mass Factors for Translational Motion," ASME Paper No. 65-WA/Unt-2.
- 5 Craudall, H., and McCalley, R. B., *Numerical Methods of Analysis, Shock and Vibration Handbook*, Vol. 2 (ed. C. M. Harris and C. E. Crede), McGraw-Hill, New York, N. Y.
- 6 Keane, J. A., "On The Elastic Vibration of A Circular Cantilever Tube in a Newtonian Fluid," PhD thesis, Carnegie Institute of Technology, Sept. 1963.
- 7 Moody, L. F., "Friction Factors for Pipe Flow," *Trans. ASME*, Vol. 66, 1944, pp. 671-684.
- 8 Fritz, R. J., and Kiss, E., "The Vibration Response of a Cantilevered Cylinder Surrounded by An Annular Fluid," KAPL-M-6539, Feb. 1966. (Available from Clearinghouse for Federal Scientific and Technical Information, U. S. Department of Commerce, Springfield, Va. 22151.)
- 9 McCalley, R. B., "Shock Analysis by Matrix Method, Notes for Short Course on Normal Modes," *Shock and Vibration*, Department of Engineering Mechanics, Pennsylvania State University, July 1966.
- 10 Private communication: items 12, 13 are due to J. H. Giermer, General Electric Co.
- 11 Fritz, R. J., "The Effects of an Annular Fluid on the Vibrations of a Long Rotor, Part 1—Theory; and Part 2—Test," *Journal of Basic Engineering*, *Trans. ASME, Series D*, Vol. 92, No. 4, Dec. 1970, pp. 923-937.
- 12 Kiss, E., "Analysis of the Fundamental Vibration Frequency of a Radial Vane Internal Steam Generator Structure," ANL-7685, *Proceedings of Conference on Flow-Induced Vibrations in Reactor System Components*, May 1970, Argonne National Laboratory, Argonne, Ill.

3720
27

Added Mass and Hydrodynamic Damping of Perforated Plates Vibrating in Water

D. F. De Santo

Senior Engineer (Dynamics),
Westinghouse Research and
Development Center,
Pittsburgh, Pa 15235
Mem. ASME

Experiments are described in which the fluid dynamic forces acting on perforated plates vibrating in water were measured. The test results are expressed in terms of added mass and hydrodynamic damping. Dimensionless formulas are presented which give accurate values for the added mass of the plates tested and which yield satisfactorily conservative lower bounds for the hydrodynamic damping force in both the linear and nonlinear (large-amplitude) damping range. The formulas for added mass and for low-amplitude damping apply to plates of any thickness that have any uniform square pattern of circular perforations. All of the results are general in that fluid density, viscosity, vibration amplitude, and frequency are all free parameters.

1 Introduction

The purpose of the investigation described in this paper is to determine the fluid-structure interaction effects of coolant liquid on the natural frequency and damping of vibrating perforated plates (such as lower core support plates), which constitute important components of nuclear reactor internals.

Natural frequency and damping are critical factors in determining the responses of reactor internals structures to various excitations including steady flow forces, pump pulsations, and seismic motions. Natural frequency is affected by the added mass associated with the inertia of the fluid that is forced to oscillate when the structure vibrates. Total damping is the sum of the hydrodynamic damping and the mechanical damping. Thus, it is necessary to evaluate the added mass and hydrodynamic damping when predicting and analyzing the vibratory responses and stresses of internals components.

Important information pertinent to the added mass and damping of perforated plates has been published in references [1 and 2], as well as in other sources. The scope of that information is limited, however, in that it is restricted to either single (mainly thin-plate) orifices, or to the linear small-amplitude regime, or to gases. The present investigation was motivated by the need to acquire reliable experimental data on configurations and conditions representative of reactor applications. These comprise:

- relatively thick plates having multiple perforations with adjacent holes spaced sufficiently close to each other to interact appreciably
- a liquid medium (water)
- large-amplitude vibrations in which nonlinear effects are important.

In this paper, the apparatus that was developed to measure the in-water added mass and hydrodynamic damping of perforated plates is described, and test results are presented in general dimensionless form. Semi-empirical formulas are given for computing the added mass and fluid damping of plates vibrating with arbitrary amplitudes and frequencies in fluids of arbitrary density and viscosity. Comparisons are made between the results of the present study and existing theory, showing close agreement over the entire amplitude range investigated in the case of added mass and, in the case of fluid damping, giving satisfactory correlation in the low-amplitude range within which the theory is valid.

2 Physical Bases of Added Mass and Hydrodynamic Damping

The term "added mass" refers to the apparent increase in the inertia of a solid object immersed in a fluid over its inertia in a vacuum, the in-fluid inertia being defined in terms of acceleration with respect to a fluid container that is fixed in inertial space. The added mass effect is a manifestation of the inertia of the fluid that must be set in motion as the immersed body is accelerated; the added mass is therefore proportional to fluid density. In the case of a perforated plate, the added mass can be very large compared with the mass of the plate itself if the total hole area is substantially less than the total (hole plus solid) plate area. Then, the flow must be accelerated to high velocities in and near the perforations as the plate moves through the fluid. This involves high inertia forces.

The added mass associated with an accelerating immersed body can be expressed in terms of the kinetic energy of the fluid

$$KE_f = \frac{1}{2} m_a V^2 \quad (1)$$

or

where m_a is the added mass and V is the velocity of a reference point on the body. Physically, the inertia force associated with the added mass consists of the resultant of fluid pressure forces acting on the body surface; this resultant force vector is collinear with and opposite in sense to the body acceleration vector. In the case of a rigid perforated plate accelerating normal to its plane, the difference in fluid pressures determined a short distance away from the plate surface on either side provides an accurate measure of the added mass. (See Sections 3.2.1 and 4.1.)

The term "hydrodynamic damping" is used to signify mechanical energy dissipation associated with the motion of a solid through a fluid. The hydrodynamic damping force is a drag force that is velocity-dependent rather than acceleration-dependent. In the case of a perforated plate, this force comprises not only the streamwise shear forces along the surfaces that are parallel to the direction of motion (i.e., the hole interior surfaces), but also the normal-pressure forces on the plate faces associated with flow separation and other energy-loss effects. These normal-pressure and shear forces are in phase with velocity and act in a sense opposing the plate motion. They are ultimately due to fluid viscosity, and at relatively low velocities are proportional to the square root of the viscosity. (See Section 4.2.)

3 Test Apparatus and Procedure

3.1 Experimental Model. A sectional drawing of the experimental model used in this investigation is shown in Fig. 1. In the model, a perforated plate is mounted on a rod sup-

ported by flat guide springs so that parallel guided motion of the plate "piston" is achieved. Sinusoidal oscillation of the plate is produced by an electromagnetic shaker; the amplitude and frequency of the plate motion are measured with a calibrated accelerometer. Different resonant frequencies can be obtained by using different titanium tuning springs.

Where the rod penetrates the end wall of the chamber in which the plate vibrates, a metal bellows is used to seal against leakage of fluid around the rod. An identical bellows is used on the other side of the plate, so that as the rod is translated, the volume source effect of the expanding bellows is compensated exactly by the volume sink effect of the other bellows. This circumvents the large springlike force (opposing the motion) which would exist if an unsymmetrical bellows arrangement were used.

The radial clearance between the edge of the plate and the inside diameter of the cylindrical chamber is about 100 microns, which is sufficient to guarantee freedom from rubbing and from any significant damping effect due to shear stresses developed in the fluid in the annulus. This, together with the guide spring design employed, the use of low-damping bellows seals, and the mounting of the model on a massive 71 cm x 71 cm x 5 cm steel spring-supported seismic base, assures that the extraneous (i.e., mechanical) damping is of a sufficiently lower order of magnitude than the hydrodynamic damping being measured.

Stainless steel and brass are used for all wetted parts, to avoid corrosion problems.

Three plates were tested. These are shown in Fig. 2. Plate 1 is a quarter-scale partial model of the orifice portion of a pressurized water reactor lower core support plate. Plate 2 has

Nomenclature

<p>A = cylinder area = $A = \pi D^2/4$</p> <p>A_b = effective piston area of one bellows seal</p> <p>A_h = hole area plus annulus area</p> <p>A_p = effective solid area of plate = $A_p = A - A_h - A_b$</p> <p>A_{p1} = $A_p = A - A_h = A_p + A_b$</p> <p>$b$ = pitch of holes in a square array</p> <p>c_f = fluid damping coefficient</p> <p>d = hole diameter</p> <p>D = cylinder diameter</p> <p>F = vibratory force applied by shaker</p> <p>F_f = hydrodynamic damping force</p> <p>f_n = natural frequency of vibration</p> <p>f_1, f_2 = frequencies (above and below the natural frequency f_n) at which drive force amplitude is stated multiple of value at natural frequency, for constant motion amplitude</p> <p>l = length of hole (thickness of plate)</p>	<p>l_{eff} = effective length of hole</p> <p>KE_f = kinetic energy of fluid motion</p> <p>m = mass of single-degree-of-freedom system</p> <p>Δm = mechanical mass increment</p> <p>m_a = added mass due to fluid inertia</p> <p>m_s = structural mass</p> <p>m_t = total mass = $m_t = m_s + m_a$</p> <p>N = number of cycles used to compute damping by decay method</p> <p>Δp = oscillatory differential pressure across plate vibrating in fluid</p> <p>Q = volume flow rate of fluid through open area of plate</p> <p>T = temperature of water</p> <p>V = absolute velocity of fluid in holes</p> <p>V_r = relative velocity of fluid in holes</p> <p>V_s = velocity of reference point on moving body</p> <p>x = displacement of plate (normal to its surface)</p> <p>\dot{x} = velocity of plate with respect to cylinder</p> <p>\ddot{x} = acceleration of plate with respect to cylinder</p>	<p>y_n = acceleration magnitude of first cycle of decaying vibration</p> <p>y_N = acceleration magnitude after N cycles of decaying vibration</p> <p>α = factor used in computing damping by bandwidth method (see equation (7) and Table 1)</p> <p>δ = log decrement damping</p> <p>δ_f = log decrement damping due to fluid</p> <p>δ_m = log decrement damping due to mechanical and windage losses</p> <p>δ_t = total log decrement damping: $\delta_t = \delta_f + \delta_m$</p> <p>$\nu$ = kinematic viscosity of fluid</p> <p>ρ = mass density of fluid</p> <p>ρ_s = mass density of structure</p> <p>ω = circular frequency of vibration</p> <p>ω_n = circular natural frequency</p> <p>$\omega_{n,air}$ = circular natural frequency in air</p> <p>$\omega_{n,water}$ = circular natural frequency in water</p> <p>$\omega_{n,\Delta m}$ = circular natural frequency with mass increment Δm</p>
---	---	---

3720 231

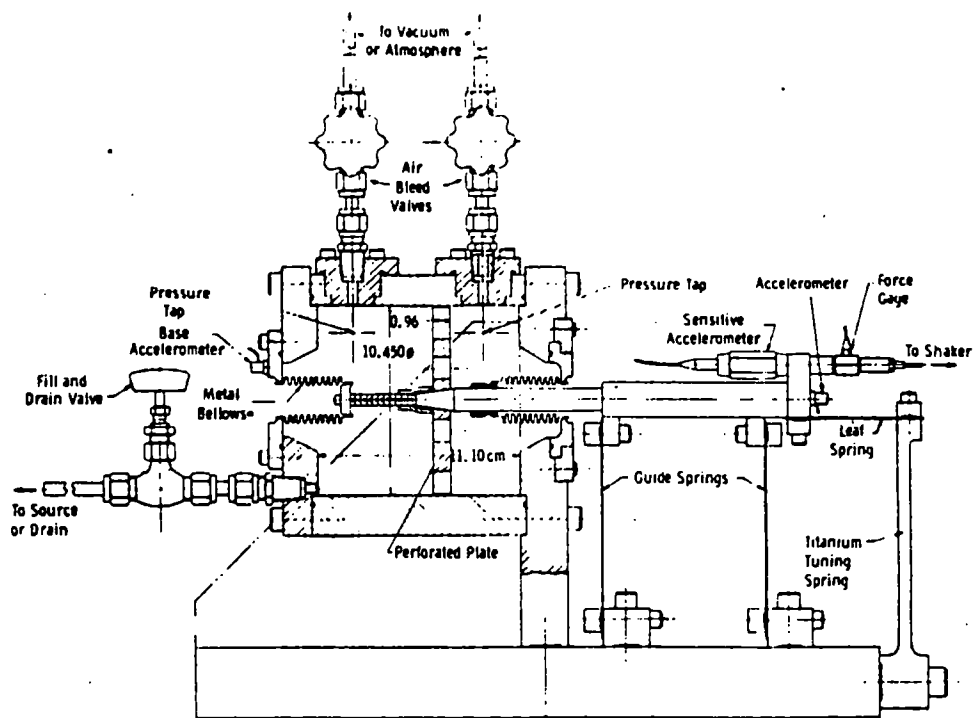


Fig. 1 Apparatus for determining added mass and hydrodynamic damping of perforated plates vibrating in water

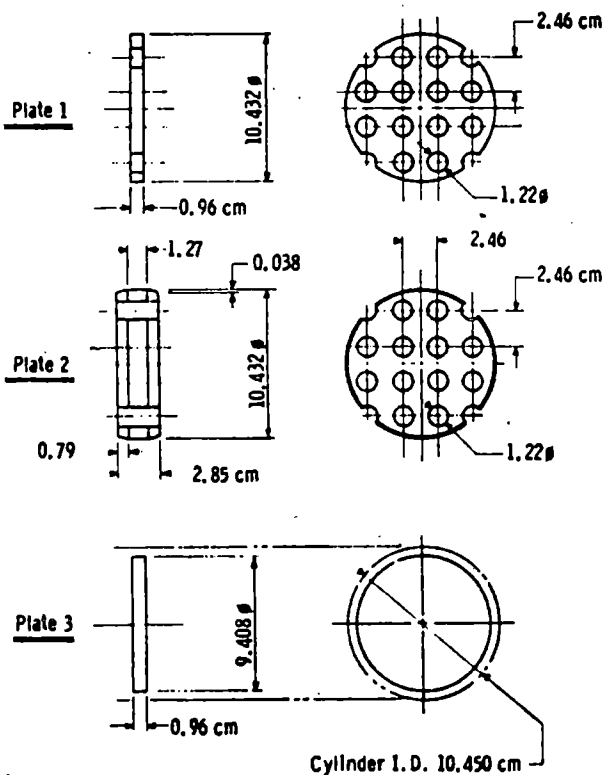


Fig. 2 Stainless steel plates used in experimental investigations of added mass and hydrodynamic damping

the same hole pattern as Plate 1 but is three times as thick; it was tested to determine the effect of hole length. Plate 3 is not perforated. Its diameter was specified to yield the same flow area between the plate outside diameter and cylinder inside diameter. All three plates are stainless steel, and in all cases the test fluid was water in room temperature.

Figure 3 is a photograph of the model.

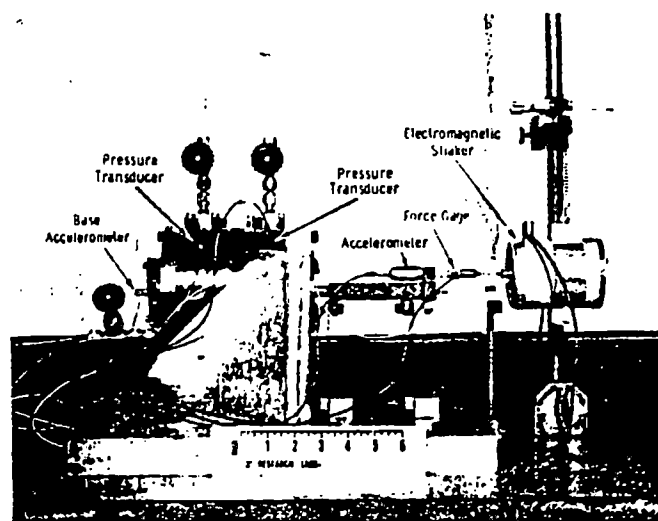


Fig. 3 Perforated-plate model test configuration with electromagnetic shaker drive

3.2 Test Procedure

3.2.1 Measurement of Added Mass. For each of the three perforated plates, the mass of the vibrating system was first determined in air. Then the apparent mass in water was determined. The added mass was found by subtracting the in-air value from the in-water value.

The vibrating mass m of a single-degree-of-freedom system¹ is given by

¹The perforated-plate model may be considered to be a single-degree-of-freedom system because the cylinder/base assembly is so much more massive than the perforated plate assembly that the base is essentially motionless. This was verified by measurements of the base vibratory acceleration.

$$m = \frac{\Delta m}{\left(\frac{\omega_n}{\omega_{n,\Delta m}}\right)^2 - 1} \quad (3)$$

where ω_n and $\omega_{n,\Delta m}$ are the natural frequencies of the system with and without the addition of an incremental mass Δm . Thus, if the natural frequency of the model is measured before and after attaching a known mass Δm to the moving platform, equation (3) can be used to compute the mass m . Performing the computation for the dry model and fluid-filled model yields the difference in apparent mass, or added mass.

Actually, since the stiffness is the same with air or water, attaching Δm need be done only for one model condition (full or empty). For example, if the incremental mass is used with the empty model the appropriate expression for the added mass m_a is

$$m_a = \Delta m \left[\frac{\left(\frac{\omega_{n,air}}{\omega_{n,water}}\right)^2 - 1}{\left(\frac{\omega_{n,air}}{\omega_{n,air,\Delta m}}\right)^2 - 1} \right] \quad (4)$$

where the subscripts have the obvious definitions.

In the experiments, a mass Δm of 190 g was used, and the natural frequencies were determined by varying the excitation frequency of the shaker until maximum motion of the plate (resonance) was obtained for a given applied force amplitude. The results of these experiments were verified by bump tests. Determinations were made at various natural frequencies of vibration, corresponding to different stiffnesses and masses of the system. Different amplitudes were also investigated.

The added mass was also determined by measuring the oscillatory differential pressure across the vibrating plate using two transducers flush-mounted in the cylindrical chamber wall a short distance from either side of the plate (Fig. 1). The value of added mass implied by the results of this type of test is given by

$$m_a = A_p |\Delta p| / |\ddot{x}| \quad (5)$$

where A_p is the effective solid area of the plate (cylinder area minus total open area minus the effective piston area of one bellows seal²), $|\Delta p|$ is the magnitude of differential pressure across the plate and $|\ddot{x}|$ is the magnitude of the plate acceleration (see Appendix).

3.2.2 Measurement of Hydrodynamic Damping. Three different methods were used to measure the damping of the plates in water at various vibration amplitudes and natural frequencies. These methods are described in the forthcoming. The first of these techniques was also used to measure the damping in air, so that allowance could be made for this relatively small nonhydrodynamic component of total damping when interpreting the in-water test results.

The *logarithmic decay* method was employed to determine the damping in air and at relatively low amplitudes in water. With the shaker disconnected, the movable platform of the model was given an impulsive motion by cutting a stretched string or striking the platform with a rubber mallet. From photographs of oscilloscope traces of the ensuing transient signal from the platform-mounted accelerometer, the logarithmic decrement δ was determined using the following well-known equation (see e.g., reference [3]):

²The effective piston area of each of the two bellows seals used in the experiments is 3.48 cm².

Table 1 Bandwidth method for determining damping at constant vibration amplitude.

Drive Force Amplitude dB up	3	6	10	20dB
Drive Force Amplitude, Multiple of Value at Resonance.	1.414	2.00	3.16	10.0
α	1	$\sqrt{3}$	3	9.95

$$\delta = \frac{\pi(f_2 - f_1)}{\alpha f_n}$$

δ = damping (log decrement)

f_n = frequency at resonance

f_1, f_2 = frequencies (above and below f_n) at which the drive force amplitude is the stated number of dB above value at resonance

$$\delta = \frac{1}{N} \ln \frac{y_n}{y_N} \quad (6)$$

where

N = number of cycles

y_n = trace amplitude of the first cycle

y_N = trace amplitude after N cycles

The total damping δ_T is the sum of the mechanical damping δ and the hydrodynamic damping δ_h , all evaluated at the same frequency and amplitude of vibration.

A second method used to determine damping was the *bandwidth* method, in which the plate/rod/platform assembly was driven at constant vibration amplitude while the excitation frequency was varied. The frequencies f_1 and f_2 at which the drive force magnitude increased by a specified amount over the force at the resonant frequency f_n were recorded and the log decrement damping, δ , was calculated by

$$\delta = \pi(f_2 - f_1) / (\alpha f_n) \quad (7)$$

where α depends on the specified amount of force increase off resonance; see Table 1. In these tests the vibration amplitude was held constant by an automatic control system while the frequency was varied manually and the force measured by a piezoelectric force gage that coupled the shaker drive rod to the moving platform (Figs. 1 and 3).

A third method employed in the damping measurements was the *damping force* method, in which the logarithmic decrement damping was determined by measuring the magnitude of the drive force, $|F|$, at resonance at given magnitudes of plate vibratory acceleration, $|\ddot{x}|$. The equation used was

$$\delta = \pi |F| / (m |\ddot{x}|) \quad (8)$$

Both the bandwidth method and the damping force method are useful in cases where the damping is strongly dependent on amplitude, as was found to be the case in water except at very low amplitudes. The decay method is particularly good when the damping is low and not too nonlinear.

4 Discussion of Test Results

4.1 Added Mass. Results obtained for the three plates

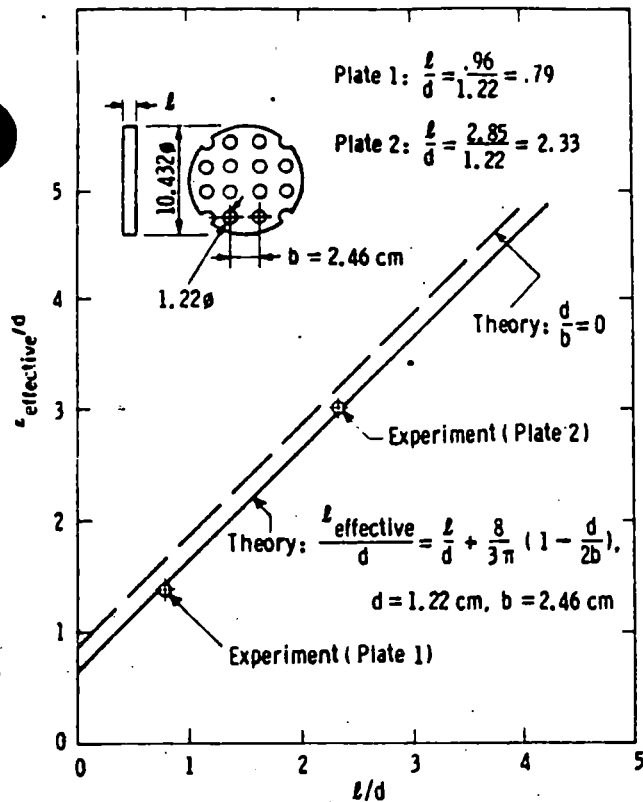


Fig. 4 Values of $l_{\text{effective}}/d$ used for determining added mass of a perforated plate vibrating in fluid

using equation (4) are shown in Table 2.³ Because of the greater amount of water in the longer holes of Plate 2 compared with Plate 1, the added mass of Plate 2 is greater.

The volume flow rate of water through the open area of the plate is

$$Q = (A_c + A_h) \dot{x} \quad (9)$$

where A_h is the total open area (hole area plus annulus area) and \dot{x} is the plate velocity relative to the cylinder. The average velocity V_r (relative to the plate) of the water in the holes is

$$V_r = Q/A_h \quad (10)$$

The absolute velocity is

$$V = V_r - \dot{x} \quad (11)$$

or, using equations (9) and (10),

$$V = A_c \dot{x}/A_h \quad (12)$$

Representing the moving fluid by a volume of cross section area A_h and effective length l_{eff} , we can express its kinetic energy as

$$KE_f = \frac{1}{2} \rho A_h l_{\text{eff}} V^2 = \frac{1}{2} \rho l_{\text{eff}} A_h^2 \dot{x}^2 / A_h \quad (13)$$

From equation (2) with V_r replaced by \dot{x} , and from equation (13) we obtain the following expression for the added mass

$$m_a = \rho A_h l_{\text{eff}} (A_c/A_h)^2 \quad (14)$$

From equation (14),

$$l_{\text{eff}} = \frac{m_a / (A_c/A_h)^2}{\rho A_h} \quad (15)$$

for any number of identical holes of length l and diameter d ,

equation (15) can be written in the following dimensionless form

$$l_{\text{eff}}/d = \frac{m_a / (A_c/A_h)^2}{\rho A_h d} \quad (16)$$

Equation (16) was used to compute values of l_{eff}/d for Plates 1 and 2. These are plotted in Fig. 4 for the values of l/d corresponding to the two plates (l is the plate thickness). Also shown in Fig. 4 is the theoretical relation between l_{eff}/d and l/d obtained when values of the test parameters are substituted in the following analytical expression (references [1 and 2]) for circular holes in a square array:

$$\frac{l_{\text{eff}}}{d} = \frac{l}{d} + \frac{8}{3\pi} \left(1 - \frac{d}{2b}\right) \quad (17)$$

where d/b is the diameter/pitch ratio. The agreement is seen to be very good.

Computations made using equation (15) and the added mass determined experimentally for Plate 3 yielded the value $l_{\text{eff}} = 2.57$ cm for this plate. This is 55 percent greater than the value 1.65 cm similarly computed for Plate 1, which has the same thickness (0.96 cm) as Plate 3 and has the same open area. The greater effective length for Plate 3 (i.e., greater added mass for the same effective solid area) implies that greater fluid kinetic energy is involved in pumping the water through a peripheral annular orifice than through distributed holes having the same total flow area. This is consistent with the fact that for circular holes, reducing the number of holes while keeping the total open area and the solid area (A_h and A_c) constant will cause d , l_{eff} , and m_a to increase (equations (17) and (14)).

4.2 Hydrodynamic Damping. In a number of cases more than one method was used to determine damping in the same amplitude and frequency range. In many of these cases the agreement between these results was very good and the values were averaged.

In other cases the results differed by as much as 20 percent. The reasons for these discrepancies are not known, but in view of the fact that damping is usually difficult to measure accurately and that experimental values generally exhibit considerable scatter (see, e.g., reference [1]), the present outcome is not surprising. The overall damping results are considered to be reliable.

(In all cases, the measured values of δ_f , the total damping in water, were corrected by subtracting out the nonhydrodynamic component, δ_s , of damping obtained from in-air decay measurements. This latter component comprises mechanical (spring plus bellows) and windage losses. It represents a relatively small correction, typically much less than 10 percent. Measured values of δ_f ranged from 0.0165 to 0.524, whereas δ_s ranged from 0.0016 to 0.0070.)

The damping results were transformed into non-dimensional form in accordance with the procedure of reference [1]. This comprised two steps. First, the hydrodynamic damping δ_f was expressed in terms of the dimensionless damping parameter $F_f / (A V_r \rho \sqrt{\nu \omega})$, in which F_f is the hydrodynamic damping force whose magnitude is given by⁴

$$|F_f| = m \omega_n |\dot{x}| \delta_f / \pi \quad (18)$$

the relative fluid velocity V_r is given by

$$V_r = \left(\frac{A_c}{A_h} + 1\right) \dot{x} \quad (19)$$

³For Plates 1 and 3, these results were confirmed by pressure measurements equation (5).

⁴The damping force magnitude $|F_f|$ is $|F_f| = c_f |v|$, in which the fluid damping coefficient c_f can be expressed as $c_f = m \omega_n \delta_f / \pi$ (see, e.g., reference [1]).

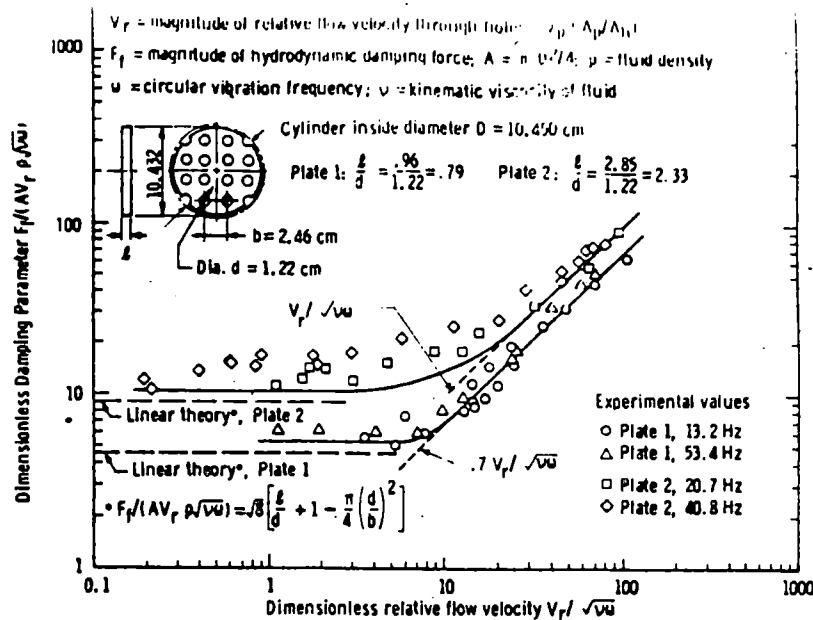


Fig. 5 Damping versus relative flow velocity through holes of perforated plates vibrating in water

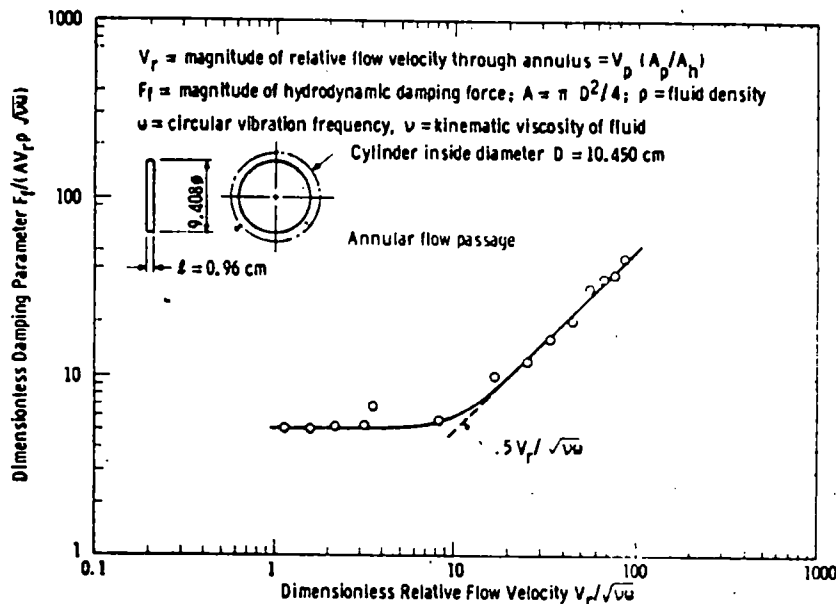


Fig. 6 Damping versus relative flow velocity through the peripheral annular clearance of a solid circular plate vibrating in water at a frequency of 50.45 Hz

in accordance with equations (9) and (10), A is the cylinder area, ω is the vibration frequency and ω_n the natural frequency, and ν is the kinematic viscosity of the fluid. The dimensionless damping parameter is then expressible as

$$F_f / (AV_r \rho \sqrt{\nu \omega}) = \frac{m \omega_n A_h \delta_l}{\pi A (A_r + A_h) \rho \sqrt{\nu \omega}} \quad (20)$$

Next, the amplitude of vibration was expressed in terms of the dimensionless amplitude parameter $V_r / \sqrt{\nu \omega}$ which in accordance with equation (19) can be written

$$V_r / \sqrt{\nu \omega} = \left(\frac{A_r}{A_h} + 1 \right) \dot{x} / \sqrt{\nu \omega} \quad (21)$$

The parameters given by equations (20) and (21) constitute the axes of Figs. 5 and 6, in which the experimental data are

plotted in dimensionless form.⁵ In this form the results are generally valid for plates of any size that are geometrically similar to those tested, and the results are valid for values of vibration frequency, fluid viscosity, and density different from the experimental ones. At low amplitudes the experimental results for the perforated plates, Fig. 5, are closely approximated by linear theory (references [1] and [2]), namely

$$F_f / (AV_r \rho \sqrt{\nu \omega}) = \sqrt{8} \left[\frac{l}{d} + 1 - \frac{\pi}{4} \left(\frac{d}{b} \right)^2 \right] \quad (22)$$

which gives slightly conservative results (the calculated damping values are about 15 percent lower than the measured

⁵ To determine values of the abscissa (dimensionless amplitude), the quantity $\omega \dot{x}$ has been substituted for x in equation (21).

Table 2 Measured natural frequencies and added masses of perforated plates

Plate No.	In-air Natural Frequency, Hz	In-water Natural Frequency, Hz	Added Mass, kg
1	15.05	13.15	0.45
	60.15	53.60	.45
	47.30	40.68	.99
	59.70	50.45	.70

values). The range of validity of the linear theory is about $V_r/\sqrt{\nu\omega} < 5$ for Plate 1 and $V_r/\sqrt{\nu\omega} < 3$ for Plate 2. Thus, for low amplitudes equation (22) is universal in that it applies to general square arrays of circular holes in plates of arbitrary thickness as well as arbitrary vibration frequency, fluid viscosity, and fluid density.⁶

Whereas at low values of $V_r/\sqrt{\nu\omega}$ the damping force is proportional to the first power of the velocity and to the square root of viscosity (equation (22)), at higher values of this parameter the damping force is proportional to the square of the velocity and is independent of viscosity. In this nonlinear range ($V_r/\sqrt{\nu\omega}$ greater than about 20), the experimental data are satisfactorily correlated by

$$F_d/(AV_r\rho\sqrt{\nu\omega}) = 0.7 V_r/\sqrt{\nu\omega} \text{ for Plate 1} \quad (23)$$

$$F_d/(AV_r\rho\sqrt{\nu\omega}) = V_r/\sqrt{\nu\omega} \text{ for Plate 2} \quad (24)$$

The values of the linear coefficients have been chosen to give slightly more conservative (i.e., lower) damping values than would be given by a least-squares fit. Unlike the linear regime, in the nonlinear regime there is no analytic expression giving the dependence of damping on l/d and h/d . Therefore for values of these two parameters significantly far outside the range investigated, accurate determination of damping require further testing.

Nondimensionalized damping results for Plate 3 are shown separately in Fig. 6. The damping is slightly lower than that of the perforated plate of the same thickness (i.e., Plate 1). Comparison of the results on an analytical basis is difficult because of the difference in shape of the flow openings. It may be noted, however, that the streamwise wetted area of Plate 3 is considerably less than that of Plate 1, which implies less drag from that source.

Results of reference [1] indicate that for single orifices in thin plates, the transition from the linear to the nonlinear viscosity-independent regime begins at a value of $V_r/\sqrt{\nu\omega} = 3$. This is in general agreement with the experiments reported here, as are the other general results of the reference [1] damping studies.

The experiments performed thus far have been restricted to the case of systems with zero steady flow component. Similar investigations of vibrating perforated plates in a flowing water system would be desirable; such tests would be considerably more complex than those performed up to now. With steady flow, the characteristics of the hydrodynamic damping can be expected to change significantly; specifically, the linear regime might disappear for steady flow velocities comparable to those in typical nuclear reactor applications. However, for configurations similar to those that have been tested, it is believed that the damping is likely to remain relatively low and that the effects of the steady flow on the added mass would not be great.

Results presented in reference [1] suggest that this and the other perforated-plate test results may be applicable to gases as well as to liquids.

5 Conclusions

- In the vibration of perforated plates typical of PWR internals, the added mass due to the water can be a significant fraction of the structural mass. The added mass can reduce the natural frequency to a value significantly below the in-air value.
- Measured values of the added mass m_a of the perforated plates tested in this study are accurately given by the following formula, which applies to uniform circular holes in square arrays:

$$m_a = \rho \frac{A_s^2}{A_h} \left[l + \frac{8d}{3\pi} \left(1 - \frac{d}{2b} \right) \right]$$

In this formula, ρ = fluid density, A_s = effective solid area of the plate, A_h = total open area, l = hole length (plate thickness), d = hole diameter, and h = hole pitch. No systematic variation of added mass occurred over the range of amplitudes and frequencies surveyed.

- The hydrodynamic damping of vibrating perforated plates comprises two regimes: 1) a small-amplitude linear (constant log decrement) regime where the damping is proportional to the square root of kinematic viscosity; 2) a larger-amplitude nonlinear regime where the damping log decrement is proportional to the vibrational velocity and is independent of viscosity.
- The nondimensionalized hydrodynamic damping of a 0.96-cm-thick plate with multiple perforations was found to be less than that of a 2.85-cm-thick plate having the same hole pattern, and slightly greater than that of a 0.96-cm-thick plate with the same solid area but having all of the open area in the form of an annulus at the periphery.
- The experimental results for the two perforated plates can be correlated to yield the following analytical expressions for satisfactorily conservative values of the hydrodynamic damping force F_d :

2.85-cm-thick plate

$$F_d = AV_r\rho\sqrt{\nu\omega} \sqrt{8 \left[\frac{l}{d} + 1 - \frac{\pi}{4} \left(\frac{d}{b} \right)^2 \right]}, V_r/\sqrt{\nu\omega} < 3$$

$$F_d = AV_r^2\rho, V_r/\sqrt{\nu\omega} > 20$$

0.96-cm-thick plate

$$F_d = AV_r\rho\sqrt{\nu\omega} \sqrt{8 \left[\frac{l}{d} + 1 - \frac{\pi}{4} \left(\frac{d}{b} \right)^2 \right]}, V_r/\sqrt{\nu\omega} < 5$$

$$F_d = 0.7 AV_r^2\rho, V_r/\sqrt{\nu\omega} > 20$$

where A = cylinder area, V_r = average relative flow velocity of fluid in the holes, ν = fluid kinematic viscosity, ω = circular frequency of vibration, and the other symbols are as defined previously.

- In those regimes where comparisons are valid, the results of this investigation are in general agreement with those reported in reference [1], which deals with single orifices in thin plates.
- An extension of the experiments described to the case of flowing water systems is desirable and would be likely to reveal significant effects of the steady flow component, especially on the hydrodynamic damping.

Acknowledgments

The author wishes to acknowledge the valuable contributions of D. V. Wright, H. J. Connors, A. R. Hess, and K. B. Wilner of the Westinghouse R&D Center to the experimental phase of this investigation.

References

- 1 Panton, R. L., and Goldman, A. I., "Correlation of Nonlinear Orifice



**Consumers
Power**

**POWERING
MICHIGAN'S PROGRESS**

General Offices: 1945 West Parnall Road, Jackson, MI 49201 • (517) 788-1636

Kenneth W Berry
Director
Nuclear Licensing

October 16, 1986

Director,
Nuclear Reactor Regulation
US Nuclear Regulatory Commission
Washington, DC 20555

DOCKET 50-255 - LICENSE DPR-20 - PALISADES PLANT -
EXPANSION OF SPENT FUEL POOL STORAGE CAPACITY -
TECHNICAL SPECIFICATION CHANGE REQUEST - REVISION 1

Consumers Power Company letter dated February 20, 1986 submitted the Technical Specification Change Request and supporting Safety Analysis Report (SAR) associated with the proposed installation of new spent fuel pool storage racks in approximately one-half of the Palisades Plant spent fuel pool. At the time of that submittal, the analyses referred to in the SAR were incomplete. Consumers Power Company letter dated April 16, 1986 provided confirmation that the analyses had been completed and the conclusions given in the SAR, with the exception of those for the pool structure, are valid. Additionally, it reported the results of analyses that showed that no modifications to the Region I racks are necessary. It also provided revised pages containing tables, figures and descriptions which were either incomplete or editorially incorrect in the February 20, 1986 submittal. Consumers Power Company letter dated April 24, 1986 confirmed that analysis of the Spent Fuel Pool structure was complete and that conclusions given in the SAR regarding the Spent Fuel Pool structure are valid.

NRC letter dated April 25, 1986 transmitted a request for additional information regarding the expansion of the spent fuel pool storage capacity. Requests for additional information were also received during discussion with the Palisades Plant NRC Project Manager. The additional information requested by letter and during discussion was provided by Consumers Power Company letter dated July 24, 1986 which also informed the Staff that Consumers Power Company would revise the Technical Specification Change Request and supporting SAR. Additionally, the July 24, 1986 Consumers Power letter informed the staff that submittal of the revised Technical Specification Change Request and supporting SAR, together with the information contained in that letter would be considered as submitted in lieu of the Summary Reports described in the Consumers Power Company letter dated April 24, 1986.

OC0886-0129-NL04

~~8610270099~~ (2pp)

449

3720

Director, Nuclear Reactor Regulation
Palisades Plant
Rev 1 - TSCR Spent Fuel Pool Capacity
October 16, 1986

2

Attachment I to this letter contains the revised (Revision 1) description of the proposed Technical Specification Changes and analysis which determines that this installation and license amendment involve no significant hazards. Attachment II contains the revised Technical Specification Change. Attachment III contains Revision 1 of the supporting SAR. The completed detailed analyses referred to in the SAR are available for review. Changes from the original February 20, 1986 submittal and from the revised pages included with our April 16, 1986 submittal are summarized as follows:

1. References to results of analyses are stated in the past tense and refer to the results of completed analyses.
2. Information provided by the completed Thermo-Hydraulic Analysis has been incorporated into Section 3 of the SAR.
3. The maximum initial U-235 loading of the fuel is stated in w/o.
4. The effect of 1,720 ppm boron in the pool water has been conservatively stated as 25 percent ΔK .

Changes made to the SAR by our letter dated April 16, 1986 have been included in the attached Revision 1. Therefore, the changes indicated by a vertical line in the right margin include those made at that time.

After approval, the specification changes requested in this Technical Specification Change Request will become effective when the installation of the new racks commences.

This letter supersedes and withdraws the May 11, 1981 Consumers Power Company letter entitled Technical Specification Change Request - Fuel Storage.

A check for \$150.00 as required by 10CFR170.21 was included with Revision 0 which was submitted on February 20, 1986.

Kenneth W Berry/rws (Signed)

Kenneth W Berry
Director, Nuclear Licensing

CC Administrator, Region III, USNRC
NRC Resident Inspector - Palisades

Attachments

OC0886-0129-NL04

3 7 2 J
4 5 0